A Hybrid Inverse Dynamic-Neural Network Approach to Lower Limb Exoskeleton Control

by

Hannah Dinovitzer

A thesis
presented to the University of Waterloo
in fulfillment of the
thesis requirement for the degree of
Masters of Applied Science
in
Mechanical and Mechatronics Engineering

Waterloo, Ontario, Canada, 2022

Author's Declaration

I hereby declare that I am the sole author of this thesis. This is a true copy of the thesis, including any required final revisions, as accepted by my examiners.

I understand that my thesis may be made electronically available to the public.

Abstract

A powered machine that is wearable over all or part of the human body can be referred to as a powered exoskeleton. The role of powered exoskeletons is usually to provide ergonomic structural support while using motor power to synchronize to and assist with intended movements. One specific category of exoskeletons is the lower limb exoskeleton.

There is a variety of applications for lower limb exoskeletons, including assistance, rehabilitation, and augmentation. A challenge in developing any of these forms of exoskeletons is the design of controllers which are able to perform well under a variety of scenarios, such as change in speed while walking or stair climbing, as well as with a variety of users. There are many different controllers that have been developed accordingly. One of these approaches involves estimating joint torques and applying these directly as control torques. This can be done in one of two ways: estimating the torques based on a few subjects and applying these prescribed torques to everyone, or estimating and applying joint torques in real-time. Many existing controllers which estimate and apply joint torques in real-time, only do so with a portion of the joint torques. For instance, this can be done by computing and applying joint torques which result from gravity only.

The challenge with the estimating and applying joint torques in real-time is developing an accurate model to represent the dynamics of the system and accurately measuring all required state signals. The signals which are most problematic for measurement is ground contact force measurements. As forceplates are not useful for continuous overground measurements and instrumented insoles can be unreliable, an alternative approach is required. To fill this gap and generate a robust real-time joint torque estimator, a hybrid inverse dynamic-neural network model is proposed. In addition, a data-driven solution is proposed and comprises of an end-to-end neural network for direct joint torque estimation.

The hybrid model computes joint torques with the use of kinematic information only. Eliminating the need for kinetic measurements allows ease with implementation in scenarios where forceplates are not available; this is done with a neural network for ground contact force estimation. The hybrid model was validated with 11 subjects during treadmill walking, including several different gait patterns. In comparison to the end-to-end direct torque estimator, the hybrid model has slightly worse performance at the knee and hip joints during treadmill walking which includes speed changes, asymmetrical walking, and start-stops. However, when testing these two approaches with a participant wearing an exoskeleton, the hybrid model outperforms the end-to-end network. This validates the versatility of the hybrid model to generalize to many different conditions and subjects.

The hybrid model was then implemented as a controller in a lower limb exoskeleton. A second pre-defined direct torque controller was also developed. The pre-defined torques

are recorded from the response of a feedback controller used on one participant. These torques are then applied as the direct torque control as a function of walking speed and gait phase. Both these controllers can be considered to be feedforward control approaches as the applied torques are not explicitly encoded by feedback errors. These controllers were tested individually and in combination for treadmill and overground walking with nine participants. A combination of the two controllers, with more contributions from the hybrid control, produces the overall best results in terms of spatiotemporal metrics. At a joint-level, all the tested controllers have similar performance in terms of range of motion and joint angle correlation to natural walking. The controller consisting of a combination of both hybrid and direct torque control, with more weight on the hybrid model, was also able to decrease the activation of four out of six muscles measured in the lower limbs, which includes knee flexors and extensors, and ankle dorsi- and plantarflexors, on average when compared to walking with the exoskeleton in passive mode. The decrease in muscle activity indicates that this control approach is able to provide assistance as well as improve the spatiotemporal performance.

As the joint-level performance was not meaningfully improved by this controller consisting of a combination of both approaches, this control alone would be insufficient for users who require assistive as well as corrective torques from the exoskeleton. For example, those who have suffered from an incomplete spinal cord injury or post-stroke hemiparesis do not have the ability to walk with a natural gait, therefore can benefit from corrections from the exoskeleton to achieve a natural gait.

The addition of corrective torques in the form of a position feedback control (FB) to the previously defined feedforward control (FF) is designed to provide both assistive and corrective torques to the user. In a pilot study with two participants for both treadmill and overground walking, the feedforward control alone has the best spatiotemporal performance while the feedback alone has the best joint-level performance. A combination of the two controllers will produce a balance of these two characteristics. All three of these controllers (FF, FB, FF-FB) were able to produce some reduction in muscle activation of the knee extensor and ankle dorsiflexor muscles, compared to passive exoskeleton walking. This indicates that all the controllers provide some level of assistance. However further testing is required to validate this hypothesis as well as optimize the method for combining these two control approaches.

This thesis demonstrated that the application of biological joint torques as an exoskeleton controller can be further improved with the addition of other control strategies. It is possible that combining biological torques with other control approaches, including those not explored in this thesis, will be more suitable for those suffering from physical impairments such as hemiparesis or severe muscle weakness.

Acknowledgements

I would like to thank my supervisor, Dr. Arash Arami, and my colleagues in the Neuromechanics and Assistive Robotics Laboratory for all their support and assistance during my time at the University of Waterloo.

I would also like to thank Dr. Stacey Acker and Dr. William Melek for being a part of my readers committee of my thesis.

Finally, I would like to thanks my loved ones for their patience and support through my work put towards this thesis.

Table of Contents

List of Figures

List of Tables

List of Abbreviations

1D-3H 1 Direct Torque Control - 3 Hybrid Control 32, 38, 41–59, 61

3D-1H 3 Direct Torque Control - 1 Hybrid Control 32, 43, 45, 46, 48–54, 57, 58

ANN Artificial Neural Network 8

BF biceps femoris 33, 51–53, 55–57, 70, 72, 74

BSIP Body Segment Inertial Parameters 7, 14, 15, 31

COP Center of Pressure 12, 21

DoF Degrees of Freedom 14, 15, 18

DTC Direct Torque Control 32, 38, 43–46, 48, 50, 52, 55, 57, 58

EMG Electromyography x, 5, 6, 10, 33, 34, 36–38, 49, 50, 59, 60, 62, 63, 70

FB Feedback 61, 65–68, 70

FF Feedforward 61, 63, 65–68, 70

FNN Feedforward Neural Network 19–22, 26

GM gastrocnemius medialis 33, 52, 53, 55, 57, 70, 73, 74

GRF Ground Reaction Force 6–8, 11, 18–23, 26, 28, 30, 76

HC Hybrid Control 30–32, 44–46, 48–55, 57–59

ID Inverse Dynamics 6, 8, 10, 20, 21

IMU Inertial Measurement Unit x, 5, 8, 28, 31, 33–36, 62

MVC Maximum Voluntary Contraction 36, 53

PCA Principal Component Analysis 35

RF rectus femoris 33, 50, 53, 55–57, 70, 72

RMSE Root Mean Squared Error 19–22, 24–28, 36

ROM Range of Motion 6, 36, 38, 47, 48, 67

SO soleus 33, 52, 55–57, 70, 73, 74

TA tibialis anterior 33, 52, 55–57, 70, 73, 74

VM vastus medialis 33, 50, 52, 53, 57, 70, 72, 74

ZMP Zero Moment Point 7, 13, 18–23, 26–28, 30, 76

Chapter 1

Introduction

Exoskeletons are intended to help the user perform a specified task. In the case of lower limb exoskeletons, these tasks include but are not limited to walking, stair climbing, and sit-to-stand movements. Those suffering from neuromuscular disorders can use exoskeletons for rehabilitation or assistive purposes [77, 10]. Exoskeletons can also be used by able-bodied subjects, in which the purpose of the exoskeleton is augmenting the user's abilities [21].

In assistive exoskeletons, the key to improving performance is in the control methods [12, 103]. Gait assistance exoskeletons can be classified into two categories: those intended for full mobilization and for partial assistance. Full mobilization exoskeletons are intended for users who have no motor control in their lower limbs, in complete spinal cord injuries for instance, thus there is no need for these exoskeletons to collaborate with the user. Meanwhile partial assistance devices are intended for users with less severe neuromuscular impairments, such as incomplete spinal cord injuries (iSCI) or hemiparesis resulting from a stroke.

The main challenge with partial assistive control methods arises when coordinating the assistance with the user's intentions [70, 77]. The controller is intended to aid more than it is hindering the user; there should be a synergy in the user-applied and exoskeleton-applied joint torques. An ideal controller would generate a torque profile that aligns with the intended movements of the user in terms of magnitude, sign, and timing. There are many different approaches to producing these motor commands.

Five common classifications of controllers includes position control, torque control, impedance control, physiological approaches, and direct joint torque estimation [12]. These approaches can be limited by signal quality, providing assistance during only certain phases

of the gait cycle, requirements for subject-specific tuning or requirements for detailed dynamic identification.

One shortcoming of many controllers is the lack of design for each user's needs. As all individuals have a unique gait in terms of both kinematics and kinetics, an ideal controller would adapt to each user. Dynamic modelling is able to highlight these differences in gait.

1.1 Objectives and outline

The main goal of this research is to develop an online joint torque estimator intended for use as a lower limb exoskeleton controller. The performance of this controller is evaluated alone as well as in combination with other common control approaches such as direct torque control and position feedback control. The main objectives of this thesis are the following:

1. Develop and validate a real-time accurate joint torque estimator for treadmill walking

2. Implement and test a feedforward exoskeleton controller based on the obtained torque estimator in 1

3. Compare the controller from 2 to a pre-defined feedforward direct torque control in experimental scenarios in order to identify an "ideal" feedforward torque control approach

4. Utilize the identified feedforward torque control identified in 3, in combination with position feedback control, to investigate the ability of the controller to correct and assist in walking

In Chapter 2, an overview of gait analysis and dynamic modelling of lower limbs is provided. Current strategies and limitations of joint torque estimation are discussed. A review of current applications of direct joint torque estimation implemented for lower limb exoskeleton control is also presented in Chapter 2. The developed hybrid model (inverse-dynamic model augmented with a neural network) as well as an end-to-end data-driven model for joint torque estimation are proposed and validated in Chapter 3. This study involves treadmill walking with various conditions (ie. speed changes, varied strides lengths, asymmetrical walking, start-stopping), which was used for the development and validation of these models. As the results from this study demonstrate that the hybrid model is better able to generalize to conditions differing from able-bodied walking, exoskeleton walking

for instance, the hybrid model was used in a controller for the lower limb exoskeleton in Chapter 4. In Chapter 4, first a series of experiments were conducted to evaluate the performance of the hybrid model (as a feedforward controller) alone and in combination with direct torque control (computed from desired trajectories). This experiment identified an ideal feedforward torque control strategy for the exoskeleton for assistance. Finally, the resulting "ideal" control from these experiments was then augmented with a position feedback control scheme to ensure both corrective and assistive torques from the exoskeleton in Chapter 5. Some concluding remarks are presented in Chapter 6. An overview of the main contributions are shown in Figure 1.1.

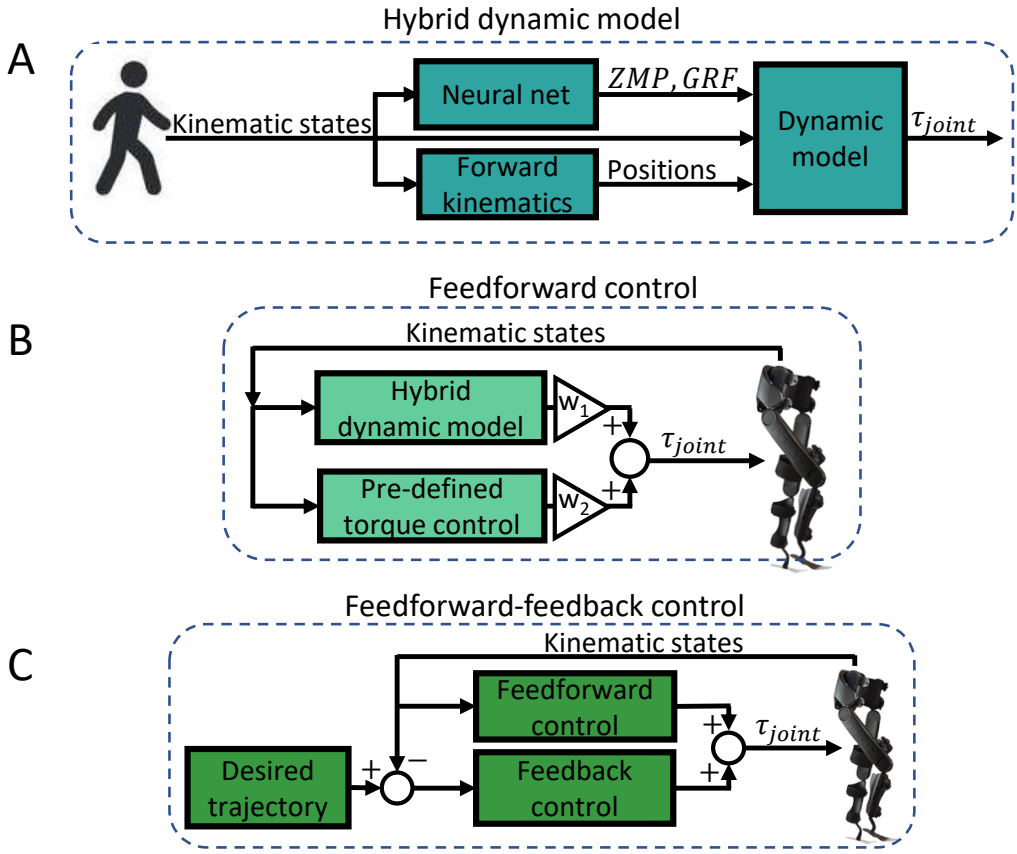

Figure 1.1: Overview of the main contributions included in (A) Chapter 3, (B) Chapter 4, and (C) Chapter 5.

1.2 Contributions

The main contributions of this research are summarized below:

1. **(Chapter 3)** Propose and validate an accurate ground reaction force estimator based on kinematic measurement
2. **(Chapter 3)** Propose and validate a hybrid inverse dynamics approach to joint torque estimation in absence of ground reaction force measurements
3. **(Chapter 3)** Propose and validate an end-to-end neural network for joint torque estimation
4. **(Chapter 4)** Evaluate the performance of an online joint torque estimator implemented as a feedforward control in a lower limb exoskeleton, in standalone mode and in combination with a pre-defined feedforward torque control in able-bodied users
5. **(Chapter 5)** Evaluate the performance of the "ideal" feedforward torque control determined previously in combination with a position feedback controller in able-bodied users

Chapter 2

Background

2.1 Human movement and gait analysis

Human movement studies is a research discipline involving the relationships between human movement and its effects on the human body. One main area of this research involves the study of human gait and locomotion. Gait analysis involves the study of locomotion in terms of body movements, body mechanics, and muscle activity [45]. This analysis has applications in biomechanics, rehabilitation, and patient assessment. For instance, gait analysis can be used as a tool for diagnosis of various neurological conditions, such as multiple sclerosis or Parkinson's disease [40], to quantify progression through rehabilitation following major surgeries [72], or in sports performance [57].

Common analysis modalities rely on physiological, kinematic, and kinetic measurements. Physiological measurements can include electromyography (EMG), electrocardiogram, or electroencephalogram signals which measure the activity of muscles, the heart, and the brain, respectively. These signals can provide a measurement of work load, or effort level as well as give insight into intended movements. EMG in particular is used in the analysis and classification of pathological gait [107].

Kinematic measurements can be resolved with motion capture systems, which are either lab-based or ambulatory systems. Lab-based systems involve fixed cameras [19, 17] while ambulatory systems involve wearable sensors. Wearable sensors used in gait analysis include inertial measurement units (IMU) [58, 3], barometric sensors [71], infrared sensors [5], or time-of flight sensors [13]. In some cases, sensors can be implanted in a smart prosthetic [8]. Kinematic analysis approaches are able to give a measure of joint or segment

positions, velocities, and accelerations which provides information about how the body is moving and highlight any abnormalities. There are many different metrics that can be used in gait analysis. Kinematic metrics can include joint ROM, segment or joint velocity, or joint angles as a function of gait phase [20]. Spatiotemporal metrics involve a combination of both spatial and temporal measurements to determine metrics such as cadence, step length, stance time, step width, and toe clearance [15]. Such metrics give clinicians the ability to quantify a patient's stability [30, 42], or fall risk [59].

External kinetic information, such as ground reaction forces (GRF) can be measured with force plates or force sensors, meanwhile internal kinetic information, such as joint moments or forces, cannot be directly measured without the use of implanted sensors. Implantable sensors are able to measure internal force and moments [46, 29, 6, 34], however require invasive procedures. For this reason, internal kinetics are commonly computed with various analytical techniques, including dynamic modelling [101].

Dynamic modeling of human movement has applications in biomechanics, for instance, in the analysis of human movement [25, 54], outcome evaluation of total joint arthroplasty and prosthetic limbs [102, 36], injury biomechanics [94], developing predictive simulations of movement, rehabilitation engineering, human motor control studies, and robotics [97, 108].

2.1.1 Dynamic modelling

There are several approaches for estimating kinetic information that cannot be directly measured, such as joint torques and forces. A few of the main approaches include sEMG, ID, and machine learning techniques.

Using electrodes, muscle activity can be measured with EMGs then mapped to muscle forces and in turn to joint torques. This mapping can be expressed via neural networks [66, 95] or forward dynamic models [16, 11] such as the Hill model [48]. As this approach relies on the quality of measured EMG signals, it is susceptible to many external factors. Signal quality can decrease as a result of improper sensor placement[18], fatigue [105], or skin-electrode conductivity changes [1].

In contrast, an ID-based approach measures external forces and body kinematics in order to compute joint torques. Having the body simplified to a kinematic chain allows the joint torques to be determined by ensuring all kinetic relationships within the model are satisfied [2]. There are four contributing factors that must be considered in the dynamic relationship: gravity, inertia, Coriolis, and external forces (see Figure 2.1). The general form of this dynamic relationship is

$$M(q)\ddot{q} + C(\dot{q}, x)\dot{q} + G(q) = \tau_{joint} + J^T F + \tau_u \tag{2.1}$$

where M, C, and G are the inertia matrix, Coriolis matrix, and gravity vector respectively. q is the vector of states describing the system, typically including joint angles and sometimes global position measurements of one selected segment. τ_{joint} is the vector of joint torques acting on each segment, τ_u includes all unmodeled dynamics, and $J^T F$ is the contribution of the external forces on the joint torques. F is a vector of external forces and J the Jacobian matrix which contains information to relate the joint angles and torques to the location and magnitudes of these forces. As the Jacobian matrix relates the position of the joints to the location of the external force, measurements of the location of external forces is required. This can be done with the ZMP. During walking, the ZMP is the location in which the GRF at the contact of the foot with the ground does not produce any moment in the horizontal direction. The unmodeled dynamics, elasticity for instance, is assumed to be negligible.

The inertia, Coriolis, and gravity matrices and vectors depend on both the state of the model as well as the BSIP. The BSIP are a set of parameters which describe the size, mass, and mass distribution of each segment.

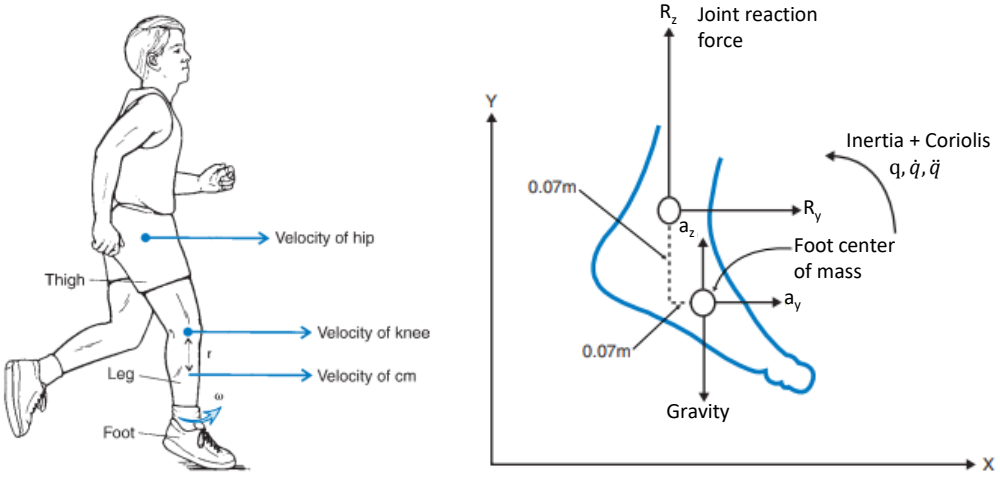

Figure 2.1: Schematic of contributions of Inertia, Coriolis and Gravity on the foot segment during running [44].

Thus, the reliability of this model is linked with the accuracy of the kinetic and kinematic measurements as well as the ability of the model to represent the body. Modelling requires many assumptions and simplifications which allow computations to be possible, however can affect the accuracy of the model's representation. Kinematic information such as joint angles, are typically measured with motion capture systems [64] or wearable inertial

measurement units (IMUs)[89, 56]. Ground contact forces and their respective locations are typically measured with forceplates[64] or instrumented insoles[35].

In the case of overground walking studies, the use of forceplates is undesirable as they are costly and not easily portable. Instrumented insoles, which are portable and less costly, can be subject to measurement inaccuracies, calibration inconsistencies, and challenges with real-time processing [27]. Due to these challenges with forceplates and instrumented insoles, approaches to estimate joint torques without the need of forceplates or instrumented insoles have been developed. These methods are generally either model-based or ANN based.

In [88], a dynamic model-based approach has been used to estimate the GRF in combination with the smooth transition assumption to eliminate the indeterminacy problem during double support. The indeterminacy occurs as during double support the force and moment equilibrium equations are insufficient to determine the forces in the system. The transition function is, however, determined through trial and error with experimental data. Therefore, it may not generalize well to other walking conditions or subjects. In addition, this transition has temporal dependencies restricting the real-time application of this method. With a focus on upper limb torque estimation, [26] demonstrated a whole body ID approach also without the use of force measurement. A similar approach as with [88] for GRF estimation was taken. The double support indeterminacy was, however, resolved with optimizing the force distribution between the left and right legs by minimizing the sum of squared net joint moment (i.e., minimizing the energetic cost). Due to the temporal dependencies and computationally expensive optimizations, none of these methods are suited for real-time applications.

There have been many uses of ANNs in the prediction of gait kinetics. Some approaches predict GRFs [81, 76] based on kinematic data. Meanwhile, other methods predict joint torques directly [31, 65, 76] by using various combinations of kinematic and kinetic data. These approaches are typically trained and tested on normal, asymmetrical, or varied stride length walking at a constant speed which restricts generalizability to different walking conditions such as varying speed.

To address the shortcomings of the existing techniques, i.e. not being able to provide a real-time estimation of joint torque and/or generalize to different walking conditions, Chapter 3 presents a real-time ID joint torque estimator which requires only kinematic measurements.

2.2 Lower limb exoskeletons

Lower limb exoskeletons can be classified into three main categories based on their intended purpose: assistance, rehabilitation, and augmentation. Assistive exoskeletons are intended for those with neurological or neuromuscular impairments that cause limited mobility or strength. These exoskeletons are designed in order to supplement the user's efforts in order to accomplish the desired movement. A rehabilitation exoskeleton is used for aiding a patient in regaining strength and mobility following a neuromuscular injury. A healthy subject using an exoskeleton to further enhance their abilities would be considered an augmentation exoskeleton. Figure 2.2 shows images of different lower limb exoskeletons.

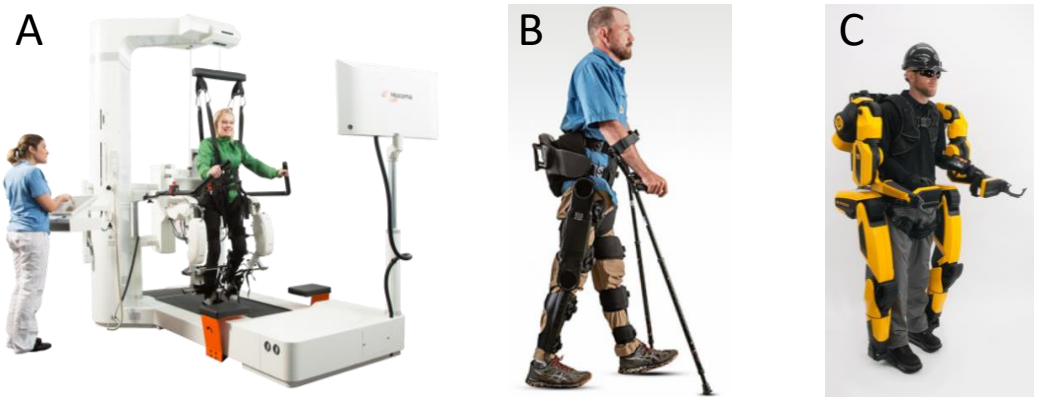

Figure 2.2: Image of exoskeletons used for (A) rehabilitation, (B) assistance, and (C) augmentation.

Improvements in the control methods will greatly improve the overall performance of assistive exoskeletons [12]. Specifically in partial assistive control, where the user contributes to some of the overall movements, challenges arise when coordinating the assistance with the user's contributions. Many of the existing approaches to resolve the challenges associated with partial assistive control can be classified into five categories: position control, torque control, impedance control, physiological approaches, and direct joint torque estimation.

A position control strategy utilizes a desired trajectory for the exoskeleton to follow. In many cases, the desired trajectories are constructed to approximate a healthy gait pattern. These gait patterns can be created as a function of gait progression [106, 22, 4], which allows the user some temporal freedom; however, these controllers do not allow for any spatial freedom. As gait naturally has some variability, imposing a strict gait pattern does not always feel comfortable to the user. However, some research has shown that it is

possible to adapt desired position trajectories based on user intention [99, 109].

A torque control consists of applying a predefined torque profile. Similar to the position control, torque control can also be a function of gait phase to allow for better synchronization with the user. The torque profiles can change over time, be optimized online [112] or offline [62]. The success of this controller relies heavily on an accurate gait phase estimation as well as a well tuned torque profile. Other control approaches are reliant on accurate detection of gait events [28].

Impedance control can be similar to a position control strategy however, in impedance control, torques will only be applied when the user deviates significantly from the intended movements. This approach is commonly applied in rehabilitation as it induces active participation from the user which in turn promotes neuroplasticity and recovery of motor control. There are several approaches to implementing an impedance control which can be through the use of stiffness modulation [51], a force field [70], or virtual energy regulation [79]. However, these approaches have more complex design and their suitability for different users and levels of injury has not been shown yet.

A physiological approach can also be taken in which EMG signals are converted into motor commands [33]. Many different approaches have evolved within this category, however, they are all subject to the same challenges. EMG signals are sensitive to skin conductance, fatigue, and sensor placement, which in turn can deteriorate the quality of the computed motor commands. In addition, users with certain neuromuscular impairments can have a decreased ability to contract their muscles which results in a high signal-to-noise ratio that is problematic for these types of controllers.

Direct joint torque estimation involves estimating, and applying to the exoskeleton, the required joint torques to achieve a certain movement. Some approaches rely on an ID model [9] while others apply a simplified model, such as considering only some components of the body dynamics [52], a spring-loaded inverted pendulum (SLIP) model [114] or a 2-degree of freedom (DoF) compass gait model [41]. These models can be implemented without timing problems as they do not rely on gait phase or time. However, the challenge to successfully implement these models is determining an accurate representation of the system in terms of kinematics and dynamics.

It can be said that there are two domains in which the exoskeleton can be controlled: position and torque domains. In general, with a position control, the movement of the exoskeleton is controlled such that it approaches a desired set of kinematic values which can include position, velocity, or acceleration of any point on the exoskeleton. Position and impedance control are both derived in the position domain. Meanwhile in the torque domain, the motions of the exoskeleton are not being directly controlled. The controller

instead computes torques directly which in turn result in the movement of the exoskeleton. The benefit to not imposing restrictions on the movements is that it gives the controllers the potential to be better suited for a variety of users without tuning.

As all individuals have their own unique walking pattern, this suggests that reference trajectories for position domain controllers should also be unique to the individual. However, a controller based on joint torque estimation as well as direct joint torque control does not impose any form of desired position trajectories, these controllers can accommodate for unique walking patterns without modifications to the controllers.

2.2.1 Control based on direct joint torque estimation

There have been many different dynamics-based approaches to estimating joint torques as a form of exoskeleton control. Some strategies apply only a component of the joint torques while others use simplified or detailed models of the human lower body to estimate and apply all components of joint torques.

In quasi-static movements, the gravitational effects dominate the dynamics which leads to some approaches be developed such that all other dynamics are ignored. For instance, a gravity compensation control strategy is implemented in the knee [39, 111] as well as in the knee and hip [53] joints of an exoskeleton during squatting. The control approach was able to reduce the participant's energy expenditure during periodic squatting. Similarly, in [113] and [52], gravity compensation, in combination with other control approaches, is applied in the stance leg during stair ascent and walking, respectively.

Although in these studies, gravity compensation is shown to assist, this control approach is not ideal for more dynamic movements such as walking as inertia and Coriolis will have a greater effect and if compensated for can have a greater assistive potential.

A joint torque estimation approach in [92] considers both the gravitational effects as well as the effects of GRFs on the computed joint torques. In this approach, the force mapping and gravity terms are considered. In including the force mapping, any external loads being carried by the user are considered in the torque computations. Similarly in [78], a gravity compensator with GRF information is implemented in walking. As with gravity compensators alone, this approach is intended for quasi-static movements. This approach is also subject to challenges with GRF measurement if implemented for overground walking conditions.

In other approaches, simplified models are implemented. For instance, in [112], a spring-loaded inverted pendulum model (SLIP) model is implemented in order to estimate

joint torques in order to be applied as assistive torques to a lower limb exoskeleton. This approach was only implemented during stance phase, leaving swing phase unassisted. A compass-gait model is implemented in [41] in which the system is simplified to 2 DoFs and is controlled across a periodic limit cycle.

In [9], the whole dynamics as shown in equation 2.1, including gravity, inertia, and Coriolis, as well as measured ground contact forces, are considered in estimating the joint torques. The gait cycle is separated into four sections, each having separate dynamical equations describing the joint torques. As the joint torque estimation switches between four models, there are discontinuities in the estimation, which renders this approach undesirable for implementation as an exoskeleton controller. A similar approach which considers all components in the Lagrangian equation (equation 2.1) is taken in [63]. In this case, the foot contact forces and COP are measured using instrumented insoles then considered in the torque computations. The use of instrumented insoles can be challenging in terms of accuracy and real time processing.

2.3 Concluding remarks

There is a need for an accurate and real-time approach to joint torque estimation that can be implemented in any setting, including those without force measurements. Having an accurate method of joint torque estimation which requires only kinematic measurements will facilitate biomechanical analysis in settings where force measurement is challenging such as continuous overground walking. In order to address this, in Chapter 3, a combination of a model-based and data-driven model are developed to compute joint torques using kinematic data alone.

This joint torque estimation model will allow for applications in exoskeleton control. This control approach, as explored in Chapter 4, will be time-independent and allow the user to have full control of their joint trajectories, without being forced to follow a predefined path. Control of joints is a result of the torques being essentially amplifications of the user's movements. The combination of an accurate joint torque estimation, direct joint torque control, and a position feedback controller has the potential to provide both corrective and assistive torques that are synchronized with the user's intentions. This is explored in Chapter 5.

Chapter 3

Accurate Real-Time Joint Torque Estimation for Dynamic Prediction of Human Locomotion

This section describes a proposed hybrid torque estimator developed by integrating an inverse dynamic model with an artificial neural network. This section also contains a comparative data-driven end-to-end torque estimator as well as experimental procedure and validation. The content of this chapter is under revision in the IEEE Transactions of Biomedical Engineering with the same title and authorship of H. Dinovitzer, M. Shushtari and A. Arami.

3.1 Methods

3.1.1 Experimental setup

Eleven participants (age 27±4.1 years, 6 female, mass: 69.9±14.0 kg, height: 1.74±0.072 m) were included in the experiment. Data collection protocols and procedures were approved by the Clinical Research Ethics Committee at the University of Waterloo (ORE#41794), and conformed with the Declaration of Helsinki.

The experimental setup consists of a split-belt instrumented treadmill (Bertec, US) with separate force plates under each foot/belt. The force plates measure ground reaction forces and torques as well as ZMP at a sampling frequency of 1000 Hz. An 8-Vero camera

optoelectronic motion capture system (Vicon Motion Systems, UK) was used to collect kinematic data at a sampling frequency of 100 Hz. Sixteen markers were placed on each participant according to [32, 60]. Fig. 3.1B shows the marker placement.

A lower limb exoskeleton (Indego, Parker Hannifin, US), shown in Fig. 3.1C, was used for one additional trial on one participant. This exoskeleton has 4 active DoF with actuators at the knee and hip joints while having a rigid ankle joint. In addition, the exoskeleton has a rigid foot plate which has been placed under the shoe insole.

3.1.2 Experimental procedure

Anatomical measurements of the participants were taken according to the relationships developed by Pavol et. al in order to determine individualized measurements of body segment inertial parameters (BSIP) [82]. These relationships are applicable to average able-bodied adults, which is the population used for this experiment. In order to test the robustness of the proposed torque estimator at different walking conditions, an experiment was designed with five consecutive walking conditions, as shown in Fig. 3.2 [98]. The first condition is constant speed walking at 0.8 m/s, with normal strides, followed by short strides, long strides, and ends with normal strides again, for 45 seconds each. The next condition consists of constant acceleration where the treadmill speed starts at 0.1 m/s, reaches 1.9 m/s, followed by constant deceleration (the treadmill speed returns to 0.1 m/s). The acceleration for this condition is ± 0.02 m/s^2. The third condition contains sharp speed jumps between 0.4, 0.8 and 1.2 m/s. The acceleration during the speed jumps is 0.4 m/s^2. The fourth condition involves asymmetrical walking, where the two belts have different speeds. The final condition consists of several repetitions of starting and stopping walking at a speed of 0.8 m/s, with an acceleration of 0.2 m/s^2.

During the exoskeleton test on one participant, the exoskeleton was in zero torque mode while the participant walked for two minutes at 0.85m/s on the treadmill. In order to consider the dynamics of the exoskeleton, it was assumed that there is no relative motion between the exoskeleton and the participant. With this, the BSIP were updated to consider each segment's added mass and inertia while the rest of the dynamic equations remain the same. However, in dynamic modelling, has been shown to be mostly affected by total mass and height of the system, rather than the mass distribution [114].

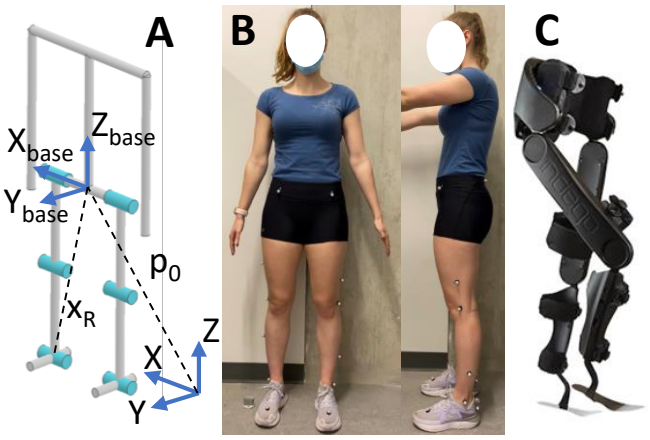

Figure 3.1: (A) Schematic of a human model with coordinate system used for derivation of dynamic equations, (B) motion capture marker placement and (C) lower limb exoskeleton (Indego, Parker Hannifin, USA) used during experiments.

3.1.3 Hybrid torque estimator

The proposed hybrid torque estimator includes a model-based and a data-driven component (see Fig. 3.3). The model-based component relies on a dynamic formulation to estimate the joint torques based on the measured kinematics and estimated kinetic obtained from the data-driven component.

Dynamic model extraction

The Newton-Euler dynamics of any system can be described using a general coordinate system. The base link of the system is selected such that the dynamic equations are derived relative to this link. In the case of modeling a human, the trunk segment can be selected in order to simplify the torque equation derivations.

Several simplifications were made in modeling the human body. Only movements in the sagittal plane were considered as these movements constitute the majority of motion during forward walking [2]. It is also assumed that the segment lengths can accurately be measured prior to experimentation and that all the joints act as pin joints. Finally, it was assumed that the BSIP remain constant and can be estimated by [82].

The human body has been simplified into a 7-segment model, the trunk and upper limbs were considered as one segment [38], with 9 DoF, see Fig. 3.1A. These DoFs include ankle, knee, and hip flexion-extension movements for both legs as well as the trunk position and orientation with respect to the global frame.

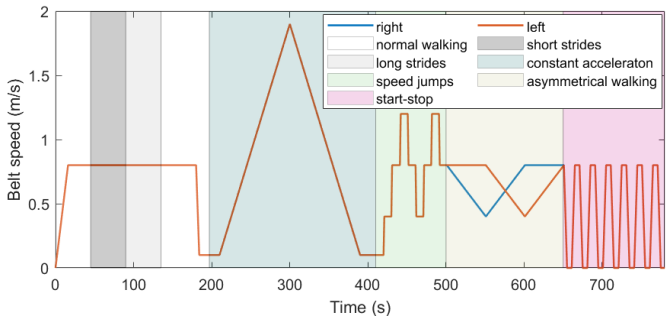

Figure 3.2: Left and right treadmill belt speeds during the experiment with the walking conditions denoted by shaded areas [98].

The general form of the equations describing this model dynamics are as follows [37],

$$\begin{bmatrix} H_{11} & H_{12} & H_{13} \\ H_{21} & H_{22} & H_{23} \\ H_{31} & H_{32} & H_{33} \end{bmatrix} \begin{bmatrix} \ddot{p}_0 \\ \ddot{q}_0 \\ \ddot{q} \end{bmatrix} + \begin{bmatrix} B_1 \\ B_2 \\ B_3 \end{bmatrix} = \begin{bmatrix} 0 \\ 0 \\ \tau \end{bmatrix} + \begin{bmatrix} I_3 & 0 \\ [x_R\times] & I_3 \\ J_{R1}^T & J_{R2}^T \end{bmatrix} \begin{bmatrix} F_R \\ N_R \end{bmatrix} + \begin{bmatrix} I_3 & 0 \\ [x_L\times] & I_3 \\ J_{L1}^T & J_{L2}^T \end{bmatrix} \begin{bmatrix} F_L \\ N_L \end{bmatrix} \quad (3.1)$$

where

- p_0 is a vector specifying the position of the base link in relation to the global coordinate system
- q_0 is a vector containing the angular orientation of the base link
- q is a vector of six joint angles
- τ is a vector of six joint torques
- F_R and F_L are vectors of ground reaction forces acting on the right and left foot, respectively
- N_R and N_L are vectors of ground reaction torques acting on the right and left foot, respectively
- H_{ij} is the inertial component of the base link ($i = 1, 2$) and for the body segments ($i = 3$)

- B_i is the Coriolis and gravitational forces for the base link ($i = 1, 2$) and for the body segments ($i = 3$)
- J_{Ri} and J_{Li} are Jacobian matrices which transform the reaction forces ($i = 1$) and torques ($i = 2$) to the respective joint torque contributions
- x_R and x_L are the position of the right and left foot with respect to the origin of p_0.

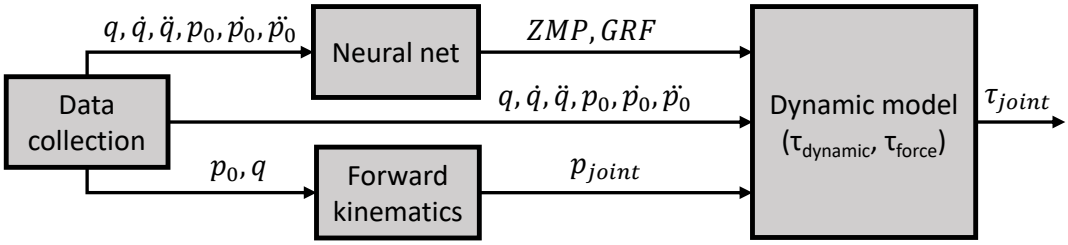

Figure 3.3: Overview of torque estimation components where q is joint angle, p is position, and τ is torque.

Using the last row of (3.1), joint torques obtain as

$$H_3 \begin{bmatrix} \ddot{p}_{y_0} \\ \ddot{p}_{z_0} \\ \ddot{q}_{x_0} \\ \ddot{q} \end{bmatrix} + B_3 = \tau + K_R \begin{bmatrix} f_y \\ f_z \\ n_x \end{bmatrix}_R + K_L \begin{bmatrix} f_y \\ f_z \\ n_x \end{bmatrix}_L \tag{3.2}$$

where

- H_3 is an inertia matrix, formed from augmenting H_{31}, H_{32}, and H_{33}
- K_R and K_L are the matrices that map the ground reaction forces and torques to the base coordinates defined in Fig. 3.1A
- b_{i3} are the components of B_3 in (3.1)
- f_i and n_i are the components of F_i and N_i in (3.1)

For clarity, (3.2) will be referred to as,

$$\tau = \tau_{dynamics} + \tau_{force}. \tag{3.3}$$

where $\tau_{dynamics}$ refers to the joint torques produced as a result of the inertial, Coriolis, and gravitational forces, and τ_{force} is the joint torques produced as a result of mapping all the ground reaction forces and torques to each joint. In order to simplify the computations, each leg in the model is considered separately as in [63]. This is possible as the dynamics of one leg has little impact on the other leg during normal walking. In addition, having each leg considered separately reduces the amount of error that can be propagated through the kinematic chain.

Dynamic model verification

A simulation was used to verify the dynamic equations derived to model lower limb joint torques. In OpenSim, a 9-DoF human musculoskeletal model (see Figure 3.4) was used in the sagittal plane [24]. The modeled skeleton walked at a constant speed of 1.23 m/s for 30 seconds during the simulation [99]. The ground contact was modeled according to [50, 47]. The simulation is torque-controlled and computes the corresponding joint kinematics and GRF. In order to validate the dynamic model and forward kinematic model (Fig. 3.3), the joint kinematics, foot kinematics, GRF and ZMP were extracted from the simulation and used to estimate the joint torques.

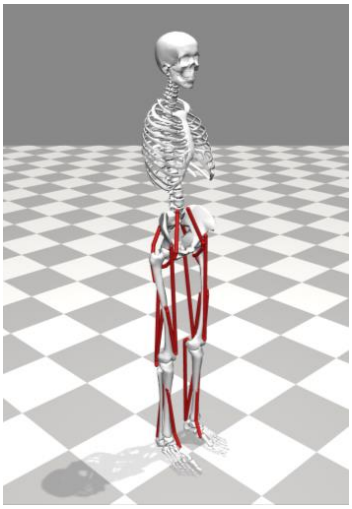

Figure 3.4: Skeletal model used in simulations constructed in OpenSim.

Data-driven GRF and ZMP estimation

In order to eliminate the need for forceplate measurements of GRF and ZMP to compute τ_{force}, a FNN is trained (force-FNN) to estimate both these values allowing the joint torque estimation method to be applied to situations in which a forceplate is not available.

The force-FNN contains two hidden layers, having 20 and 10 neurons, and was trained using the Levenberg-Marquardt algorithm [110] to minimize a mean squared error (MSE) loss function computed using both GRF and ZMP estimates. As the collected dataset consists of multiple subjects, the GRF and ZMP values were normalized by total body weight (BW) and foot length (L_{foot}), respectively. This would give the network the ability to account for differences due to anthropometric variability across subjects. The anterior-posterior component of ZMP has been utilized as the position for force application to the base link as this eliminates the need for considering the ground reaction moments in the force mapping. As the ZMP is measured relative to the heel, the forward kinematics equations have been derived starting from the stance foot, rather than the trunk. This ultimately produces the same relationship between the collected data and the estimated torques.

GRF and ZMP estimation validation

A leave-one-subject-out cross validation approach was used such that the test subject was excluded and the network was trained on the remaining dataset. The validation subject for early stopping was randomly selected from the remaining training subjects. This process was repeated eleven times, such that the network was tested on each participant once. GRF and ZMP of the proposed method were compared to those measured by the forceplates in the instrumented treadmill. RMSE, and Pearson correlation coefficient (R) were used to compare the results. A Wilcoxon signed rank test with Bonferroni correction was used to compare the RMSE and R of force-FNN results obtained across different walking conditions.

3.1.4 End-to-end joint torque mapping

As a comparative approach, a data-driven end-to-end joint torque mapping was developed. This model consists of a FNN, with two hidden layers with 15 and 8 neurons, that was trained to directly estimate the joint torques using kinematic data only. The same features and training procedure as with the GRF and ZMP estimator (force-FNN) were used. The torques were normalized by $BW * height$ for each subject.

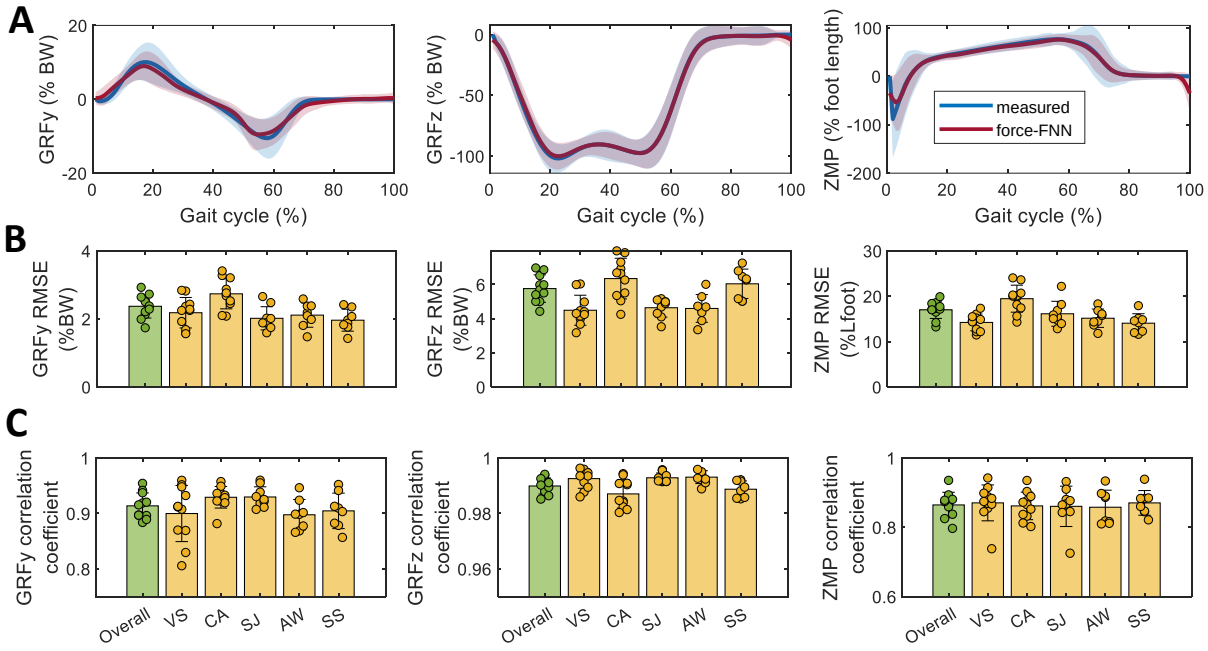

Figure 3.5: (A) Average estimated GRF and ZMP compared to forceplate measurements. The overall performance for the estimator as well as the performance for each walking condition, including varied stride lengths (VS), constant acceleration (CA), speed jumps (SJ), asymmetrical walking (AW), and start-stops (SS), are reported in terms of (B) RMSE, and (C) Pearson correlation coefficient. Each point represents the result of an individual subject.

3.1.5 Torque estimation validation

The same leave-one-subject-out cross validation approach to the GRF and ZMP estimator validation were implemented with the hybrid and end-to-end torque estimators. RMSE, and Pearson correlation coefficient (R) were used to compare the torque estimators results to the reference torque, which was the ID-computed torques based on Vicon computations. The Vicon ID torques are computed based on motion capture and forceplate measurements, and are considered as the gold standard for gait analysis. These metrics of RMSE and R are compared at different tested walking conditions. However, as the Vicon computations are based on a different approach, which includes different assumptions and simplifications to the model, than that being proposed in this chapter, there are expected differences between these models regardless of the accuracy of each component of the hybrid model.

The exoskeleton experimental data was not included in the development of either FNNs,

and is used as an additional validation condition for the two torque estimators. The ID-algorithm used in the Vicon program was designed for use with subjects with an average body composition. However, during the exoskeleton experiment, the inertial properties of the human-exoskeleton system no longer match those of an average body composition. Hence, there will be some resulting estimation errors. Nonetheless, the results from the Vicon-estimated torques are likely to be close to the true values as [87] demonstrated that variations in inertial parameters do not have a significant effect on lower limb ID for torque estimation. Therefore, the Vicon torques will still be treated as the reference torques.

In analyzing the overall performance of the hybrid and end-to-end joint torque estimators (walking without or with exoskeleton), one-tailed Wilcoxon signed rank tests were implemented using a level of significance of 0.05. The performance of the hybrid and end-to-end torque estimators were also compared at each walking condition (e.g., varied stride length, speeds jumps, etc) without exoskeleton. For this comparison at each joint, similar statistical tests were used while a Bonferroni correction was also applied.

3.2 Dynamics discussion

An analysis was conducted separately to demonstrate the overall performance of the torque estimators as well as their components, the force-FNN and the dynamic model.

3.2.1 GRF and ZMP estimation

Average RMSE of 2.30±0.34% BW, 5.75±0.80% BW, and 17.01±1.89% foot length are obtained on the test participants for horizontal GRF, vertical GRF, and the anterior-posterior ZMP estimation, respectively. Figure 3.5A compares the average profile of the FNN-estimated GRF and ZMP with their measured values across test subjects.

The ZMP of each foot is reported relative to the respective heel such that positive values indicate a location in front of the heel in the y-direction. For the ZMP data, there is a slightly larger standard deviation in the measured values compared to the FNN-estimated values. This is particularly more evident in the loading response and the pre-swing phase of the gait cycle. This is expected as studies have found that COP, and consequently ZMP, during walking, particularly during the loading response and pre-swing phases, have more variability among individuals [14, 104]. It is also noted that the normalized ZMP at heel strike is negative at the beginning of the gait cycle. This caused by the treadmill belt

making contact with the foot at this instant which results in a measured ground reaction moment, in turn causing the ZMP to be measured as negative.

The mean RMSE and the correlation coefficient between the measured and estimated values are further investigated in Figure 3.5B-C indicating an almost uniform performance of the force-FNN across different walking conditions. When comparing the performance of the force-FNN across all walking conditions, no significant RMSE or correlation coefficient difference was found between any two walking conditions.

The FNN estimates horizontal GRF with a slightly lower correlation coefficient (0.91 ± 0.023) than the vertical GRF (0.99 ± 0.003). This could be due to the inputs provided to the force-FNN are not rich enough to quantify these small variations in the force profile. For instance, footwear has been shown to cause changes in the GRF peaks during walking [96]. During this study, participants wore their footwear of choice which has the potential to introduce some small variability in the GRF .

As seen in Figure 3.5 there is little variation in the performance of the force-FNN across different walking conditions, demonstrating the robustness of this network to different walking conditions.

3.2.2 Dynamical model verification

The developed dynamical model is initially validated in Opensim. The simulated and estimated joint torques from dynamic modeling are plotted in Figure 3.6. The RMSE and correlation coefficient (R) between the estimated and simulated joint torques across one gait cycle are 4.6, 5.6, and 2.1 Nm and 0.99, 0.98, and 0.99, respectively for the ankle, knee and hip joints. The small amounts of error between the simulated and estimated torques arise from the simplifications made to the dynamic model during derivations which do not match those of the model being applied in the simulation. The overall estimated torques are, however, acceptable as the errors are relatively small and the estimates follow the same trend as the simulated values (confirmed also by high R values). This verifies that the dynamic model represents the gait kinetics and kinematics accurately enough to be used in the hybrid torque estimator.

Further validation of the dynamic equations in the hybrid model are performed with experimental data from all 11 subjects. In this case, the measured GRF and ZMP are used as an input to the dynamic model along with kinematic measurements. The resulting computed torques are shown in Figure 3.7A. When compared to the gold standard Vicon-computed torque estimation, the overall RMSE of all subjects for the ankle, knee and hip joints are 0.8 ± 0.14, 1.0 ± 0.28, and 1.4 ± 0.39 %BW*height while the corresponding

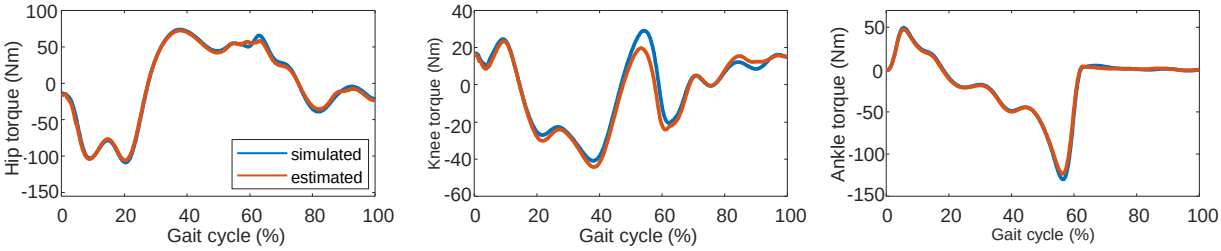

Figure 3.6: Comparison of simulated and estimated joint torques using dynamic modeling for the hip, knee, and ankle for one gait cycle. RMSE is the root mean squared error, and R is the Pearson correlation coefficient.

correlation coefficients are 0.97±0.02, 0.69±0.12, and 0.75±0.12. As components of the hybrid model, the GRF and ZMP estimator and the dynamical equations, have been validated, further analysis was conducted on the hybrid model as a whole.

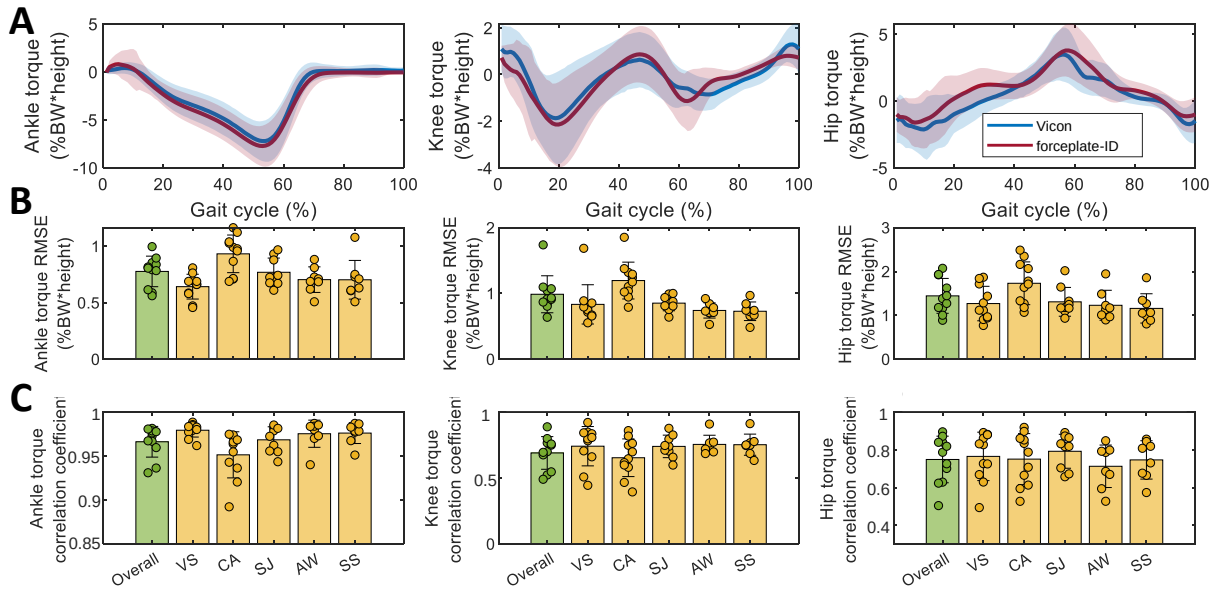

Figure 3.7: (A) Average computed torques using the dynamic model with forceplate-measured GRF and ZMP compared to a gold standard Vicon joint torque estimation approach. The overall performance as well as the performance for each walking condition, including varied stride lengths (VS), constant acceleration (CA), speed jumps (SJ), asymmetrical walking (AW), and start-stops (SS), are reported in terms of (B) RMSE, and (C) correlation coefficient. The points represent the individual subjects.

3.2.3 Torque estimation

Figure 3.8A shows the average estimated torques from the hybrid and end-to-end model compared with the Vicon-estimated torques across the test participants throughout the entire experiment.

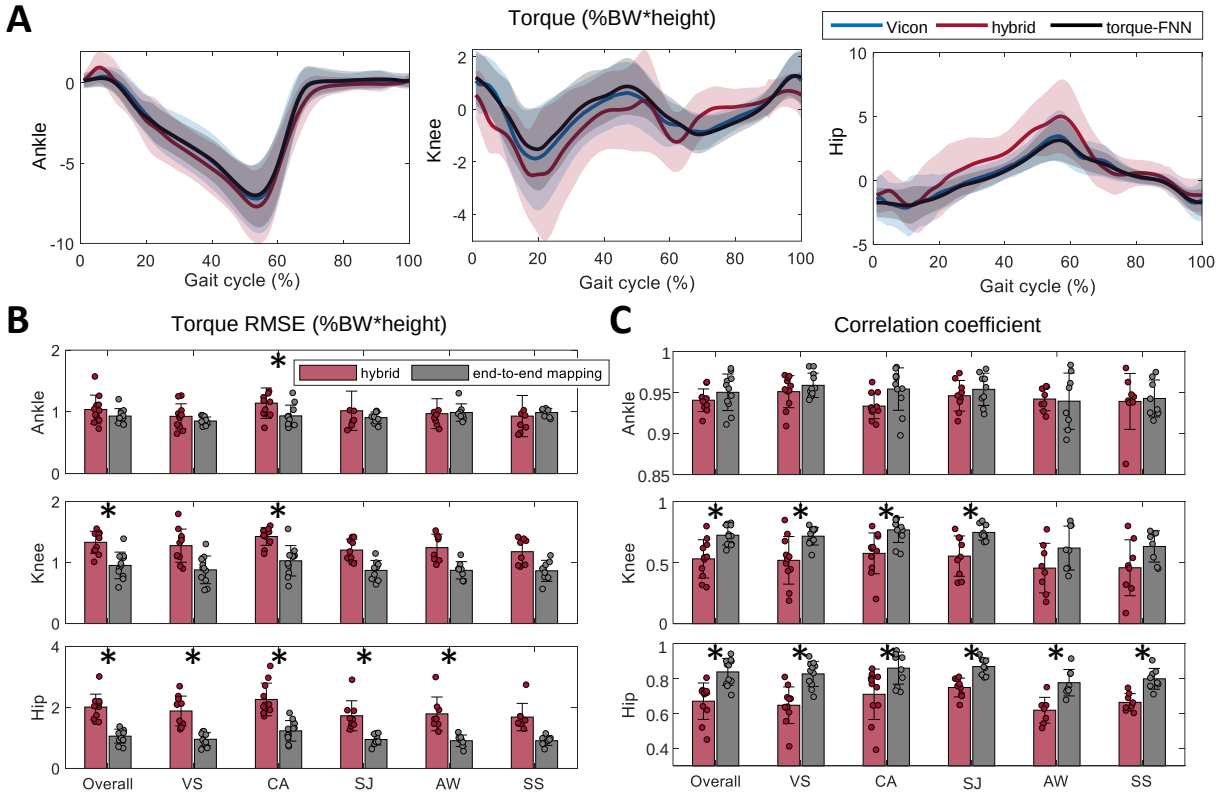

Figure 3.8: (A) Average computed torques using the hybrid model, end-to-end estimator compared to Vicon-computed joint torques. The overall performance as well as the performance for each walking condition, including varied stride lengths (VS), constant acceleration (CA), speed jumps (SJ), asymmetrical walking (AW), and start-stops (SS), are reported in terms of (B) RMSE, and (C) correlation coefficient. The points represent the individual subjects. The asterisk denotes a significant difference between the two models.

Figure 3.8B-C shows the RMSE and correlation coefficient of both models during each of the tested conditions. The end-to-end mapping has slightly better overall performance (RMSE=0.9±0.12, 1.0±0.22, and 1.1±0.23%, R=0.95±0.02, 0.72±0.08, and 0.84±0.08 for the ankle, knee and hip) than the hybrid model (RMSE=1.0±0.23, 1.3±0.18, and

2.0±0.42%, R=0.94±0.01, 0.53±0.15, and 0.67±0.10 for the ankle, knee and hip) in terms of the RMSE and correlation.

Wilcoxon signed rank tests are performed to identify any significant differences in RMSE and correlation coefficient of the two torque estimators across the whole experiment and at different walking conditions (the latter with Bonferroni correction). No significant difference is identified between the RMSE or the correlation coefficient of the hybrid model and the end-to-end torque estimator in the ankle joint for the overall experiment (p_{RMS}=0.46, p_R=0.94). When comparing the torque estimators at each specific walking condition, a significant difference is observed in RMSE only during constant acceleration condition (p_{RMS}=0.0055), while no significant difference between the correlation coefficients are obtained (p_R>0.20). At the knee joint, there are significant differences in RMSE and correlation coefficient for overall data (p_{RMS}=0.039, p_R=0.0078). There are significant correlation coefficient differences when comparing the torque estimators at variable strides (p_{RMS}=0.15, p_R=0.0078), and speed jump (p_{RMS}=0.023, p_R=0.0078). There are significant differences in both RMSE and correlation coefficient at the knee when comparing them at constant acceleration (p_{RMS}=0.0078, p_R=0.0078). The performance of the two torque estimators is not statistically different during asymmetrical walking (p_{RMS}=0.38, p_R=0.016, as compared to corrected significance level of 0.05/5) and start-stopping (p_{RMS}=0.20, p_R=0.38) conditions. There are significant differences between the performance of the two estimators at the hip during overall experiment and when comparing at different walking conditions (p_{RMS}=0.0078, p_R=0.0078), except the RMSEs are not significantly different at start-stopping (p_{RMS}=0.016, comparing to a corrected significance level of 0.05/5).

Despite the performance of end-to-end torque estimator shows statistical superiority over the hybrid torque estimator at the hip (for all conditions) and knee (for three out of five conditions), the difference in estimated normalized torque RMSE was in range of ([0.28% 1.8%]) at hip and ([-0.016% 0.89%]) at knee joint. This indicates that the performance of the two estimators are close and not meaningfully different.

The performance of the end-to-end estimator is heavily governed by the richness of the training dataset. For this reason, the model would likely require retraining on cases where the type of gait abnormality is not covered in this experiment or individuals with atypical anthropometry.

The hybrid model tends to have larger errors in the hip joint than the knee and ankle joints, particularly during the stance phase. This is due to the force-FNN estimation errors and the forward kinematic error which is more evident at the hips as the kinematic chain originates at the foot. In addition, model simplifications including decoupling the legs, are

also sources of error for the hip joint torque estimation.

The joint torque estimation errors in the hybrid model, that stem from errors in the force-FNN, occur during stance phase and are more apparent in the knee and hip joints. This is because the knee and hip joints have larger moment arms to the ZMP, which in turn causes a larger contribution to τ_{force}, in comparison to the ankle joint. As seen in Figure 3.7, the torque estimation errors are remarkably reduced when using measured rather than estimated values of GRF and ZMP.

The estimated ankle torque from the hybrid model has the best performance as it is largely only impacted by the τ_{force} while $\tau_{dynamics}$ is small, as seen in [63]. However, as the moment arm for this joint is relatively small, it is less sensitive to errors in GRF and ZMP. The remaining errors in the hybrid model can be attributed to kinematics measurement error as well as the effects of assumptions made in creating the dynamic model.

3.2.4 Exoskeleton testing

The analysis of the exoskeleton data consists of the GRF and ZMP estimation as well as the torque estimation.

GRF and ZMP estimation

Figure 3.9A shows the average estimated GRF and ZMP of one subject walking with a lower limb exoskeleton. As exoskeleton data was not included in the training set for the FNNs, a decrease in GRF and ZMP estimation performance when applied to exoskeleton data is expected compared to walking without the exoskeleton. The decrease in estimation accuracy while wearing the exoskeleton is more evident in the ZMP estimates (RMSE=30.18%, R=0.77) than the GRF estimates (RMSE=2.93 and 7.24%, R=0.89 and 0.99 for the y- and z-directions, respectively).

There is a notable increase in the standard deviation, when compared to walking without the exoskeleton, of the measured ZMP (measured by the instrumented treadmill) during the loading response and pre-swing phase of the gait cycle as a result of the fixed ankle and rigid insole of the exoskeleton. This leads to limited transverse and coronal plane movements causing less consistency between the strides. The force-FNN is, therefore, not able to capture the profile or standard deviation of the ZMP at these points. The hybrid model is, nevertheless, minimally affected as the GRFs are small during the loading and pre-swing phases.

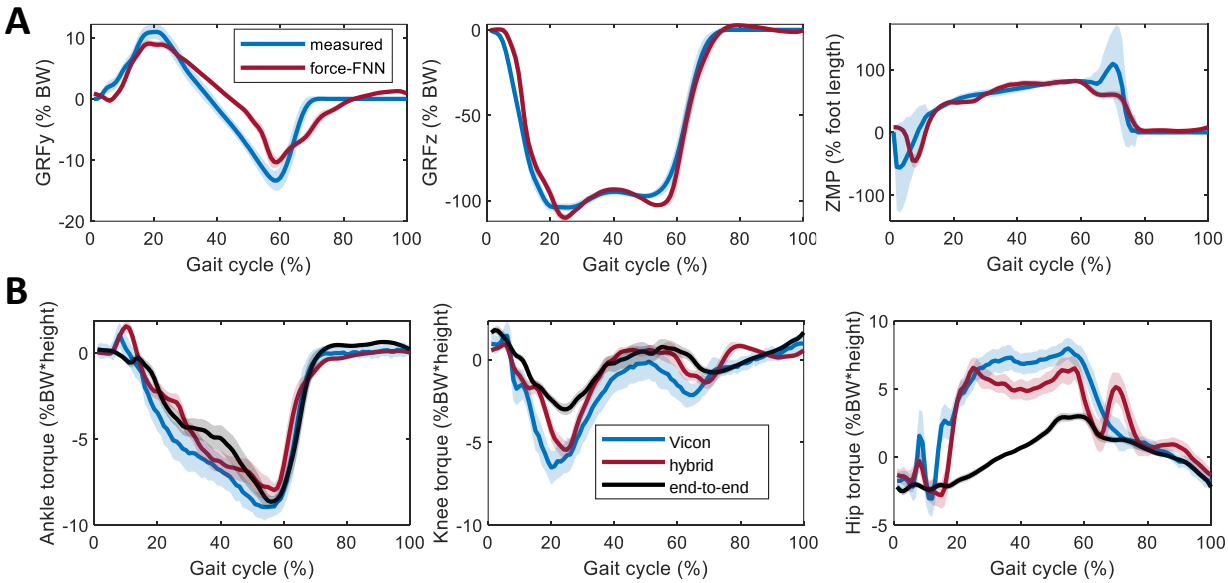

Figure 3.9: Measured and estimated (A) normalized GRF and ZMP, and (B) normalized joint torques for the exoskeleton test averaged over one gait cycle. The standard deviations are illustrated by the shaded area. RMSE is the root mean squared error, and R is the correlation coefficient.

In addition, an error increase is noticeable in the estimated ZMP within 20-50% of the gait cycle, when comparing Figure 3.9A to Figure 3.5A. It is likely that the rigid insole and ankle joint impacts the ZMP location due to restricting the ankle flexion in addition to toe extension at the metatarsophalangeal joint which typically occurs at this interval in a normal gait [67, 93]. As the force-FNN was trained with normal walking, the network is unable to capture these modifications to the ZMP location. In order to mitigate these errors, the force-FNN should be trained on gait data collected while wearing the exoskeleton which is beyond the scope of this study. In addition, implementing this force-FNN tests whether the dynamic modelling aspect of the hybrid model allows for sufficiently accurate torque estimation even with worsened ground contact force estimation.

Torque estimation

The estimated joint torques as well as the Vicon torques are shown in Figure 3.9B.

The hybrid model has significantly smaller RMSE ($p<0.05$) in all three joints when compared to the end-to-end torque mapping. In addition, the hybrid model has correlation coefficients significantly larger ($p<0.05$) than the end-to-end mapping in the knee and hip

joint while no significant difference has observed at the ankle joint (p=0.42). In contrast to the without exoskeleton walking condition, the hybrid model (RMSE=1.4±0.26 and 2.0±0.28%, R=0.87±0.03 and 0.87±0.03 for the knee and hip joints) outperforms the end-to-end torque mapping (RMSE=1.9±0.36 and 4.4±0.30%, R=0.83±0.05 and 0.59±0.04 for the knee and hip joints) for the knee and hip joints while having comparable performance at the ankle joint (RMSE=1.2±0.28, R=0.96±0.009 and RMSE=1.1±0.28, R=0.96±0.01 for the hybrid and end-to-end models respectively). This demonstrates that the due to an explicit encoding of human dynamics, the hybrid model generalizes better to conditions differing from those included in the training data set such as addition of the exoskeleton which modifies joint mobility as well as the mass distribution of the subject.

In the event that these models are applied to individuals with physical impairments, for instance due to incomplete spinal cord injuries or post-stroke hemiparesis, these individuals would also have markedly different joint mobility and may have different mass distributions than an able-bodied person. In such cases, it is likely that the proposed hybrid torque estimator also outperforms the end-to-end neural network based torque estimators.

3.3 Conclusion

A hybrid joint torque estimator is developed with a combination of a dynamical model and a data-driven GRF and ZMP estimator. An end-to-end feedforward neural network is also used as a comparative baseline. Both models are trained on the data collected from 11 participants walking on a treadmill with different speeds and gait patterns. Even though the end-to-end network outperforms the hybrid model in walking conditions close to the training data, the hybrid model has better generalization as it outperforms the end-to-end model during walking with an exoskeleton as it benefits from an expressive GRF estimator and the generalizability of a closed-form dynamical equation at the same time.

The proposed approach provides real-time estimation of torques at different joints and can be used in control of lower limb exoskeletons. As many exoskeletons have built-in joint angle measurements and IMUs, this is a reasonable next step for the developed hybrid model. The estimated joint torques in this case would be a combination of the exoskeleton applied torques and the human applied torques. Therefore, it is possible to isolate the human applied torque as the exoskeleton applied torques are known. This can be used as a measure of the level of exertion which can be useful as some exoskeleton controllers aim to reduce the require human exertion.

A further analysis of the two torque estimation approaches can further highlight their

differences. For instance a stability analysis can be beneficial for real-time implementation in an exoskeleton controller.

Chapter 4

Lower Limb Exoskeleton Direct Joint Torque Control

4.1 Control strategy

As previously mentioned, a control strategy constructed in the torque domain (for instance feedforward control) is advantageous as it does not explicitly enforce any joint trajectories [55]. In this experiment two different torque domain control strategies are investigated: direct joint torque estimation and direct torque control. These controllers are both similar to feedforward control approaches as the kinematic error is not explicitly used in the control law). However, the feedforward torque, in both controllers, is a function of estimated gait phase at each moment. Therefore, it can be seen as a state feedback control as well. This chapter will determine whether a direct joint torque estimation or pre-defined torque profile, or a combination of both, provides better control performance when used by human participants.

4.1.1 Direct joint torque estimation

The hybrid joint torque estimator presented in Chapter 3 was modified in order to be used in real-time with the exoskeleton-measured signals. This torque control based on the hybrid torque estimator, developed in Chapter 3, will be called HC in the rest of this thesis. There are a few differences in the implementation. As the exoskeleton being used does not measure kinematic information of the ankle joint, the NN used for GRF and ZMP

estimation was retrained to require only knee and hip kinematic information. The training and testing data is the same as used in Chapter 3.

In order to determine the global position and orientation of the exoskeleton, p_0 and q_0 in equation 3.1, the IMUs in the exoskeleton were used. As the exoskeleton limits all movement to the sagittal plane, all position computations consider 2D movements only. Thus allowing simple kinematic relationships to be used rather than 3D rotation matrices.

The IMUs are located in the thigh segments and in order to determine the position of the hips, knees and ankles, which are used in τ_{force} and τ_{dyn}, rigid body kinematic relationships between the segments were applied. The global Cartesian position of the thigh IMU, P_{thigh} is determined by correcting the local acceleration measurements to global coordinates by using the orientation of the local frame, θ_{thigh}, which is computed directly by the exoskeleton. The acceleration signals are then double integrated and filtered with a highpass Butterworth filter with a cutoff frequency of 0.1 Hz in order to remove low frequency drift. The position of each joint is then determined with respect to P_{thigh},

$$\begin{aligned} P_{hip,y} &= P_{thigh,y} - L_{hip} * sin(\theta_{thigh}) \\ P_{knee,y} &= P_{thigh,y} + L_{knee} * sin(\theta_{thigh}) \\ P_{ankle,y} &= P_{knee,y} - L_{shank} * sin(\theta_{thigh} - \theta_{knee}) \end{aligned} \tag{4.1}$$

where L_{hip}, L_{knee}, and L_{shank} are the distance of the IMU to the hip, the IMU to the knee, and the shank segment respectively. P_i is the Cartesian position of joint i. A similar approach to equation 4.1 can be taken for the other dimensions as well.

As the HC was developed based on experimental data without the use of an exoskeleton, this approach can be implemented with any exoskeleton. With different exoskeleton, there will be changes in the BSIP, however, this is accounted for in the dynamical equations of the controller.

4.1.2 Direct torque control

As an additional approach, a direct torque control was used. The torque profile was determined based on the computed torques from a position feedback controller implemented with one subject's own gait trajectories used as the reference trajectory. The proportional (K_p) and derivative (K_d) controller gains at the hip are 3 and 0.25 respectively. At the knee, these gains are 0.9 and 0.08. Further details of the measured torques and angles are presented in Section 4.3.1.

The final torques were evaluated at a series of speeds ranging from 0.4 to 1.2 m/s, then resampled to form a lookup table based on gait phase and speed. The torques were normalized by subject BW*height. This control approach will be referred to as DTC for the remainder of the thesis.

In order to implement this lookup table as a control algorithm, a robust gait phase and speed estimator is needed. The gait phase estimator is a neural network trained on eleven different participants and five walking conditions as done in [98]. The walking speed is estimated based on the step length divided by the step time of the previous step. The step time is determined directly from the gait phase estimator while the step length is determined from a simple forward kinematic equation, treating both legs as a serial manipulator. However, as the exoskeleton does not record kinematic information of the ankle, the step length is measured as the distance between the two ankle joints.

As the final torques are a function of gait phase and walking speed, this controller performs differently than a traditional position feedback controller as the controller is essentially blind to the joint-level kinematics.

4.1.3 Control application

Although the HC and the DTC approaches are both constructed in the torque domain, they will have different torque profiles and thus different performances. The DTC will produce essentially the same torque profile at each gait cycle regardless of the user's varying joint kinematics. Meanwhile the HC is sensitive to different joint and segment kinematics, and will produce torque accordingly.

In order to compare these two approaches individually and in combination, both control methods were scaled such that their magnitudes of torques are comparable. Four different torque controllers are being tested: DTC alone, HC alone, 75% HC with 25% DTC, and 25% HC with 75% DTC. These four controllers will be referred to as: DTC, HC, , and .

4.2 Experimental design

In this section, an in-depth description of the experimental setup and procedure are followed by the data analysis performed. The experiment consists of testing the controllers during treadmill and overground walking. In order to compare the performance of the controllers, various metrics are computed. This includes spatiotemporal (walking speed,

step time, percent stance, step length), kinematic (range of motion, angle correlation to natural walking), and EMG-based (effort level, activation time, co-contraction) metrics.

4.2.1 Experimental setup

The experimental setup consists of a split-belt instrumented treadmill (Bertec, US), a lower limb exoskeleton (Indego, Parker Hannifin, US), six IMUs (MTw Awinda, Xsens, NL), and 12 EMGs (Trigono, Delsys, US). The exoskeleton, IMUs, and EMGs have sampling rates of 200, 100, and 2000 Hz, respectively. The EMG sensors were placed on both legs on the following muscles: RF, VM, BF, TA, GM, and SO. The IMUs were placed with one on each foot and shank, one on the right thigh and one on the torso. For the thigh and shank, the IMUs were placed on the lateral side of each segment, approximately about the midpoint of the distal and proximal joints. The torso IMU was placed on the Xiphoid process and the foot IMUs were placed on the laces of the participant's shoes. Figure 4.1 shows the experimental setup. The exoskeleton has actuated hip and knee joints while having no direct effect on the ankle joints.

Figure 4.1: Placement of EMG and IMU sensors.

4.2.2 Experimental procedure

Nine healthy subjects (age 26±3.0 years, 2 female, mass: 74.6±8.8 kg, height: 1.82±0.065 m) participated in this experiment. Data collection protocols and procedures were ap-

proved by the Clinical Research Ethics Committee at the University of Waterloo (ORE#41794), and conformed with the Declaration of Helsinki.

Once all the sensors have been placed on the subjects, functional calibration and maximum isometric contractions were recorded. The functional calibration involves flexion-extension movements of the hip, knee, and ankle on each leg along the sagittal plane for five repetitions followed by the trunk also for five repetitions as done in [7, 80]. The isometric contractions were recorded while the subject contracts each of their leg muscles as hard as possible for five seconds each while standing in a neutral position. The EMG sensors were not moved between different trial as to ensure comparability in the measured muscle activity.

The experiment included both overground and treadmill walking during six different conditions. The conditions include one with passive exoskeleton, four with active exoskeleton (one for each controller), and one natural walking trial without the exoskeleton. The passive exoskeleton case is when the exoskeleton applies no torques to the joints while during the active cases, the exoskeleton applies the torques generated by the controllers to each joint.

The participants walked on the treadmill at 0.6 and 0.8m/s for 40 seconds each, with a transition acceleration of 0.04m/s^2 for each condition. The participant then walked overground for a total of 36m at a self-selected walking pace for each of the six conditions.

Each participant was asked to rank the exoskeleton trials from 1 to 5 where 1 is the best in the following categories: effort level, stability, natural walking, and overall performance. The rating was completed immediately following the treadmill and overground sessions separately. Minimal effort would occur when the user is not required to put much force into walking as the exoskeleton is compensating some or all of this force.

4.2.3 Data analysis

The data from the IMUs and EMGs are processed in order to compute various performance metrics. First the gait events are detected (as described in section 4.2.4) with the IMU signals, then joint angles are computed also from the IMU data (see section 4.2.5), and finally the EMG data is processed to quantify muscle activity (see section 4.2.6).

4.2.4 Gait event detection

The shank gyroscope measurements are used for toe off detection as done in [3, 91] where the negative peaks immediately preceding the prominent positive peaks. Heel strikes are

detected at the negative peak in vertical acceleration, in the local coordinate system, of the foot which immediately follows the prominent positive peak in the shank gyroscope data [90]. A sample of event detection is shown in Figure 4.2.

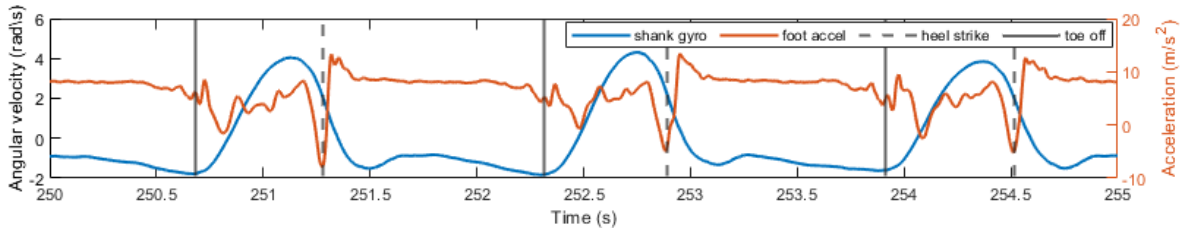

Figure 4.2: Shank gyroscope and foot vertical acceleration during treadmill walking. Event detection of heel strike and toe off are shown.

The detected heel strike and toe off are used to determine stance time, and step time. Using the detected heel strikes, all measured data is then segmented into gait cycles for further analysis.

4.2.5 Kinematic and spatiotemporal computations

The IMUs are also used to compute joint angles, similar to [73]. A PCA is applied to the gyroscope data of each IMU during the functional calibration movements. The computed principal axis is then in the direction of the axis of rotation of each joint, normal to the sagittal plane. The coefficients from the PCA are then used to transform the gyroscope data throughout the whole experiment. The following equations describe this process,

$$\omega^T\omega = \begin{bmatrix} u_1 & u_2 & u_3 \end{bmatrix} \begin{bmatrix} d_{11} & 0 & 0 \\ 0 & d_{22} & 0 \\ 0 & 0 & d_{33} \end{bmatrix} \begin{bmatrix} u_1^T \\ u_2^T \\ u_3^T \end{bmatrix} = UDU^T \tag{4.2}$$

$$\omega_{proj} = (\omega^T u_1)u_1 \tag{4.3}$$

where ω is the gyroscope data (an $N \times 3$ matrix) before transformation, U is the matrix of normalized left eigenvectors, and D is a diagonal matrix of singular values. The principal component of the gyroscope data following the transformation is ω_{proj} and u_1 is the principal axis, direction of interest, corresponding to the dominant axis of rotation.

Segment orientations are computed as the integral of the transformed gyroscope data and the initial angle is set to zero for all segments as this occurs during a neutral standing pose. By definition, the segment angles in a standing neutral pose are zero. A strapdown

integration was not implemented as the rotation essentially occurs about one axis, especially while wearing the exoskeleton as it limits all movements to the sagittal plane. Any drift in the signal is removed by subtracting a moving average of the signal with a window width of 5 seconds. This window length was selected as the window width should be at least twice the period of the signal [75]. Signals in a gait cycle can be considered periodic with respect to the step time. The selected window length respects this criterion. Window lengths of 5, 3, and 2 seconds were tested. The window size of 5 seconds had the highest correlation to gold standard measurements (R=0.95) compared to the two other windows (R<0.91) while the range of angles was changed by less than 0.5 degrees for all window lengths.

Based on the computed joint angles, the ROM of each joint is computed for each stride. ROM is computed as the difference between the maximum and minimum joint angle. In addition, the average correlation coefficient between natural walking joint kinematics and exoskeleton walking kinematics is computed for each subject separatelyThe RMSE between the experimental and natural walking joint angles were not computed as this metric is largely affected by any offsets in the data. As the approach taken for computing joint angles relies on IMU data, the computed angles have some offsets.

As walking with loads, such as a back pack or heavy exoskeleton, has been shown to have significant effects on kinematics at a joint-level [68, 86], it is expected to see significant changes between the exoskeleton conditions compared to natural walking. A controller which is able to effectively assist the user should render the kinematic measures more similar to natural walking than passive exoskeleton walking.

The step lengths are computed from the foot acceleration data with orientation correction similar to [69]. The forward acceleration with respect to the inertial/global frame is integrated twice to compute position. Drift is corrected at each step such that velocity and position are set to zero at foot flat. Foot flat is identified as the gyroscope signals go to zero at this point. From the computed step lengths, the walking speed is computed for each stride as the step length divided by step time.

4.2.6 EMG processing

The EMG data is first filtered with a bandpass filter with cutoff frequencies of 5 and 100 Hz [74]. The signal is then full-wave rectified and an envelope is computed by taking the moving average with a window of 50 ms. Each EMG signal is normalized by its respective MVC. The MVC of each muscle is computed as the maximum measured contraction during either walking or during the isometric contraction data collection.

Based on the EMG activation during each stride, a measure of effort level is computed as the integral of the squared EMG activation [83, 23]. For the overground walking trials, as the walking speed is not fixed between trials or subjects, the EMG measurements are normalized by walking speedas effort level increases with walking speed. The measured effort level e for one gait cycle is computed as

$$e = \frac{1}{v} \int_t EMG^2 \tag{4.4}$$

where v is the walking speed, EMG is the processed muscle activity during one gait cycle, and t is the step time.

Additionally, co-contraction between agonist-antagonist muscle pairs were also compared across conditions. These pairs are RF-BF, VM-BF, TA-GM, and TA-SO. The co-contraction is computed as the product of the two muscle activation signals [100]. Similar to muscle effort, the co-contraction of each stride is quantified by the integral of the aforementioned product signal across the step and is normalized by walking speed.

Finally, the percent of the gait cycle in which each muscle and co-contraction pair are active are determined. The threshold for determining activity is the average activation while the muscle is known to be inactive during non-exoskeleton walking plus two standard deviations of the signals.

4.2.7 Statistical analysis

The first and last five steps from each condition were excluded from the analysis in order to eliminate the transition effects from speeds changes and adjustments to different control algorithms. The average of each metric was computed for each controller and each subject across all gait cycles being considered. The statistical significance of each metric was tested with a one-tailed Wilcoxon signed rank test as this test will determine which controller has significantly better performance in the metric being tested. For spatiotemporal and kinematic metrics, a Bonferroni correction was applied to the significance level such that p=0.05/10 as all conditions are compared with each other. However, for the EMG metrics, a Bonferroni correction of 4 is applied as each active condition is compared only to the passive case. This is because one goal of the controllers is to reduce the required muscle activity compared to the passive case rather than compared to the other active controllers.

Although an ANOVA is generally useful in the statistical analysis of experiments with multiple conditions, such as this experiment, it was not implemented as the data is not normally distributed.

4.3 Results and discussion

A separate analysis of the applied torques, spatiotemporal parameters, kinematics, and EMG were conducted to compare each of the five exoskeleton trials. Finally, the results from the questionnaire are compared to the related analytical results.

Table 4.3 shows a summary of the results from the analysis where the controller was shown to have the best performance. A more detailed discussion of each metric follows.

4.3.1 Applied torques

Figure 4.3A shows the joint angle lookup table used for the feedback controller in the generation of DTC as described in Section 4.1.2. The average and standard deviation of the measured joint angles as well as the desired angles are plotted in Figure 4.3B for walking at 0.6m/s for 45 seconds. The average and standard deviation of the torques generated for this walking speed are shown in 4.3B. The measured and desired joint angles are plotted in 4.3B. Both the measured torques and angles have small standard deviations, which indicates that using the average torque profile is sufficient for capturing the effects of these torques. Figure 4.3D shows the complete torque lookup table of DTC, which includes walking speeds ranging from 0.2 to 1.2 m/s.

As the controllers being tested are sensitive to differences in kinematics and walking speed, the applied torques vary between subjects. The applied command torque profiles for each of the controllers for subject 2, 6, and 8 walking on the treadmill at 0.8 m/s are plotted in Figure 4.4. Each subject had similar torque profiles at 0.6m/s compared to 0.8m/s. These three subjects were randomly selected to show variation between participants.

The standard deviation of the DTC torque profile of subject 8 (Figure 4.4C) is much larger than that of subject 2 and 6. This is an indicator of inconsistencies with the inputs of velocity and gait phase into the DTC lookup table. As this was collected with constant speed treadmill walking, it is expected that the DTC torque profiles have a very small standard deviation; therefore, this indicates inconsistencies in the gait phase and velocity estimator. The subjects not shown in the graphs have similar torque profiles to those of subject 2 and 6.

A more in depth analysis of the kinematics of subject 8 indicates a much smaller ROM in the knee joint than normal walking. Thus, the walking pattern is sufficiently different than the training data of the gait phase estimator network which leads to worsened gait phase estimation for such gaits. This error is then propagated to the velocity estimation.

Metric		Performance			
		Overground	Treadmill 0.6m/s	Treadmill 0.8 m/s	Overall
Spatio-temporal	Walking speed	1D-3H	*	*	3D-1H has best performance in terms of spatiotemporal
	Percent stance	1D-3H	HC	HC	
	Step time	1D-3H	1D-3H	HC	
	Step length	3D-1H / 1D-3H	HC	DTC	
Kinematics	Hip correlation	HC	HC	DTC	No meaningful improvements in performance across metrics or conditions
	Knee correlation	3D-1H	1D-3H	3D-1H	
	Ankle correlation	1D-3H	1D-3H	1D-3H	
	Hip range of motion	HC	1D-3H	3D-1H	
	Knee range of motion	3D-1H	DTC	3D-1H	
	Ankle range of motion	1D-3H	HC	HC	
EMG	Muscle effort	1D-3H / 3D-1H	1D-3H / 3D-1H	1D-3H / 3D-1H	1D-3H has best performance in terms of effort and co-contraction
	Active time	**	**	**	
	Co-contraction	1D-3H	1D-3H	1D-3H	
	Co-contraction time	**	**	**	
Feedback	Effort	1D-3H	1D-3H	1D-3H	1D-3H rated the best
	Stability	1D-3H	1D-3H	1D-3H	
	Natural	1D-3H	1D-3H	1D-3H	
	Overall	1D-3H	1D-3H	1D-3H	

Table 4.1: Overview of analysis results where the controller having the best performance for each metric is displayed in the table. However, it should be noted that the improvements in performance reported in this table can be small. Refer to the discussion for further details.

* not applicable to treadmill walking

** no conclusive results

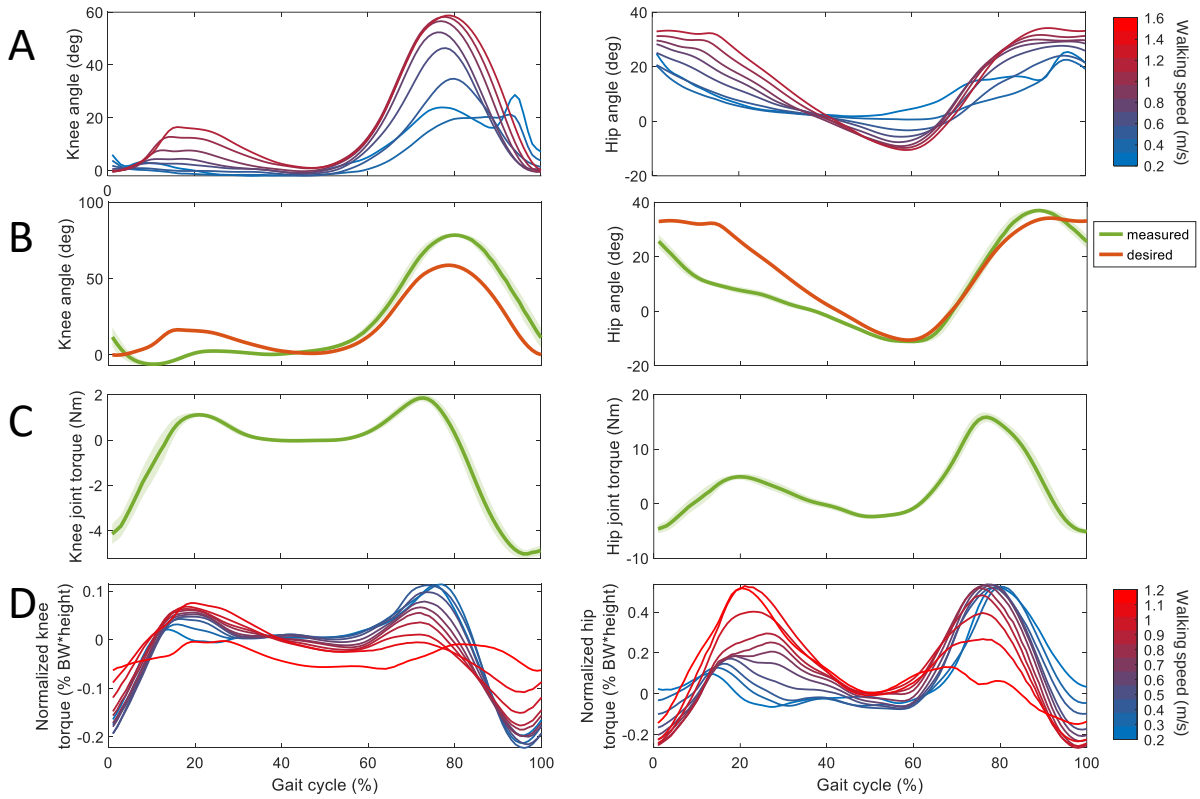

Figure 4.3: (A) The joint angle lookup table used in the generation of DTC. The average (B) angles and (C) torques generated while walking at 0.6m/s, the standard deviations are shown by the shaded areas. (D) DTC profiles for each walking speed.

As subject walks at a speed of 0.8m/s on the treadmill, the estimated velocity is 1.1m/s. However, the overall torque profile is generally similar to those of other subjects, and still has the potential to assist in gait.

The dependence on a gait phase and velocity estimator is thus a drawback from this approach. This suggests that a more robust gait phase estimator would be required for use with individuals having atypical gaits, such as individuals suffering from hemiparesis or iSCI.

The commanded torques for overground walking for the same subjects are shown in Figure 4.5. The standard deviation of each torque profile has increased as there is more kinematic variability in overground walking compared to treadmill walking. However, the kinematic profiles of each subject for treadmill and overground walking appear to have

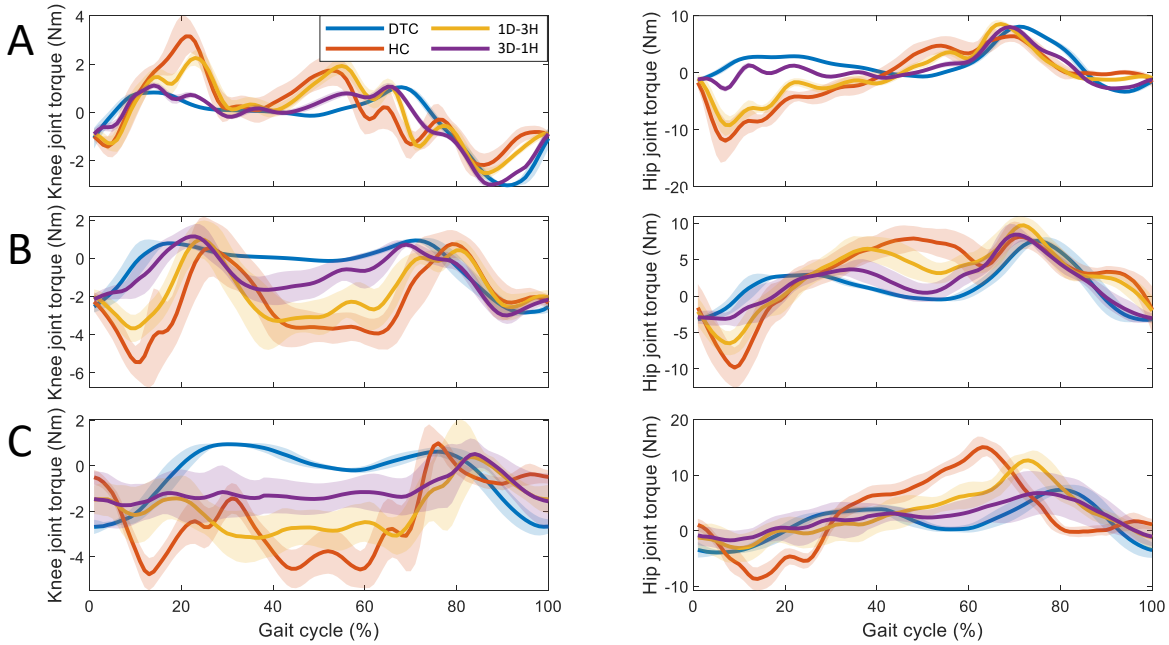

Figure 4.4: Average command torque for (A) subject 2, (B) subject 6, and (C) subject 8 for each controller while treadmill walking at 0.8m/s. The shaded area shows the standard deviation of the torques.

many similarities in terms of average profiles. In general, the torque profiles generated by the controllers at the hip had more similar shapes when comparing between participants than at the knee. Further testing is required to determine whether these differences are accurately capturing the differences in kinetics among people or a result of external factors.

4.3.2 Spatiotemporal gait analysis

The spatiotemporal gait analysis presented in this section includes an analysis of walking speed, percent stance, step time, and step length. Metrics in the lateral direction, such as step width and lateral sway, are not considered as the exoskeleton restricts movement to the sagittal plane in the knee and hip joints. As this exoskeleton does not control the ankle joint, spatiotemporal metrics which are primarily affected by the ankle angle, such as strike foot angle, and lift off foot angle, are not considered.

The spatiotemporal metrics are computed for each subject and compared to their respective metrics during natural walking. Overall, the shows the performance closest to

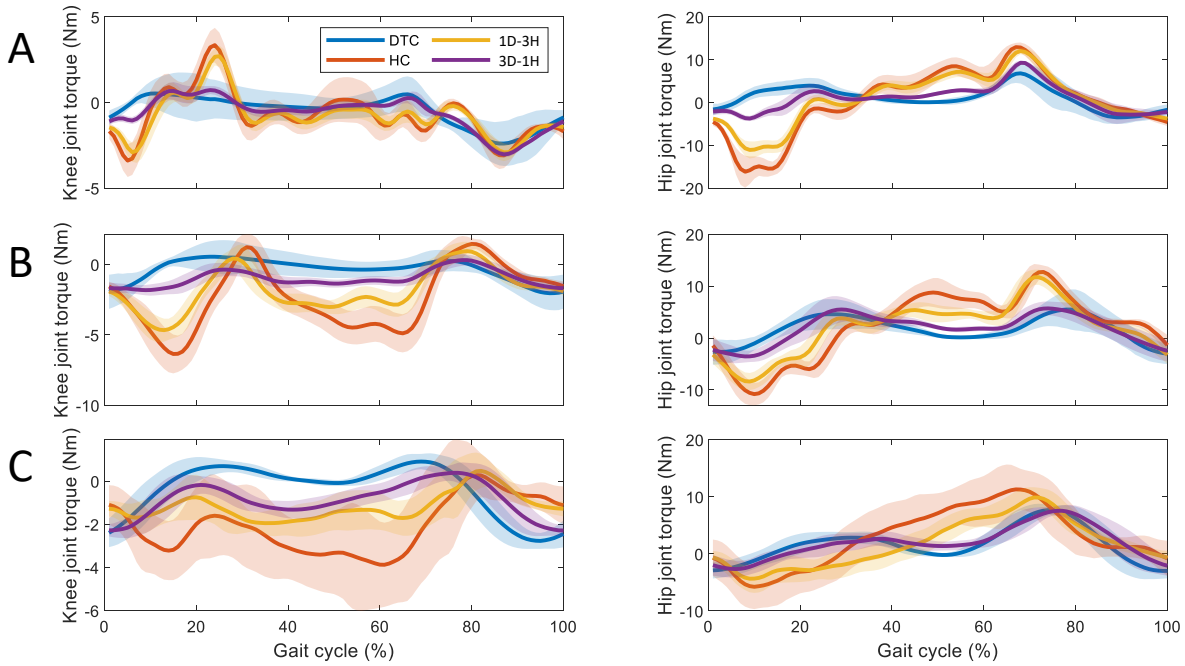

Figure 4.5: Average command torque for (A) subject 2, (B) subject 6, and (C) subject 8 for each controller for overground walking. The shaded area shows the standard deviation of the torques.

natural in terms of spatiotemporal metrics. Figure 4.6 shows the average overground walking speed for each trial. Figure 4.7 shows the percent stance time, step time, and step length for each exoskeleton trial normalized by natural walking metric of each respective subject. The standard deviation of the spatiotemporal metrics are shown in Figure 4.8.

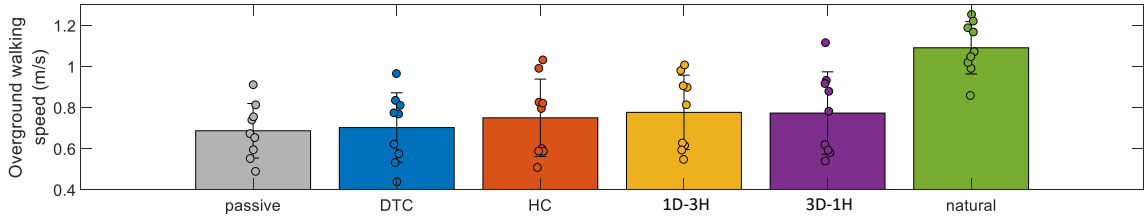

Figure 4.6: Overground walking speed of each exoskeleton condition and natural walking speed. The points show each subject separately and the error bars show the standard deviation.

The average overground walking speed at is the fastest out of all overground exoskeleton

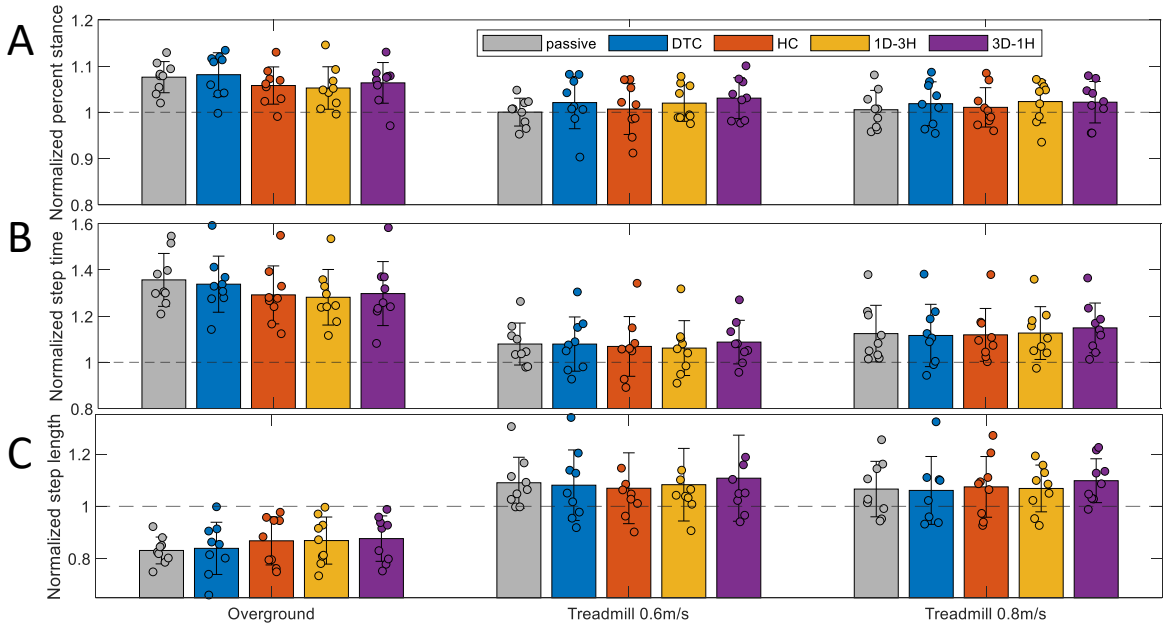

Figure 4.7: Spatiotemporal analysis of overground and treadmill walking at 0.6 and 0.8 m/s. Average measures of (A) percent stance, (B) step time, and (C) step length are reported normalized by natural walking at each condition. The points show each subject separately and the error bars show the standard deviation.

trials. The natural overground walking speed of all participants was measured as faster than all exoskeleton walking trials, therefore also has the most natural walking speed. The only has a slightly slower speed. There is a significant difference between the walking speed with and compared to walking with DTC ($p<0.0039$) while not with the other conditions ($p>0.0098$). The average standard deviation of walking speed for overground and treadmill walking are 0.059 and 0.035, respectively. The standard deviation of walking speed are shown in Figure 4.8D. During overground walking, the average walking speed variation most similar to natural is with , with a variation of 0.062. During treadmill walking, the speed variations are much larger than natural. DTC and have the most similar variations for 0.6 and 0.8m/s respectively. The increase in walking speed can be considered a measure of the assistance level of the controller in combination, while more natural speed variation can be an indicator of stability and comfort of the participants with the controller. These results suggest the offers better assistance level and stability for overground walking.

Overall during overground walking, the has the percent stance most similar to natural

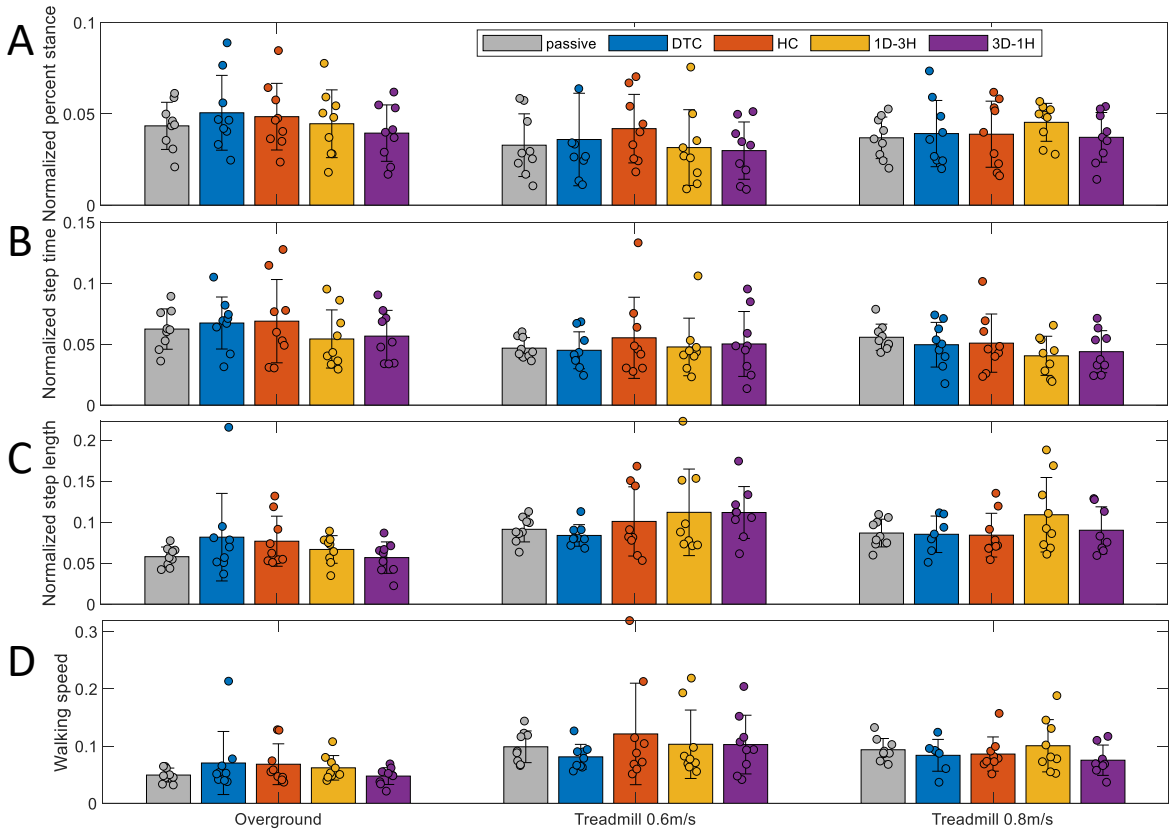

Figure 4.8: Spatiotemporal analysis of overground and treadmill walking at 0.6 and 0.8 m/s. Standard deviation of normalized measures of (A) percent stance, (B) step time, (C) step length, and (D) walking speed are reported at each condition. The points show each subject separately and the error bars show the standard deviation.

walking. The performance of is closely followed by the HC. There are no significant differences between the different controllers ($p>0.0195$). However, during treadmill walking, passive exoskeleton walking has the closest percent stance time to the natural gait with the being the second closest. At 0.6m/s the passive exoskeleton walking has a percent stance significantly ($p<0.002$) closer to natural walking compared to DTC. There are no significant differences for the other conditions and speeds ($p>0.0098$). Overall, the and are the control approaches which achieve the most natural percent stance for overground and treadmill walking, respectively. Studies have shown that increases in percent stance time are an indicator of decreased stability [42, 43]. On average, DTC has the highest percent stance during overground walking. Based on participant feedback for overground

walking, DTC was rated on average, the least stable of the controllers (see section 4.3.6). During treadmill walking, the percent stance of the controllers are very similar; however, the participant feedback also indicates that DTC is on average the least stable.

The standard deviation of percent stance during natural walking is 0.016 and 0.025 for overground and treadmill walking respectively. The standard deviation of percent stance is most similar to natural walking for all walking conditions with . However the standard deviation of the other controllers is very similar.

The has the closest average step time to natural walking for both overground and treadmill walking at 0.8 m/s. During treadmill walking at 0.6m/s however, DTC has the most natural step time on average. There are no significant differences between the conditions for overground ($p>0.0059$) or treadmill walking ($p>0.0645$). The standard deviation of step time for overground and treadmill walking are 0.039 and 0.018 respectively. During all walking conditions, has a variation most similar to natural walking. In general has the most natural step time and variation during all walking conditions.

During overground walking, the average step length is most similar to natural walking with and closely followed by and HC. Both the and are significantly closer to natural gait than DTC ($p<0.0039$). Treadmill walking at 0.6 and 0.8m/s results in a more natural step length at HC and DTC, respectively. There are no significant differences between these conditions ($p>0.0645$). The standard deviation of step length for overground and treadmill walking are 0.065 and 0.023 respectively. During overground walking, has an average standard deviation of 0.66, which is most similar to natural walking of all the controllers. During treadmill walking, the step length standard deviation is much larger than natural where DTC has a slightly more natural variation. Overground walking has the most natural step lengths with while treadmill walking with DTC.

These spatiotemporal metrics demonstrate the effectiveness of the controllers to produce some aspects of a natural gait in terms of both mean and standard deviation of these metrics. A more in depth analysis of the joint-level effects of each controller will illuminate further whether the resulting gait is similar to natural walking.

4.3.3 Joint kinematics

Figure 4.9 and 4.10 show the average and standard deviation correlation of each joint to the recorded natural walking (of that subject) during all of the exoskeleton test conditions and controllers. During natural overground walking, the correlation of each stride to average profile for each joint is 0.98 ± 0.01. During natural treadmill walking, the correlation of the hip and knee to average normal walking joint profiles are 0.98 ± 0.01 while the ankle

angles exhibited a correlation of 0.90±0.04. As the average correlations are high and the standard deviations are small, especially for the knee and hip, comparing joint angles in the presence of different controllers to the average joint angles during natural walking is meaningful.

The average correlation coefficients at the hip joint are high for all conditions and controllers (R≥ 0.8), however, this is lower than during natural walking. During overground and treadmill walking at 0.6m/s, HC produces the highest correlation (R= 0.93±0.04 and 0.89±0.06 respectively) to natural walking at the hip. Meanwhile DTC has the highest correlation during 0.8m/s treadmill walking (R= 0.90±0.06). During treadmill walking at 0.6m/s, there is a significant difference between the passive and DTC performance (p=0.002, where the significance level is 0.05/10 as a result of the Bonferroni correction); however, there are no other significant differences between conditions (p>0.0098).

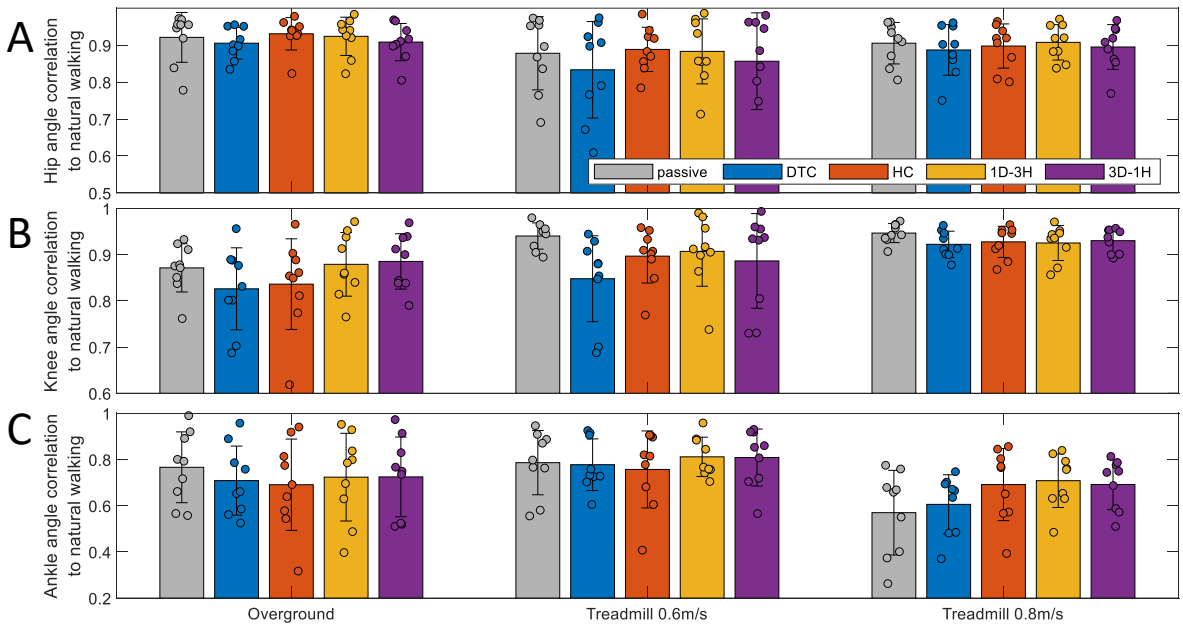

Figure 4.9: Correlation to natural walking joint trajectories measured during overground and treadmill walking for the (A) hip, (B) knee, and (C) ankle.

The average correlations at the knee joint are slightly lower, ranging between 0.8 and 0.95. Treadmill walking produces the highest correlation to natural walking at the knee joint during the passive conditions. The second highest correlations for treadmill walking at 0.6 and 0.8m/s are during and , respectively. Meanwhile during overground walking, has the highest knee correlation. However none of the conditions have statistically significant

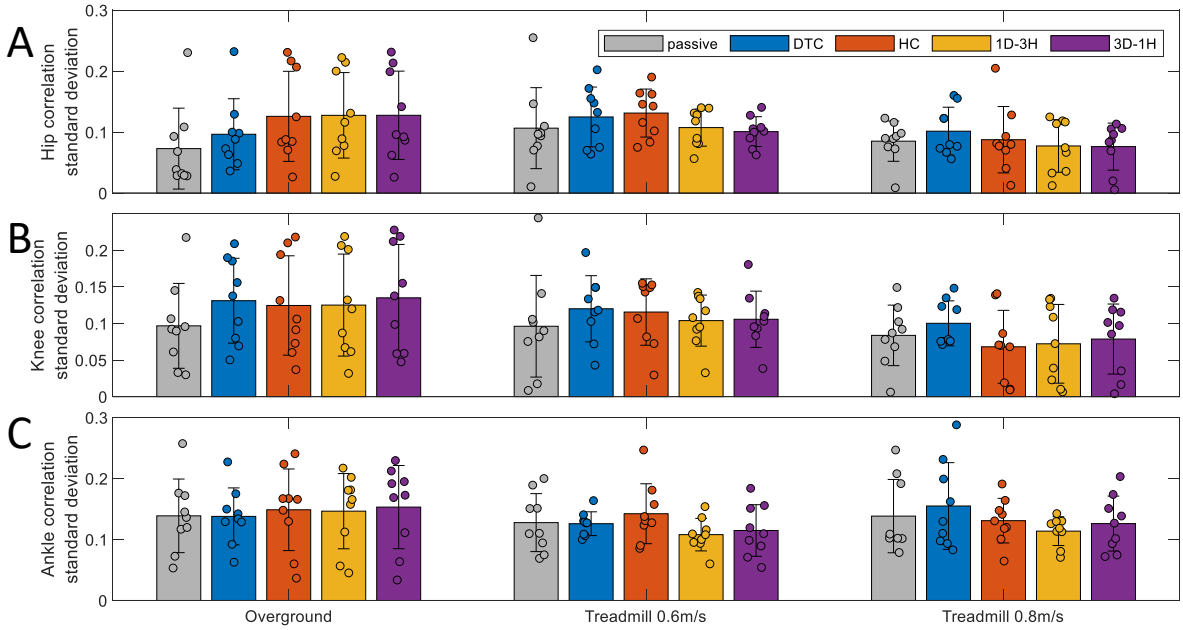

Figure 4.10: Correlation standard deviation to average natural walking joint trajectories measured during overground and treadmill walking for the (A) hip, (B) knee, and (C) ankle.

improvements ($p>0.0059$).

The ankle joint has the lowest correlations which range between 0.5 and 0.8. The highest correlation at the ankle joint occurs during and passive walking for treadmill and overground walking, respectively. None of the improvements in correlation are statistically significant ($p>0.0273$).

The average standard deviation of correlation during exoskeleton walking is larger than that of natural walking and is close to 0.1 for all controllers and joints. There are no significant differences between the standard deviations at any joints between conditions or controllers ($p>0.0098$). The average difference between the standard deviation of correlation between conditions is small. This indicates that the controllers are equally able to generate consistent walking patterns in terms of joint profiles.

Figure 4.11 shows the average ROM of each joint during the exoskeleton walking conditions normalized by the ROM from natural walking. Similar to studies analyzing the effects of load on gait kinematics [68, 86], in general walking with the exoskeleton tends to increase hip and ankle ROM, while decreasing the knee ROM compared to no-load walking.

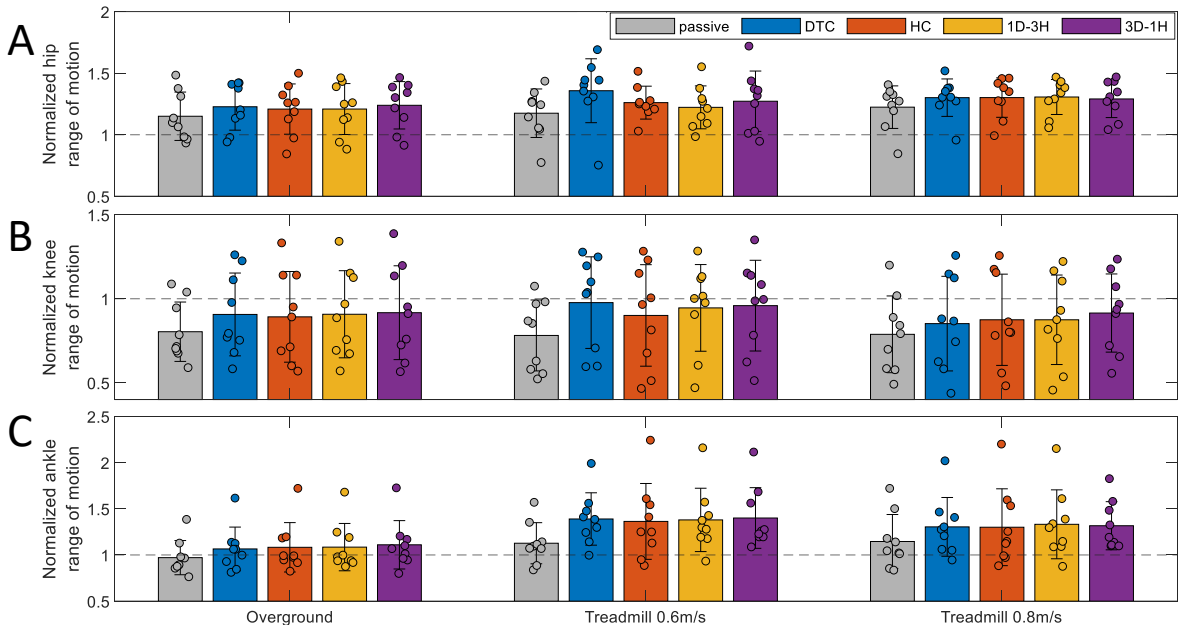

Figure 4.11: Range of motion during overground and treadmill walking for the (A) hip, (B) knee, and (C) ankle. The ranges are reported in terms of percent change from natural walking range for each participant.

The ROM of the hip joint is, on average, 20% larger than that of natural walking. This corresponds to an increase of approximately 8 degrees. During overground and treadmill walking, passive exoskeleton walking has the most natural hip ROM. Out of the active control cases, HC, , and have the most natural ranges for overground, treadmill at 0.6m/s, and treadmill at 0.8m/s respectively. However, none of these conditions are significantly better than the other one ($p>0.082$).

On average, the knee ROM decreases by 15% compared to natural walking, which corresponds to close to 9 degrees. At the knee joint during overground walking and treadmill walking at 0.8m/s, the most natural ROM occurs during , meanwhile the most natural range occurs during DTC for treadmill walking at 0.6m/s. There are no significant differences between any of these conditions or controllers ($p>0.0098$).

The ankle joint shows little change in ROM during overground walking and an average increase during treadmill walking of close to 30%. This increase corresponds to approximately 7 degrees. The has, on average, the most natural ankle ROM during overground walking, and the second most natural range during treadmill walking. The most natural during treadmill walking is the passive exoskeleton condition. During treadmill walking

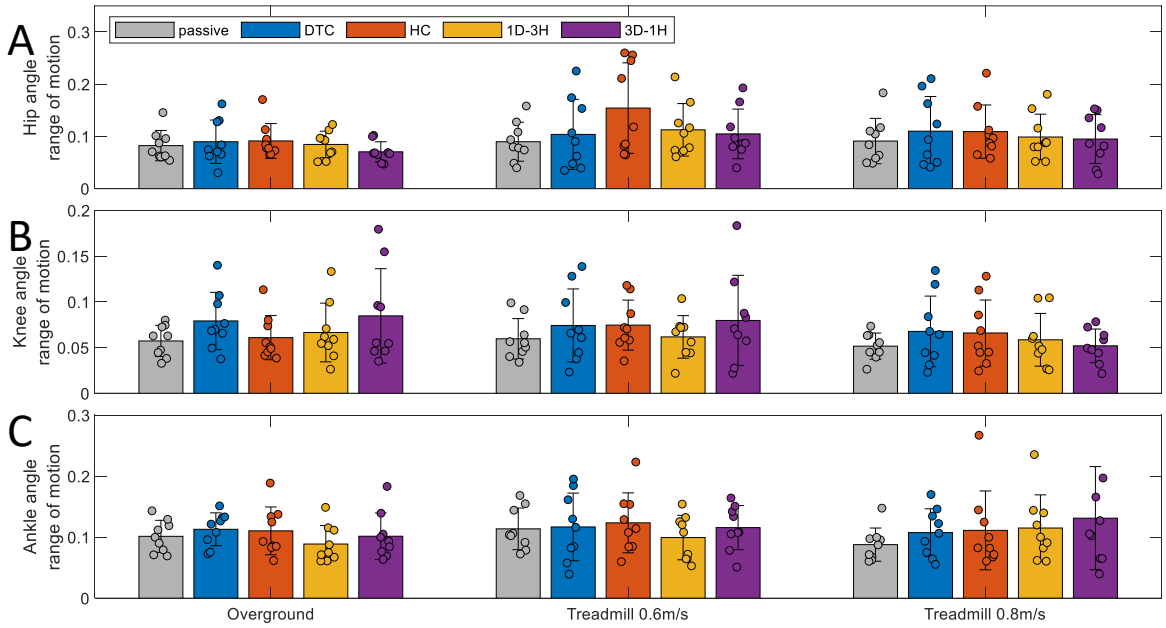

Figure 4.12: Standard deviation of range of motion during overground and treadmill walking for the (A) hip, (B) knee, and (C) ankle. The standard deviations are reported in terms of percent change from natural walking range for each participant.

at 0.6m/s, the passive condition is significantly ($p<0.0039$) more natural than the and . There are no significant differences between the other controllers for treadmill ($p>0.0098$) or overground ($p>0.248$) walking.

This analysis demonstrates that the controller which produces the most natural joint-level kinematics depends on the joint and walking condition. Overall at the hip joint, HC and show the best performance. Meanwhile, at the knee joint, and have the best performance. At the ankle joint, each controller appears to have a similar performance. As is preferable at both the knee and hip joints, it is sensible to conclude that this controller, in agreement with the spatiotemporal analysis, produces the most natural gait.

As the controllers being tested do not directly control joint angles, any observed differences in joint trajectories provide insight into how the exoskeleton is assisting or restricting the movements. An additional measure of whether the controllers are able to assist the movements can be seen in EMG measures.

4.3.4 Muscle activation

In this section, the change in muscular effort (equation 4.4) as a result of using different controllers overall and for each muscle, followed by a measure of time of activation is presented. The overall muscular effort is computed as the sum of each individual muscular effort and is shown in Figure 4.13 as being normalized by effort of walking with the passive exoskeleton. On average, the overall muscle effort with HC, , and decreases when compared to passive exoskeleton walking for both treadmill and overground walking. With DTC, there is negligible changes in overall effort compared to the passive case for both walking conditions. The contributions of each muscle are analyzed individually.

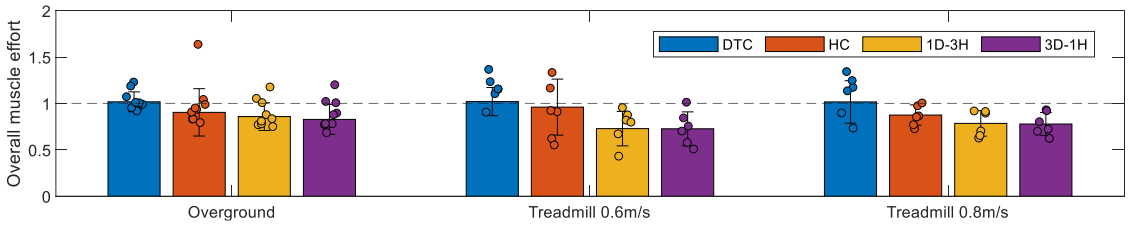

Figure 4.13: Overall muscular effort, computed as the sum of all individual muscle efforts, during the whole gait cycle normalized by passive exoskeleton walking.

The measure of effort, defined as the integral of squared EMG across the gait cycle is computed for each muscle and normalized by the effort during passive walking (Figure 4.14).

In the RF muscle, the effort increases with DTC compared to passive exoskeleton walking during overground and treadmill walking by approximately 10 and 55% respectively. Both and have a decrease in muscle effort ranging from 18 to 57% during all conditions; however these decreases are not statistically significant ($p>0.016$). The and show the best ability to reduce the effort in the RF muscle for both treadmill and overground walking. The RF functions as a hip flexor as well as knee extensor; thus, the decrease in effort indicates that these controllers are able to assist with movement at these joints.

The VM muscle, during overground walking, shows no change in muscle effort with DTC while decreases with all other controllers. The decrease in activation with is statistically significant ($p=0.0039$) when compared to passive exoskeleton walking. During treadmill walking, there is an increase in effort with DTC, HC, and and a small decrease with . When comparing the four controllers, and require the least effort from the VM for overground and treadmill walking, respectively. The VM is a knee extensor muscle, indicating that these controllers are best able to assist with this movement.

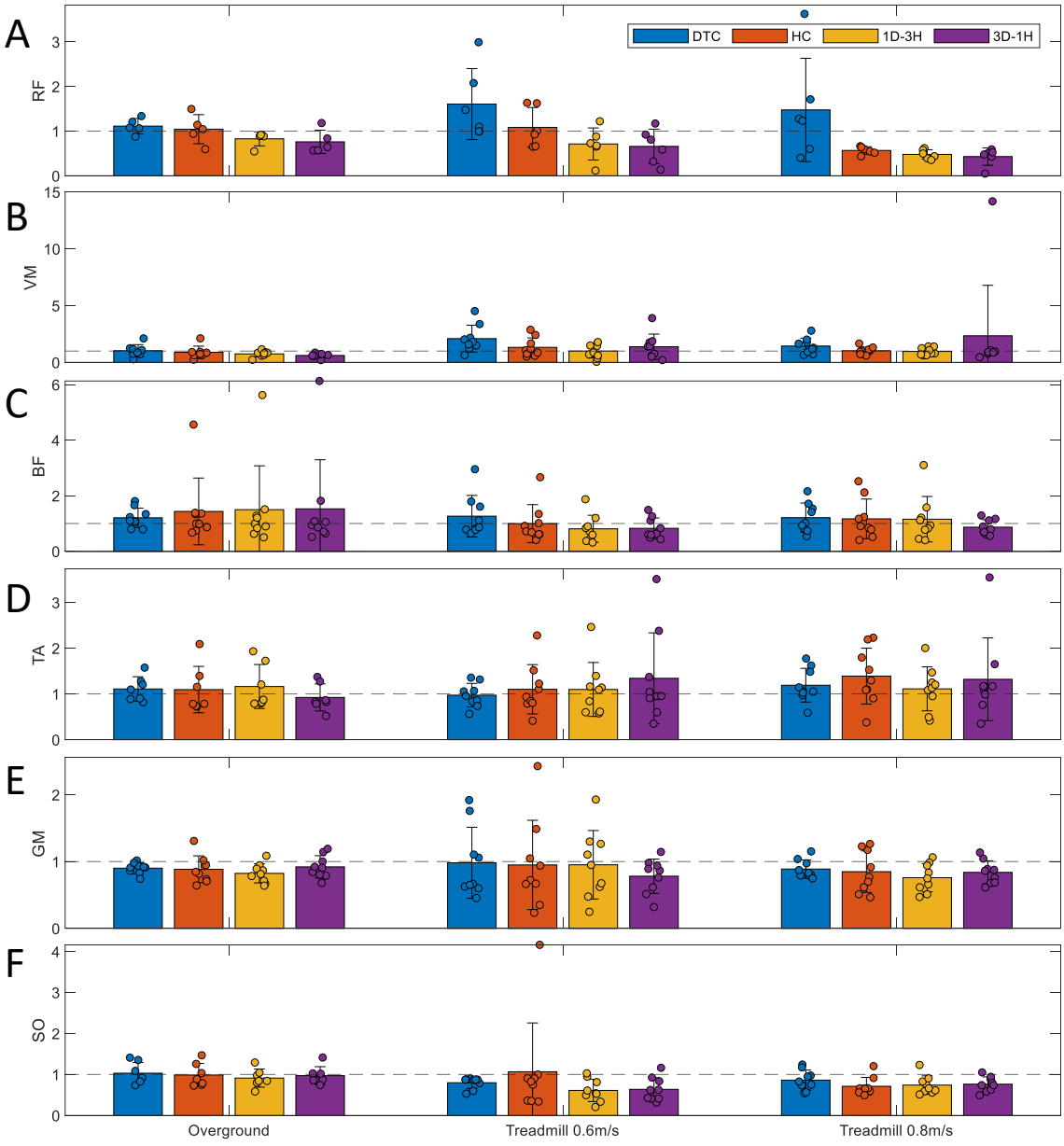

Figure 4.14: Muscular effort during the whole gait cycle normalized by passive exoskeleton walking.

The BF shows an increase in effort for all controllers during overground walking. However, there appears to be an outlier with HC , , and which is artificially increasing

the average required effort. This participant has an effort with these controllers of up to 600% larger than that of passive exoskeleton walking. Without this outlier, these three controllers demonstrate an average decrease of 5%. During treadmill walking, there is an average decrease during for both speeds and a decrease with and HC at 0.6m/s. However, these changes are not statistically significant (p>0.049). The overall increase or no change in BF effort compared to passive exoskeleton walking is due to co-contraction of this muscle with the knee extensor muscles (BF and VM) as it has an important function for stabilizing the pelvis during stance.

In the TA muscle, there are increases in effort ranging from 10 to 30% during all conditions with the exception of during overground and DTC during 0.6m/s treadmill walking. The decreases in these two cases are less than 8%. The TA muscle is a ankle dorsiflexor. During walking, the TA's primary role is toe flexion during late swing and stabilizing ankle (co-contracting with plantar flexors [61]) during stance. As the exoskeleton does not affect the ankle joint during swing phase, the increase in activation during treadmill walking can be attributed to needing more stabilization in order to coordinate their walking with the exoskeleton controls.

The GM shows an average decrease in effort for all conditions ranging from 2 to 25%. The effort inthis muscle is significantly less than passive exoskeleton for the overground walking with (p=0.0098) and treadmill walking at 0.8m/s with and (p<0.0098). This muscle indicates the best performance with the and . The GM is primarily an ankle plantarflexor and a knee flexor. This is an indicator that the controllers are able to assist during knee flexion. In addition, as the controller is able to assist with hip and knee movements, the ankle is not required to exert as much power to attain the same walking speeds.

At the SO muscle, all conditions decrease with the exception of HC during treadmill walking at 0.6m/s. During this condition, there is one outlier which increases the average. Without this outlier the average effort would be similar to that of DTC . The decreases in and 72 DTC are statistically significant during treadmill walking at both speeds (p<0.0058) as well as HC at 0.8m/s (p=0.0058) and DTC at 0.6m/s (p=0.0020). The SO is a uniarticular muscle and its muscle's primary function is ankle plantar flexion. Although the exoskeleton does not directly control the ankle joint, decreases in SO effort are able to demonstrate improved stability and improved assistance at other joints. Similar with the GM, as the exoskeleton assists more at the knee and hip, the participants do not have to compensate with effort at the ankle during push off.

Although many of the average muscle effort decreases, compared to passive exoskeleton walking, that are shown in Figure 4.14 are not statistically significant, on average the

and are better able to decrease the required muscle effort for walking compared to the passive exoskeleton condition. For overground walking, this decrease in muscle effort is more notable as the average walking speed at these conditions is significantly faster which by nature tends to increase required muscle effort. Therefore this demonstrates that these exoskeleton controllers would be able to decrease overground walking effort even more if the speed remained constant for all trials.

Figure 4.15 show the average activation time of each muscle during each of the exoskeleton controllers and walking conditions. The decrease in activation time of the GM during treadmill walking at 0.6m/s with HC compared to passive walking are significant ($p<0.0098$). This decrease corresponds to nearly 25% of the passive exoskeleton activation time. In the RF muscle, there are large increases in activation time by up to 10% of activation time during passive exoskeleton walking however, the overall effort decreases according to Figure 4.14, which indicates that the amount of contraction is much less during the active cases compared to passive walking. The changes in activation time are very small in the remaining muscles.

4.3.5 Muscle co-contraction

The average co-contraction of each muscle pair is shown in Figure 4.16 where the activity of each muscle is normalized first by its MVC before computing co-contraction.

The muscle pairs in the thigh segment are the RF-BF and VM-BF . The RF-BF pair shows a decrease in co-contraction during all conditions with as well as with HC and during treadmill walking. The decreases during overground and treadmill walking are in the range of 25% to 40% and 5% to 20% respectively. However the differences between the effort with these controllers and passive exoskeleton walking are not statistically significant ($p>0.015$). The VM-BF muscle pair shows decrease in co-contraction with all controllers during overground walking (by 9% to 45%) and increases with nearly all controllers on the treadmill (by 80% to 800%). The co-contraction decrease compared to passive exoskeleton walking for and are statistically significant ($p<0.0039$). During treadmill walking at 0.8m/s, there is a large increase in co-contraction with HC. This behaviour is exhibited with only six of the participants while the remaining participants have a negligible increase. The large standard deviation of this the co-contraction could be an indicator of measurement inaccuracies. Further data collection should be done to further understand the cause of the extreme variations between participants.

The RF-BF pair is responsible for hip and knee stabilization by modulating joint mechanical impedance [49] while the VM-BF pair is only involved in knee stiffness modulation

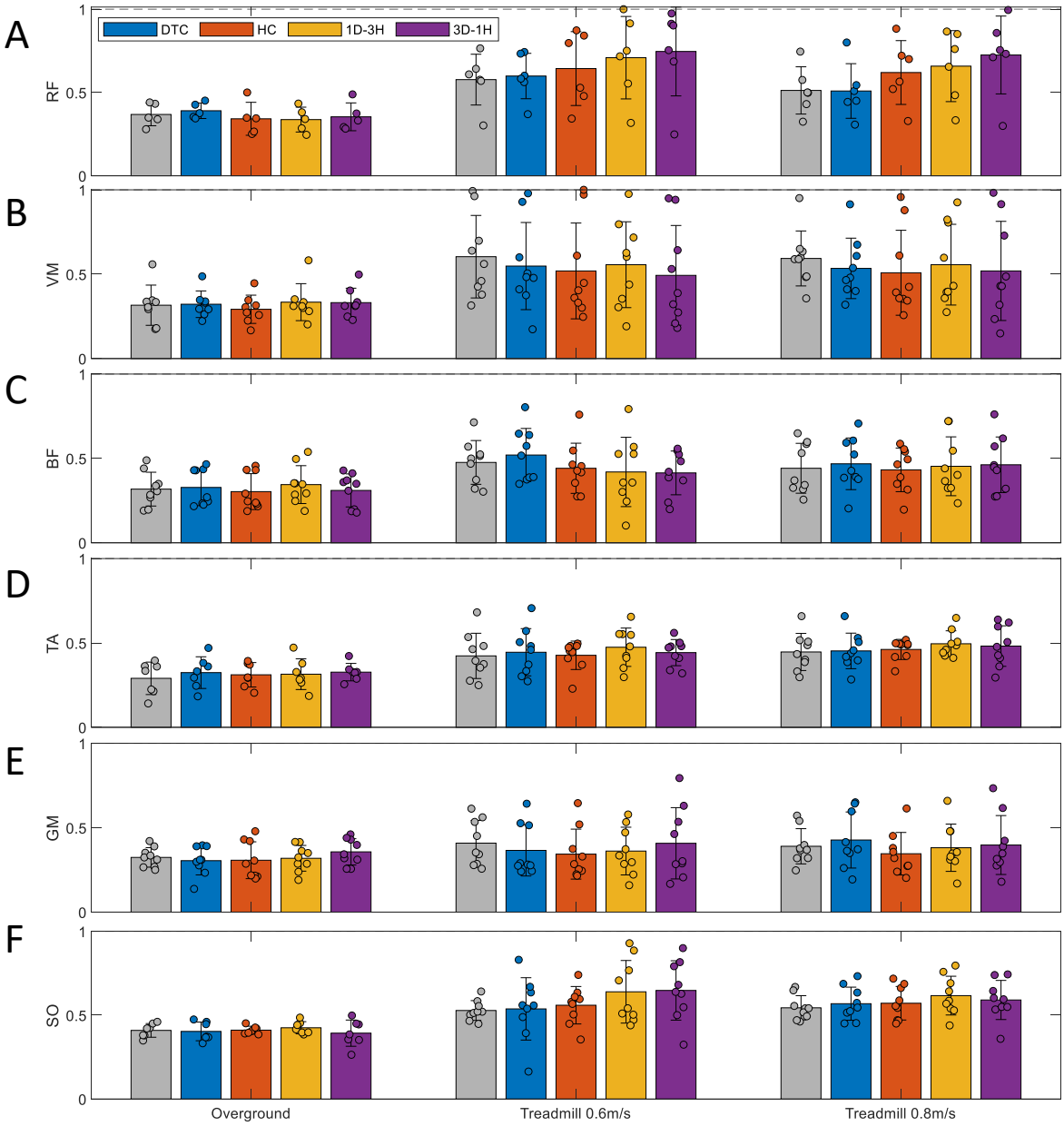

Figure 4.15: Percent of gait cycle with each muscle active.

and stabilization [85]. As there are decreases in both muscle pairs during overground walking with HC, , and , this indicates that the controller does not induce instability at these

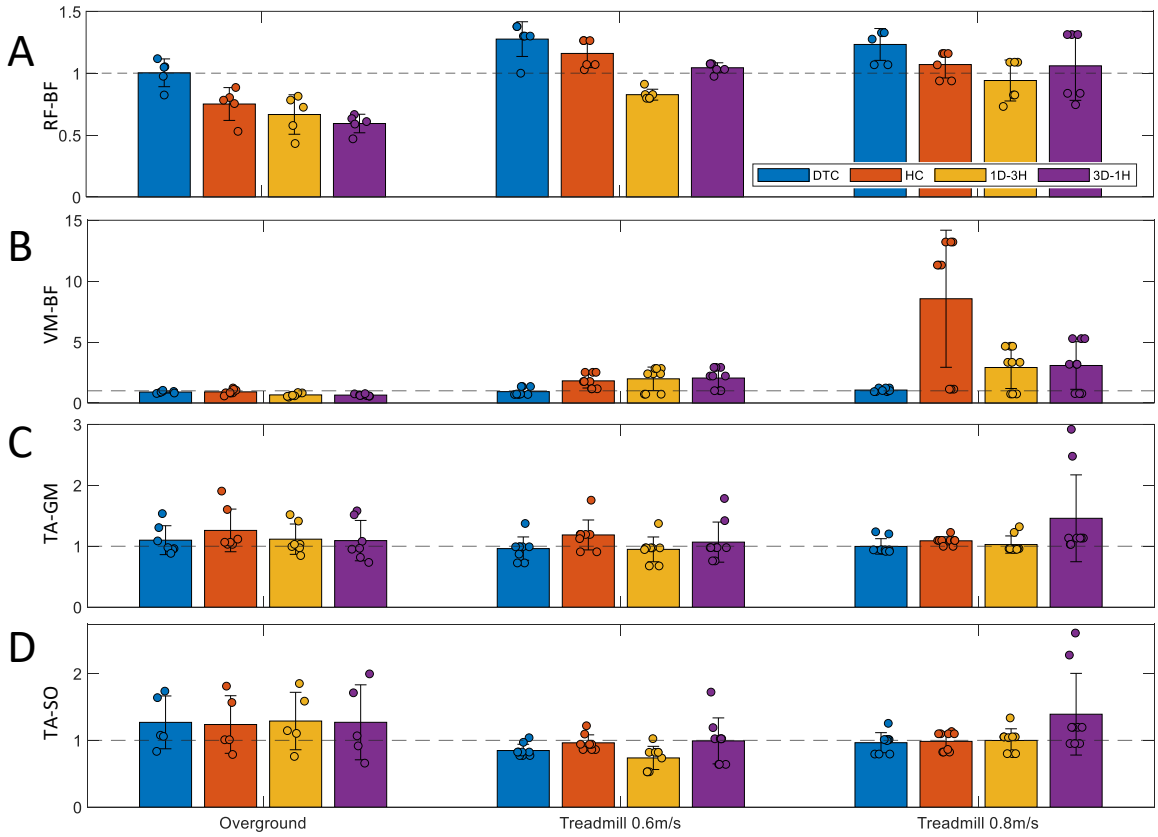

Figure 4.16: Average integrated co-contraction for each active controller normalized by passive exoskeleton walking.

joints. The increase in stability could be due to the timing of applied torques and intended movements being synchronized. As the is able to decrease co-activation in both pairs during treadmill walking and in RF-BF during treadmill walking, this controller is best able to provide stability to the participant.

The TA-GM and TA-SO are the muscle pairs in the shank segment that modulate the ankle mechanical stiffness. There is a slight decrease in TA-GM co-contraction during treadmill walking at 0.6m/s with DTC and HC ($p>0.025$) while the rest of the controllers and walking conditions show an increase in co-contraction. With the TA-SO muscle pair, there is a decrease in co-contraction with all controllers during treadmill walking at 0.6m/s. The decreases with DTC and are statistically significant ($p<0.0059$).

The TA-GM muscle pair is involved in knee and ankle stiffness modulation and in

turn stabilization. The TA-SO pair is only responsible for ankle stiffness modulation and stabilization. The increase in co-contraction of both pairs during overground walking is due to the increased walking speed compared to passive exoskeleton walking [84]. During treadmill walking where the speed is constant, the decreases in co-contraction indicates an increase in stability at the ankle joint.

On average, the co-contraction is lowest with the controller which indicates that less joint stiffness modulation and stabilization from the participants is required. This is in agreement with the increased stability detected in these controllers with a decreased percent stance.

Figure 4.17 shows the average co-contraction activation time normalized by the passive exoskeleton condition.

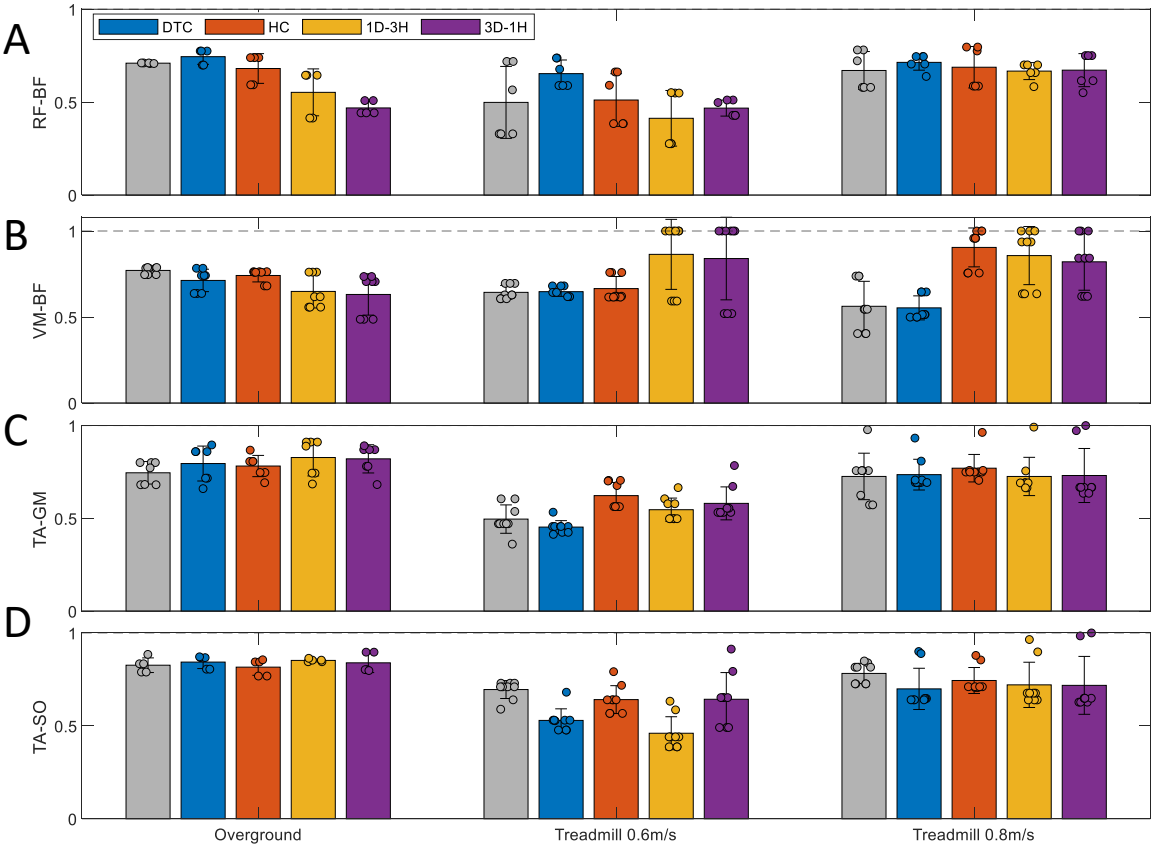

Figure 4.17: Average percent co-contraction time.

Compared to active exoskeleton walking, there is a decrease in RF-BF co-activation

time during overground and treadmill walking with and ($p>0.015$). The co-contraction time in VM-BF decreases with all controllers during overground walking when compared to passive exoskeleton. This decrease is significant ($p<0.0039$) with all controllers except for HC ($p=0.043$). As the integrated co-contraction also decreases (Figure 4.16), this further demonstrates that these controllers provide a sense of stability at the knee joint. These two muscle pairs show no change or an increase in active time for the treadmill conditions.

In the TA-GM and TA-SO muscle pairs for overground walking, the co-contraction time increases slightly (by 1% to 14%) with the active controllers. During treadmill walking, the TA-GM co-contraction time tends to increase (by 1% to 25%) with all controllers with the exception of DTC at 0.6m/s (decrease of 10%). With the TA-SO pair, activation time decreases for all active cases. The decrease is statistically significant for DTC ($p=0.0039$) and ($p=0.0039$) at 0.6m/s and DTC at 0.8m/s ($p=0.0078$). Similar to the increase in integrated co-contraction of these muscle pairs for overground walking, the increase in co-contraction time can be attributed to increased walking speed. Meanwhile during treadmill walking, the co-contraction time decreases which demonstrates the improved stability at the ankle joint with these controllers at constant speeds.

4.3.6 Participant feedback

Figure 4.18 shows the average ranking of each exoskeleton condition where 1 is the best and 5 is the worst in each category of effort, natural feel, stability, and overall performance.

On average, the effort level is reported highest during passive exoskeleton walking Each of the active controllers have a similar rating on effort level. The reduction in effort level of the active controls compared to passive walking are seen in the RF, GM, and SO, for all walking conditions (Figure 4.14. However, there are activation increases in the remaining muscles. Perceived effort is contributed to by many different muscles, including those not being measured in this study. There is a relationship between perceived effort and measured muscle activity, however, it is beyond the scope of this study as there are many muscles not being measured.

The DTC and HC are rated on average the least natural. This is in agreement with the kinematic and spatiotemporal analysis in Sections 4.3.3 and 4.3.2 respectively. During overground walking, and passive walking are rated the best, on average. Correspondingly, has the most natural step time, percent stance, and step length in terms of both magnitude and variation. Passive walking, tends to have less natural spatiotemporal measures, however, the joint-level correlation it has the highest correlation and range of motion to

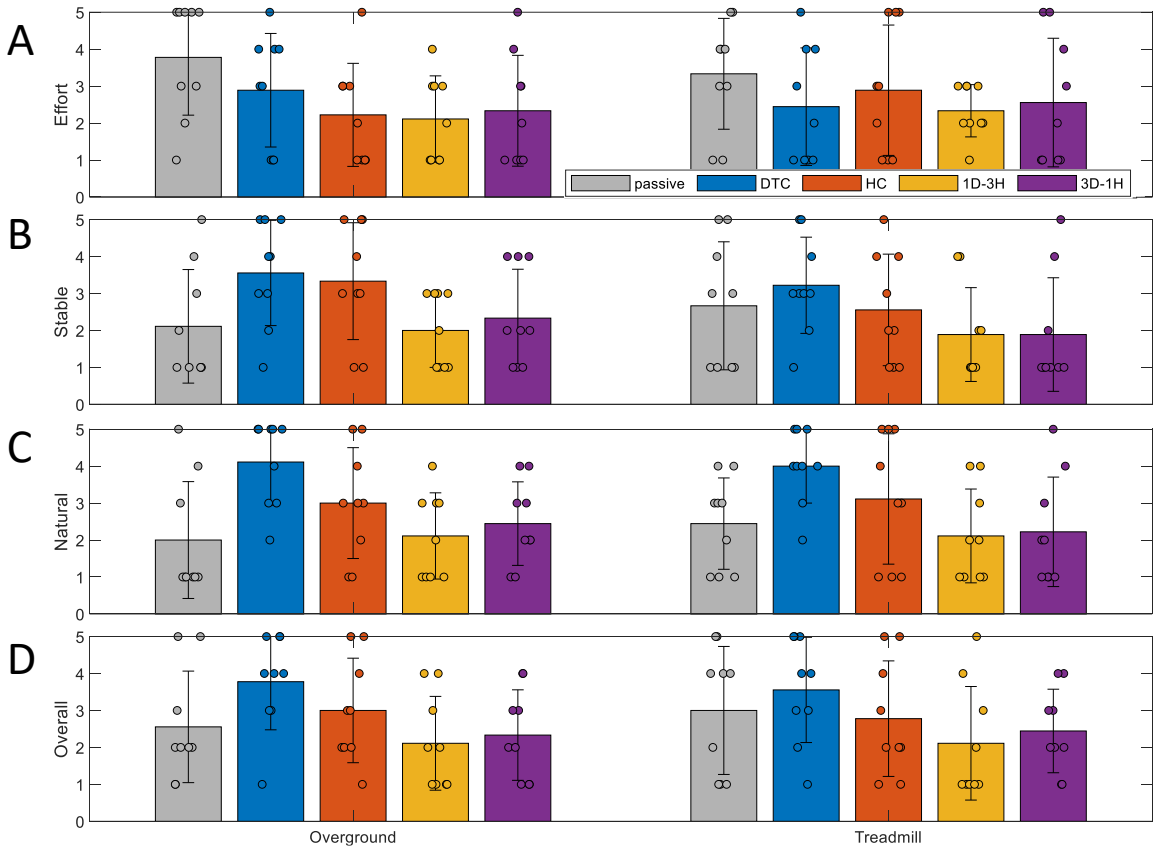

Figure 4.18: Average participant feedback on effort level, natural walking, stability, and overall performance for treadmill and overground walking with each exoskeleton condition where 1 is the best and 5 is the worst. Each point shows the rating of each participant.

natural walking at a joint-level. During treadmill walking, and are rated the most natural. Both these controllers have the most natural walking speed and speed variation.

The stability of these controllers is also rated the lowest DTC while has the best rating, which is in agreement with the reported co-contractions in Figure 4.16. The nature of HC allows the controller to completely conform to the user's movements, thus not restricting the movements. However, as HC is entirely dependent on the measured kinematics, it can become unstable. Meanwhile, DTC has a stable and predictable nature. This however, can lead to restrictive torques or asynchrony with the user. The combination of the two control approaches is able to incorporate benefits of both approaches; synchrony from HC and stability from DTC. However, the perceived stability of DTC is worse than its true

nature. This could be the result of asynchrony between the user's intentions and the control torques which can feel like instability to the user.

Interestingly, although HC computes the current joint torque, which is subject to signal delays, rather than that required to move to the desired positions, users did not report any lag in the timing of HC control with their intended movements. Further testing is required to determine whether a predictive joint torque controller would improve the performance of HC.

In general, is rated the highest across all metrics as well as with the overall rating reported in Figure 4.18. As participant feedback is a subjective measure, further investigations should be done to determine specifically which factors are considered in participant's ratings. For instance, in rating in terms of natural feeling, participants could value more overall gait timing rather than joint level-performance, or vise versa.

4.4 Conclusion

A hybrid model, including model- and data-driven components, for direct joint torque estimation was implemented in real time as an exoskeleton controller. A separate pre-defined direct torque control was developed. These two controllers were compared individually and in combination for both overground and treadmill walking with 9 participants.

During overground walking, a weighted sum of both control methods, with more weight on the hybrid control, was able to generate the fastest walking speeds. This same combination of controllers was also able to produce the closest spatiotemporal measures to those of natural gait. At the joint-level, each of the controllers had similar ability to produce natural trajectories. On average, the weighted sum of controllers was able to decrease the muscle activation of four out of six measured muscles when compared to activation during passive exoskeleton walking. Co-contraction tends to decrease in the thigh segment during overground walking with any controller. Meanwhile co-contraction tends to increase in the shank segment during overground walking, which could be due to the increase in walking speed [84]. During treadmill walking, only a combination of the controllers can decrease co-contraction in one pair of thigh muscles and both shank muscle pairs.

Participant feedback, in terms of effort, feeling of natural walking, stability, and overall performance, was also recorded. On average, the best controller identified with the spatiotemporal, kinematics, and EMG analysis is also identified to have better performance than the other controllers. Several consistencies between perceived natural walking were

identified with the metrics for spatiotemporal and joint-level performance. Although relating EMG activation and co-contraction to measures of effort and stability also shows some consistency, further studies should be done to investigate this relationship.

Overall, the combination of controllers tends to provide the most assistance and stability compared to the other controllers. In order to have more of an effect at a joint-level, this controller can be augmented with a feedback controller such as a path controller which will impose a desired trajectory at each joint.

In order to further improve the controllers, testing can be done with more varieties of walking conditions. For instance speed changes, non-straight walking, or ramp walking. As the hybrid controller was trained on a set of walking conditions, which doesn't include non-straight or ramp walking, it is possible that the network within the hybrid model should be re-trained for these cases. In addition, exploring different weights for the combination of the two controllers has the potential to further improving controller performance.

In this chapter, a variety of performance metrics were defined to evaluate the controller. These metrics are intended for validating the controller, meanwhile, a different set of performance metrics would be required for applications in rehabilitation. These metrics would be define based on the goal of the application; however, this is beyond the scope of this thesis.

Chapter 5

Lower Limb Exoskeleton Feedforward-Feedback Control

5.1 Control strategy

In this chapter, a FF-FB control approach is explored in a pilot experiment. A block diagram of the FF-FB control is shown in Figure 5.1. Based on Chapter 4, was shown to have preferable performance above the other tested controllers. For this reason, this control approach will be used as the feedforward torques. A position feedback controller is implemented based on an ideal trajectory based on each subject, with fixed gains. The proportional (K_p) and derivative (K_d) controller gains at the hip are 3 and 0.25 respectively. At the knee, these gains are 0.9 and 0.08. These gains were determined with human-in-the-loop optimization. In this case, a lookup table based on gait phase and walking speed is constructed based on previously recorded treadmill walking data of each subject. As in Chapter 4, the gait phase estimation is based on the approach taken in [98].

During experiments, both the FF and FB controllers were tested individually. In addition, these two controllers were tested in combination. The three control conditions will be referred to as: FF, FF-FB, and FB.

5.2 Experimental design

In this section, an in-depth description of the experimental setup and procedure are followed by the data analysis performed. Similar to Chapter 4, the experiment includes treadmill

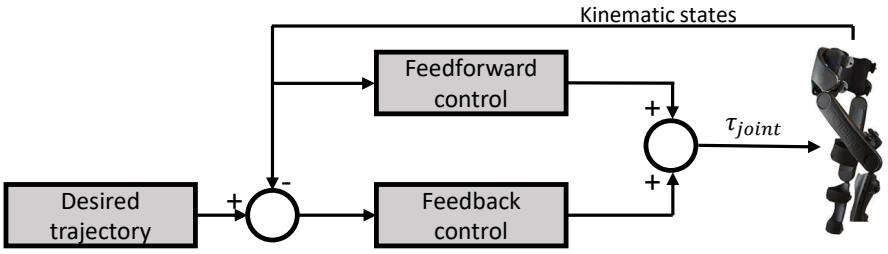

Figure 5.1: Block diagram showing the feedforward-feedback structure.

and overground walking, and the controllers are evaluated in terms of spatiotemporal, kinematics, and EMG-based performance metrics.

5.2.1 Experimental setup

The same setup was used as in Chapter 4 which includes a lower limb exoskeleton (Indego, Parker Hannifin, US), an instrumented treadmill (Bertec, US), six IMU sensors (MTw Awinda, Xsens, NL), and 12 EMG sensors (Trigono, Delsys, US). Two able-bodied subjects (age 23 and 25 years, 1 female, mass: 63 and 77 kg, height: 1.7 and 1.9 m) participated in this experiment. Data collection protocols and procedures were approved by the Clinical Research Ethics Committee at the University of Waterloo (ORE#41794), and conformed with the Declaration of Helsinki.

5.2.2 Experimental procedure

Similar to the experiment in Chapter 4, both treadmill and overground walking were tested. Each participant completed one minute of walking with the passive exoskeleton, and each of the three controllers at 0.6 and 0.8m/s. Following this, participants walked 36m overground with these same conditions. Finally, the participants repeated the same walking conditions with no exoskeleton.

5.2.3 Data analysis

The same approaches with gait event detection and joint angle computation with IMUs as well as EMG processing was implemented as in Chapter 4 (sections 4.2.4 and 4.2.5, and 4.2.6). In terms of spatiotemporal measures, the following metrics are computed and

compared between controllers: walking speed, step length, step time, and percent stance. At a joint-level, the correlation between joint trajectories of each stride and the respective natural trajectories are computed as well as range of motion. Finally, the integral of EMG squared during each stride as well as percent activation time. The same measures of co-contracting muscle pairs are computed with the product of the two EMG signals.

A statistical analysis is performed on metrics computed for each subject separately. Fifteen steps are randomly selected, with the exclusion of the first and last five steps, from each controller and compared with an unpaired t-test with a Bonferroni correction. As there are four control conditions (one passive and three active), this results in six comparison which gives a corrected significance level of 0.05/6.

5.3 Results and discussion

Each of the controllers are compared in terms of torque profiles, spatiotemporal measures, kinematics, and EMG. The aim of these controllers is to generate a natural gait profile, for this reason, many of these parameters are compared to each subject's natural walking pattern.

5.3.1 Applied torques

Figure 5.2A shows the joint angle lookup table used for subject 1 with the FF control is shown in Chapter 4, Figure 4.4A. The joint trajectories for subject 2 are similar. Figure 5.2B-C and Figure 5.3 shows the average applied joint torques for both subjects for treadmill at 0.8 m/s and overground walking respectively for all three of the controllers. The torques are defined such that positive torques are in the direction of joint flexion.

The torque profiles are very similar between overground and treadmill walking, indicating that the algorithms work similarly during these two conditions. The standard deviations about the torque profiles of subject 2 are an indicator that the subject walks with more variation between strides than subject 1. However, the FF torques have smaller standard deviations than the other controllers which indicates that the control is able to enforce the desired trajectories. The sign of the torques matches well with the signs of the angular velocities of each joint. At the hip joint, the velocities are generally positive from 20 to 90% of the gait cycle, this trend is also shown in the joint torques. The knee velocities are generally positive from 10 to 80% of the gait cycle. The corresponding joint torques within this range are either positive or close to zero. As the signs of the joint

torques and velocities are inline, this indicates that the torques are assisting, rather than resisting the movements.

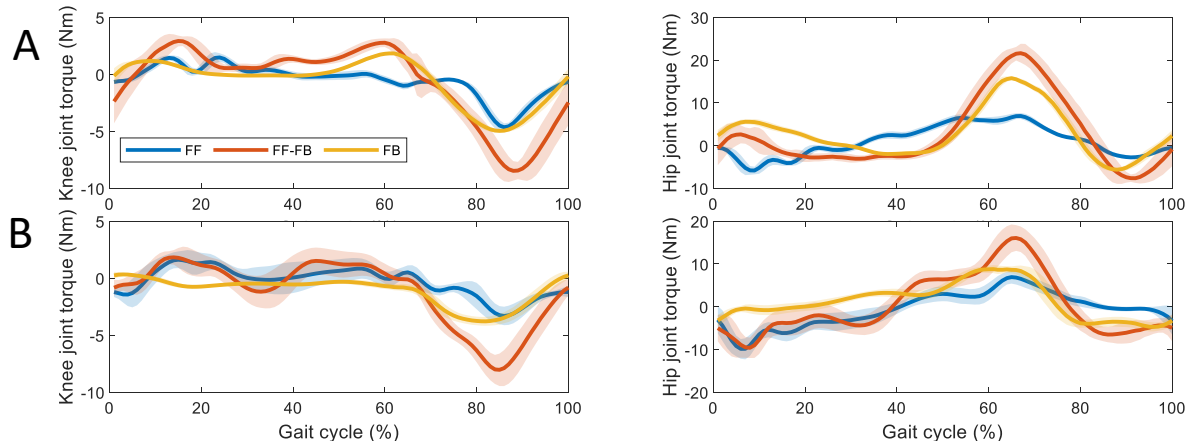

Figure 5.2: Average control torque for subject (A) 1, and (B) 2 for each controller for treadmill walking at 0.8m/s. The shaded area shows the standard deviation of the torques.

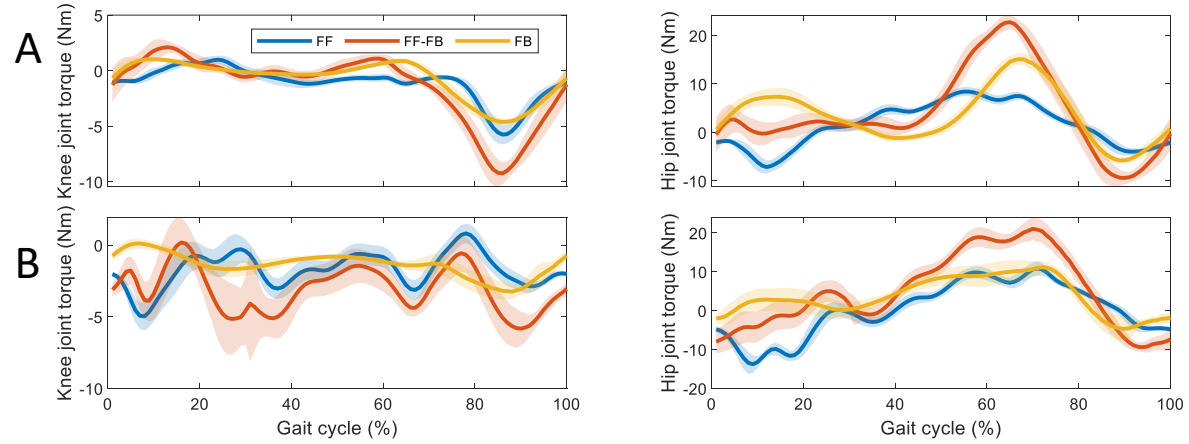

Figure 5.3: (A) Average control torque for subject (A) 1, and (B) 2 for each controller for overground walking. The shaded area shows the standard deviation of the torques.

5.3.2 Spatiotemporal gait analysis

Figure 5.4D shows the average and standard deviation of walking speed of both subjects during all exoskeleton conditions as well as the respective natural walking speed. The

exoskeleton reduces the average walking speed in both subjects. Both subjects walk faster with FF and FF-FB control compared to the other exoskeleton conditions. The increase in speed indicates that these two controllers are best able to assist the subjects.

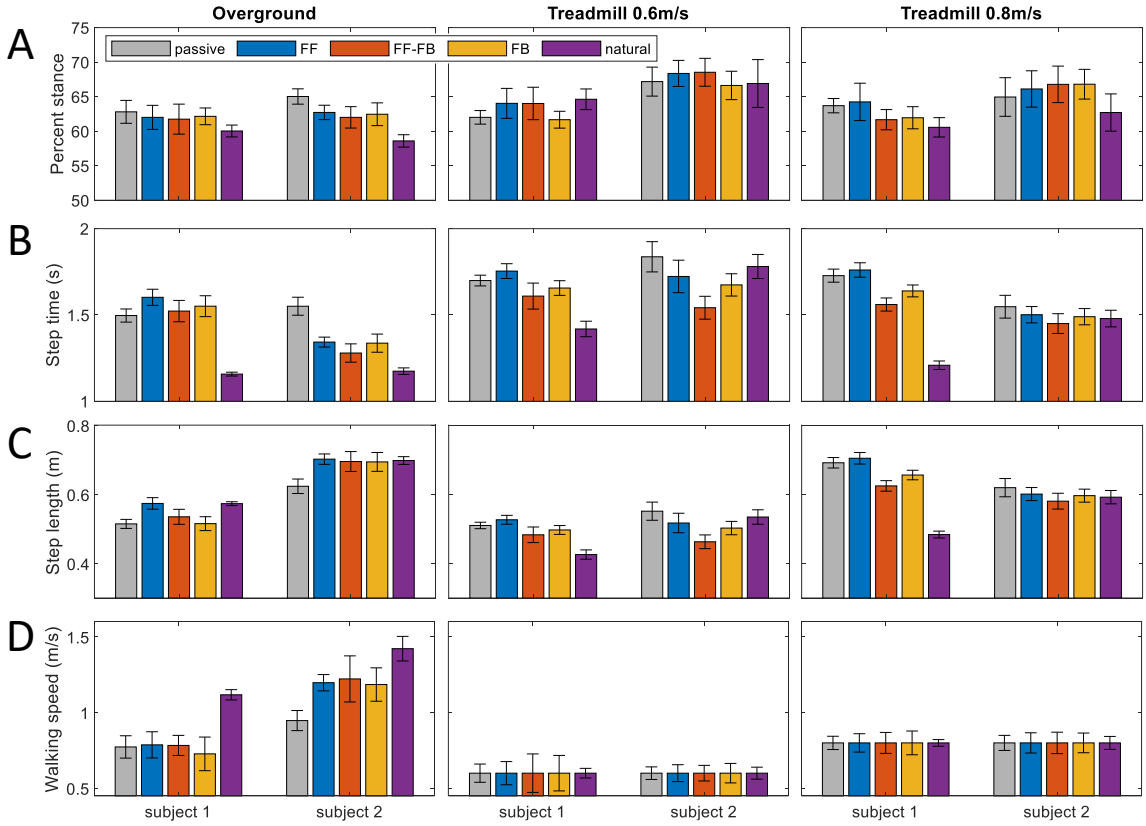

Figure 5.4: Spatiotemporal analysis of overground and treadmill walking at 0.6 and 0.8 m/s. Average measures of (A) percent stance, (B) step time, and (C) step length for all exoskeleton conditions and natural walking.

The walking speed of subject 1 with FB is nearly the same as passive exoskeleton walking. While the walking speed of subject 2 increased (by 25%) compared to passive walking. As the primary function of the FB control is to provide corrective torques, its effects will not necessarily be demonstrated in walking speed.

The spatiotemporal analysis including percent stance, step time, and step length, are shown in Figure 5.4A-C. During treadmill walking at 0.8m/s and overground walking, both subjects have higher percent stance (62% and 62%) when wearing the exoskeleton compared to natural walking (60% and 61%). Subject 1 has, on average, a percent stance

most similar to natural walking with FF-FB control (61%). The step time during natural walking is significantly different than passive and FB treadmill walking at 0.8m/s as well as FF treadmill walking at 0.6m/s ($p<0.003$). None of the other conditions are significantly different ($p>0.029$). Subject 2 has, on average, the closest percent stance with FF-FB to the natural gait during overground walking and passive walking during treadmill walking. Subject 2 passive walking has step time significantly different than natural gait step time, and more distant than all other conditions during overground walking ($p<1e-6$) while more natural during treadmill walking at 0.8m/s ($p<0.0045$).

Subject 1 has the step time most similar to natural walking during treadmill walking with FF-FB and is significantly different than all other walking conditions ($p<0.0034$). During overground walking, the most natural is passive walking and FF-FB being the second most natural. FF-FB is significantly closer to natural walking than FF ($p=0.0004$) but not FF ($p=0.038$). Subject 2 has a significantly more similar step time to natural with FF-FB during overground walking ($p<0.0007$). Meanwhile during treadmill walking FF and FB have the most natural step time at 0.6 and 0.8m/s respectively. Neither of these controllers are significantly different than the other controllers ($p>0.01$).

FF-FF has step lengths significantly more similar to natural walking than all the other controllers for treadmill walking ($p<0.0034$) for subject 1. During overground walking, FF significantly the most natural step lengths ($p<1e-7$). Subject 2 has very similar step lengths across all controllers during overground and treadmill walking at 0.8m/s. At 0.6m/s, subject 1 has the most natural step lengths with FF-FB, however this is only significantly different than passive walking ($p=0.0033$).

Overall, subject 1 has more natural spatiotemporal metrics of walking with FF-FB compared to all other controllers. Meanwhile subject 2 has most natural walking with FF, or FF-FB control depending on the metric and condition. Based on this and the walking speed comparison, the FF-FB control appears to achieve more natural walking, however, additional participants are needed to further investigate this claim.

5.3.3 Joint kinematics

Figure 5.5 shows the average joint angles for each of the exoskeleton controllers during overground walking. Treadmill walking resulted in very similar joint angles. There are some noticeable changes in the profile and range of the joint angles each controller. The angular profiles resulting from the FB and FF-FB controllers appear to be more similar than the FF as a result of the imposed trajectories in the FB controller. A more in depth analysis of these features is presented in this section.

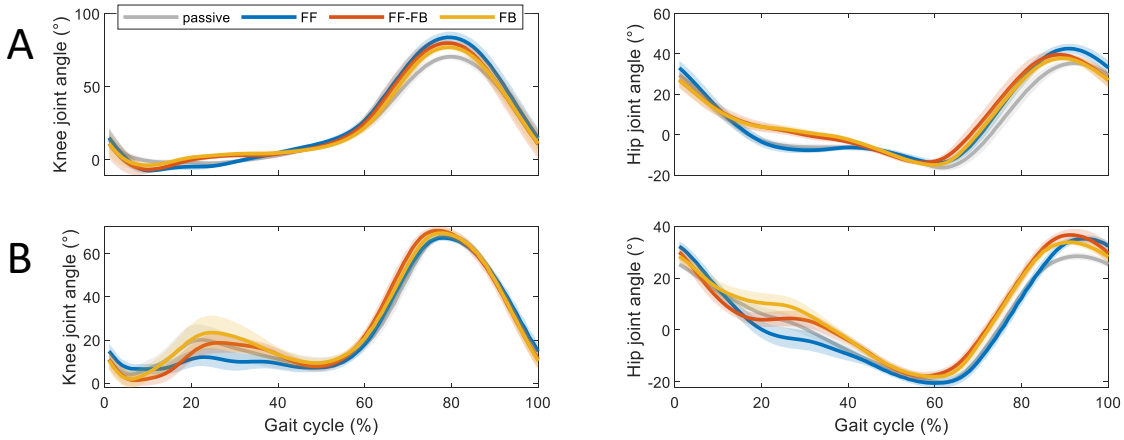

Figure 5.5: Average joint angles during passive and active exoskeleton walking for (A) subject 1 and (B) subject 2 during overground walking.

Figure 5.6 shows the ROM of each joint during exoskeleton and natural walking for both subjects. As seen in Chapter 4, the weight of the exoskeleton changes the ROM of each joints. In many cases, the passive exoskeleton ROM is most similar to natural walking. Out of the active cases, there is no clear controller which is best able to improve the ROM across conditions and subjects.

The Pearson correlation coefficient of the joint trajectories while wearing the exoskeleton to natural walking are shown in Figure 5.7.

During natural walking, the correlation of each stride to the average joint profile for subject 1 and 2 at the hip are 0.996±0.0035 and 0.998±0.0016 respectively. At the hip, FF control is able to significantly increase ($p<0.0080$) the correlation to natural walking in subject 1 compared to all other conditions with the exception of passive overground walking ($p=0.62$). Subject 2 has the most natural hip trajectories with FF control during overground walking and FF-FB during treadmill walking. During overground walking, FF is significantly closer to natural than all other controllers ($p<0.0013$). FF-FB is only significantly more natural than FB during treadmill walking at 0.8m/s ($p=0.0007$) while there is no significant difference between the other conditions ($p>0.015$).

During natural walking, the correlation of each stride to the average joint profile for subject 1 and 2 at the knee are 0.999±0.00089 and 0.999±0.0012 respectively. At the knee joint, the FB control has the highest correlation to natural walking with the exception of treadmill walking at 0.8/s for subject 2 where the most natural is passive walking. The knee trajectory of subject 1 is significantly more natural than passive and FF ($p>0.001$)

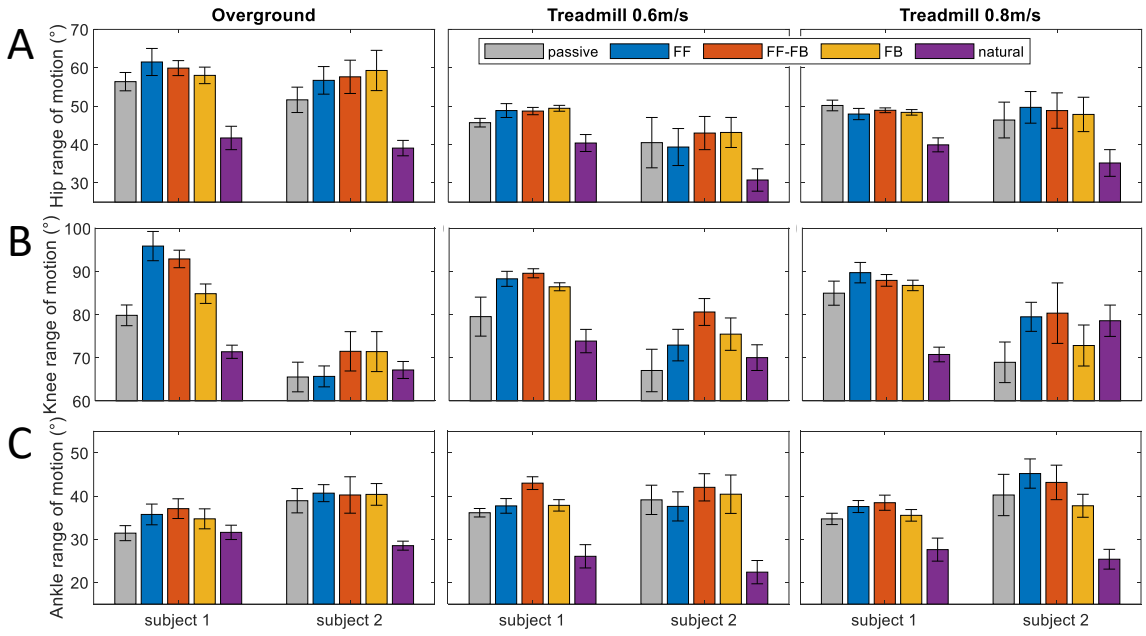

Figure 5.6: Average measured joint range of motion at the (A) hip, (B) knee, and (C) ankle for all exoskeleton conditions and natural walking.

for both treadmill and overground walking in addition to more natural than FF-FB during treadmill walking at 0.6m/s ($p=0.0029$). Subject 2 has significantly more natural knee trajectories with FB than all conditions during treadmill walking at 0.8m/s ($p<0.0031$) as well as more natural than FF and FF-FB ($p<0.0025$).

During natural walking, the correlation of each stride to the average joint profile for subject 1 and 2 at the ankle are 0.989 ± 0.0073 and 0.986 ± 0.0089. At the ankle joint, FB also tends to have the most natural joint angles. This increase is significant for subject 1 when compared to passive and FF during treadmill and overground walking ($p<0.0056$) as well as FF-FB during treadmill walking at 0.8m/s ($p=0.001$). Subject 2 has a significant increase during overground passive and FF walking as well as FF-FB treadmill walking at 0.8m/s ($p<0.002$).

In general, the joint trajectories tend to be more natural, especially in terms of correlation, with FB control alone. However, FF-FB is also able to increase the naturalness of the joint angles as well, although to a lesser extent. This is due to the corrective nature of the FB control. Therefore, in order to achieve a natural gait at a joint level, some contributions of FF are required. However, as the FB control has less natural spatiotemporal performance, compared to FF, this indicates that a combination of these two control

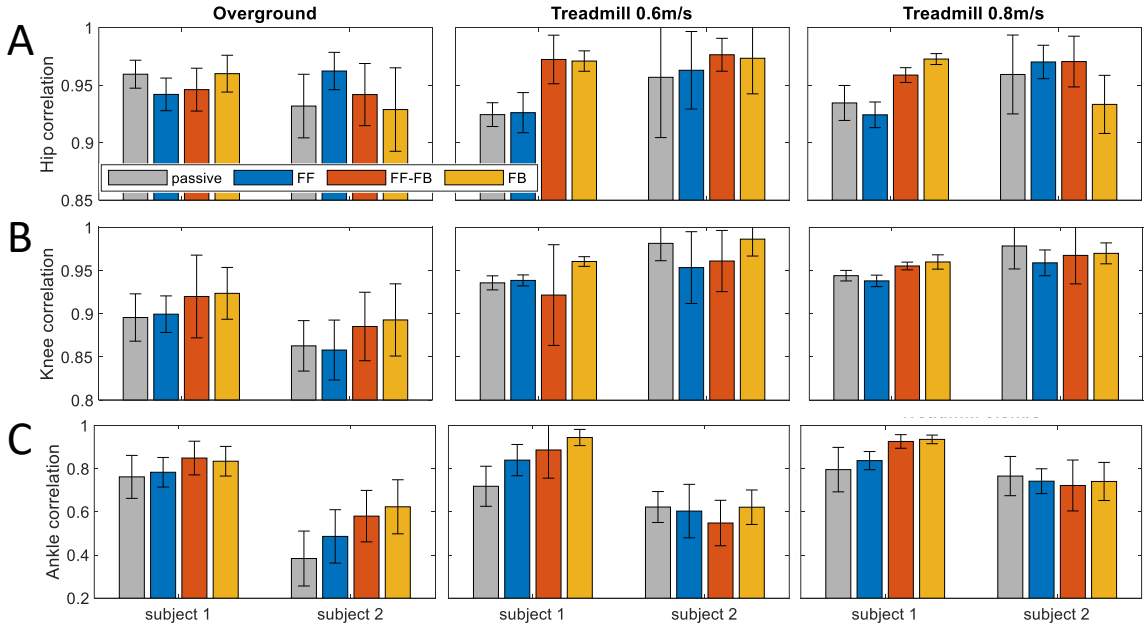

Figure 5.7: Average correlation of the (A) hip, (B) knee, and (C) ankle joint angles with natural walking for all exoskeleton conditions.

approaches can achieve improved kinematic as well as spatiotemporal performance.

5.3.4 Muscle activation

Figure 5.8 shows the overall effort level, computed as the sum of all muscle effort, across each gait cycle. There is no consistent increase or decrease in overall muscle effort between controllers, walking conditions, or subjects. For this reason, further analysis on each muscle individually is completed.

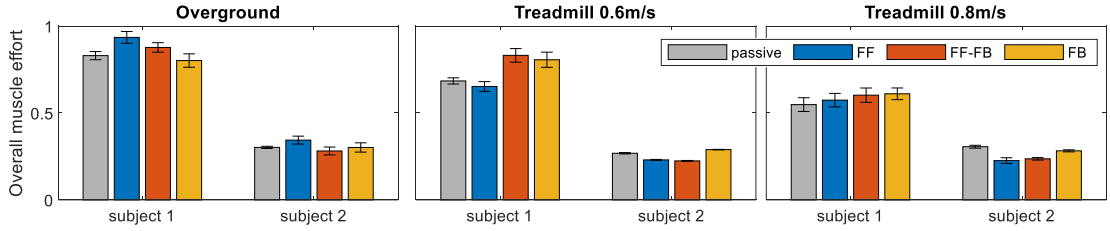

Figure 5.8: Overall effort level normalized by walking speed.

Figure 5.9 shows the effort level computed for each muscle across each gait cycle. The knee extensor muscles, RF and VM, have on average higher EMG activity with the exoskeleton in passive mode. This decrease is only statistically significant for subject 1 VM during overground walking ($p<0.0015$). This indicates that the active exoskeleton modes are able to assist in knee extension. The BF muscle, a knee flexor, has on average lower EMG activity during passive exoskeleton walking. This difference is only statistically significant for subject 1 for all walking conditions ($p<0.0045$). This increase in BF activation during active control is due to an increase in stabilization required as the exoskeleton provides some assistance to movements. This is also referred to as co-contraction and further analyzed in Figure 5.11.

The TA muscle shows some slight decrease in activation during active conditions compared to passive, although these decreases are small (less than 0.1). FF-FB activation is significantly lower than passive walking for subject 1 during overground ($p=0.0003$) as well as with subject 2 during treadmill walking at 0.6m/s ($p=0.0028$). This decrease in activation could be a result of the decrease in co-contraction in the shank muscles, indicating an increase in stability at the ankle joint as this is one of the main functions of the TA muscle during walking (see Figure 5.11). The activation of the ankle plantar flexor muscles (GM and SO) do not show consistent changes between subjects or conditions. Any changes seen in these muscles are small and likely not an indicator of controller assistance levels.

Figure 5.10 shows the fraction of the gait cycle in which each muscle is active. In the knee extensor muscles (RF and VM)), there is in general a slight decrease in activation time when comparing passive mode to the three controllers. This, in agreement with the EMG magnitude in Figure 5.9A-B, further shows that the controllers are able to effectively assist the subjects. However, the decrease compared to passive walking is only significant in subject 1 during treadmill walking at 0.8m/s ($p<0.0034$). In the knee flexor muscle (BF), there are only small differences between the activation time during passive mode and active. Although the EMG amplitudes in Figure 5.9C showed increases with the active control, since the activation time did not increase accordingly, this implies that the controllers are not resisting the user's movements.

In general, the TA muscle shows decreases in activation time when the controllers are applied. In addition to the decrease in EMG amplitude reported in Figure 5.9, this indicates an increase in stability at the ankle (see Figure 5.11). The decrease in activation time compared to passive walking is significant only for subject 1 with overground walking ($p<0.0016$). The GM and SO have very little change in activation time between the active and passive cases. Similar to the activation magnitude, this demonstrates that the activation time of these muscles is not an effective indicator of the performance of these controllers.

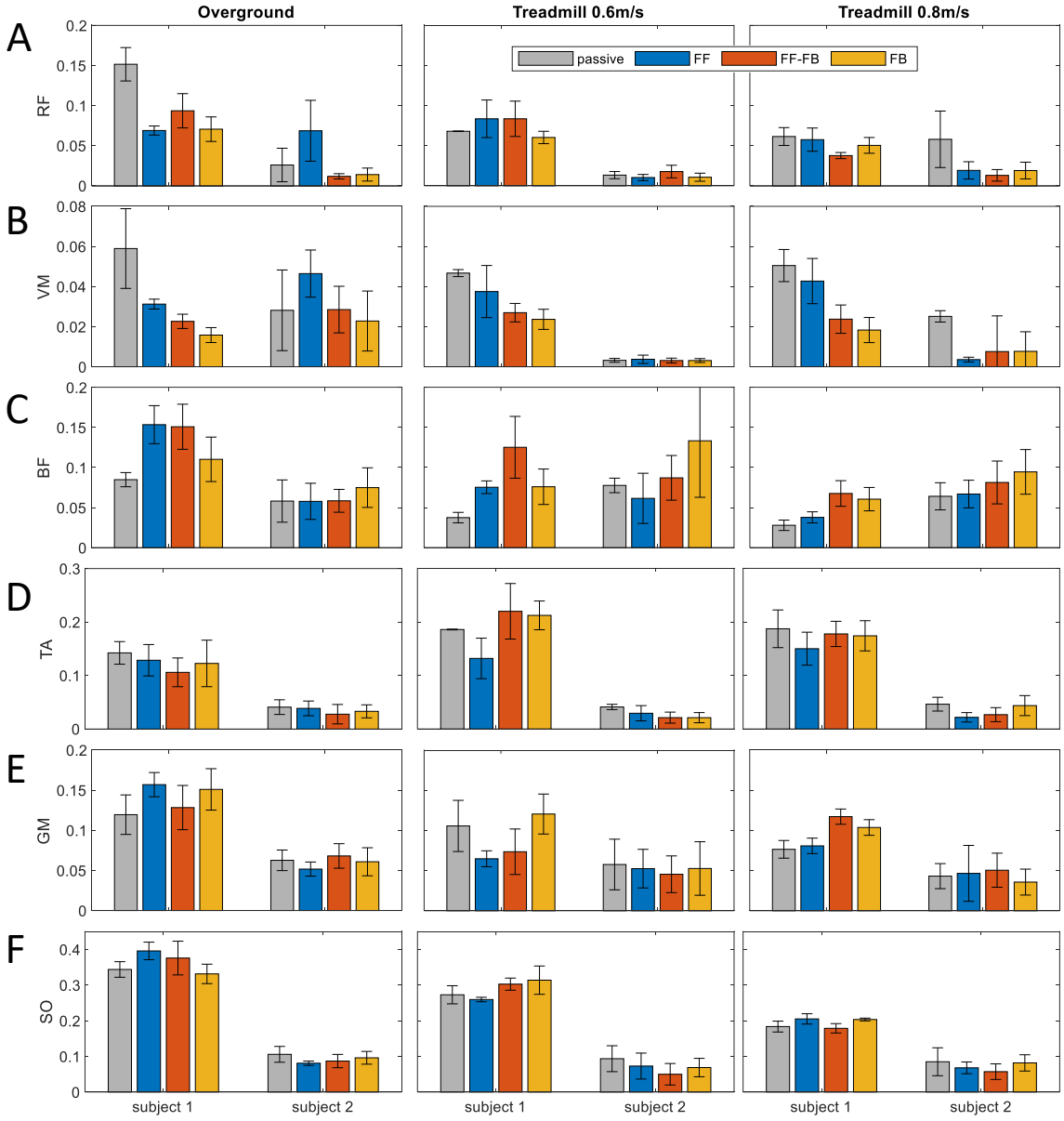

Figure 5.9: Average effort level normalized by walking speed for all muscles.

5.3.5 Muscle co-contraction

Figure 5.11 shows the average co-contraction during one gait cycle for each exoskeleton condition, normalized by walking speed. With the exception of subject 1 during overground

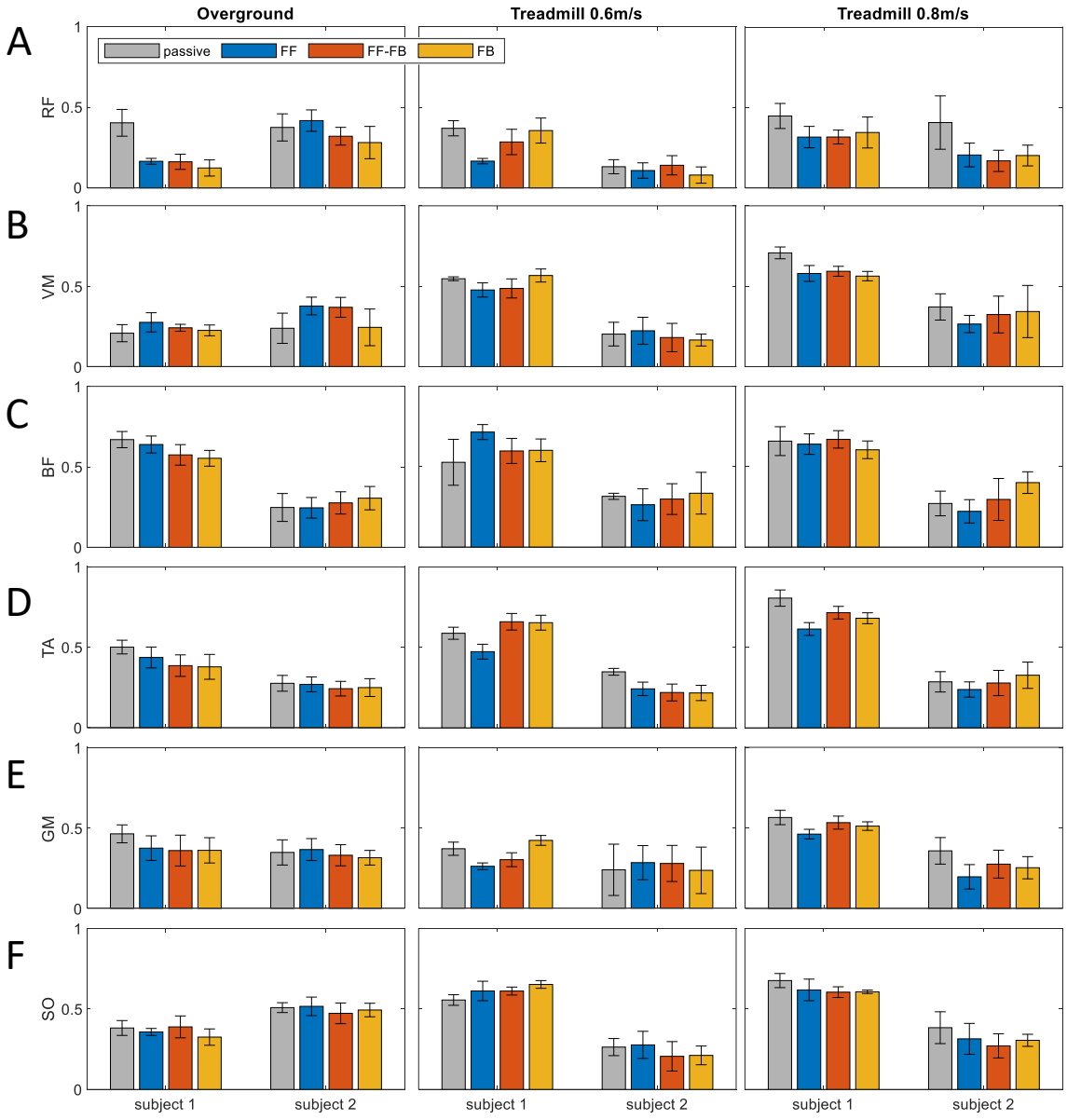

Figure 5.10: Fraction of gait cycle with muscle active.

and subject 2 during treadmill walking at 0.8m/s, there is an increase in the RF-BF and VM-BF muscle pairs co-contraction during active versus passive walking. Subjects increase those co-contractions when the exoskeleton is controlling their joint, possibly as the user

not feeling to be in full control of their joint movements (as with passive walking). However, these increases are small (less than 0.02). The increases are only statistically significant for subject 1 during treadmill walking ($p<0.0046$).

On average, there is a decrease in TA-GM and TA-SO co-contraction during active versus passive controllers, however these decreases are only statistically significant for TA-SO with subject 1 during overground walking ($p<0.002$). This indicates that the ankle joint requires less stiffness modulation which indicates that the ankle is more stable during the active cases compared to passive walking. As the exoskeleton does not directly control the ankle joint, the decrease in co-contraction is reduced as the exoskeleton is supplying more support to the knee and hip joints, thus relying less on the ankle.

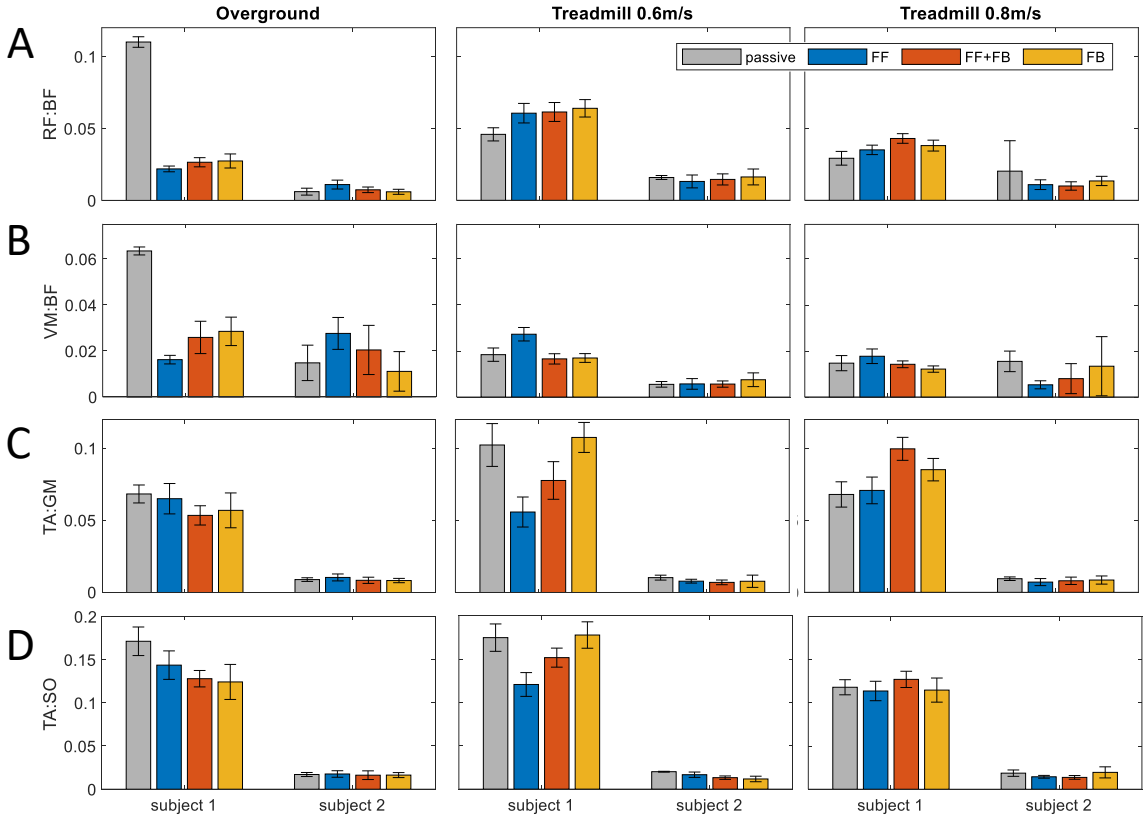

Figure 5.11: Average amount of co-contraction during each gait cycle, normalized by walking speed.

Figure 5.10 shows the fraction of the gait cycle in which co-contraction occurs. With the exception of subject 1 during overground walking, there is very little change in the

co-contraction time of the VM-BF and VM-BF muscle pairs. There is a slight decrease in the co-contraction time of the TA-GM and TA-SO muscle pairs during active versus passive walking; however these decreases are not statistically significant ($p>0.0095$) with the exception of subject 1 TA-SO during overground walking ($p<0.006$). This further demonstrates that there is a decrease in joint stiffness, and increase in stability, at the ankle joint, which in turn requires less co-contraction in these muscle pairs.

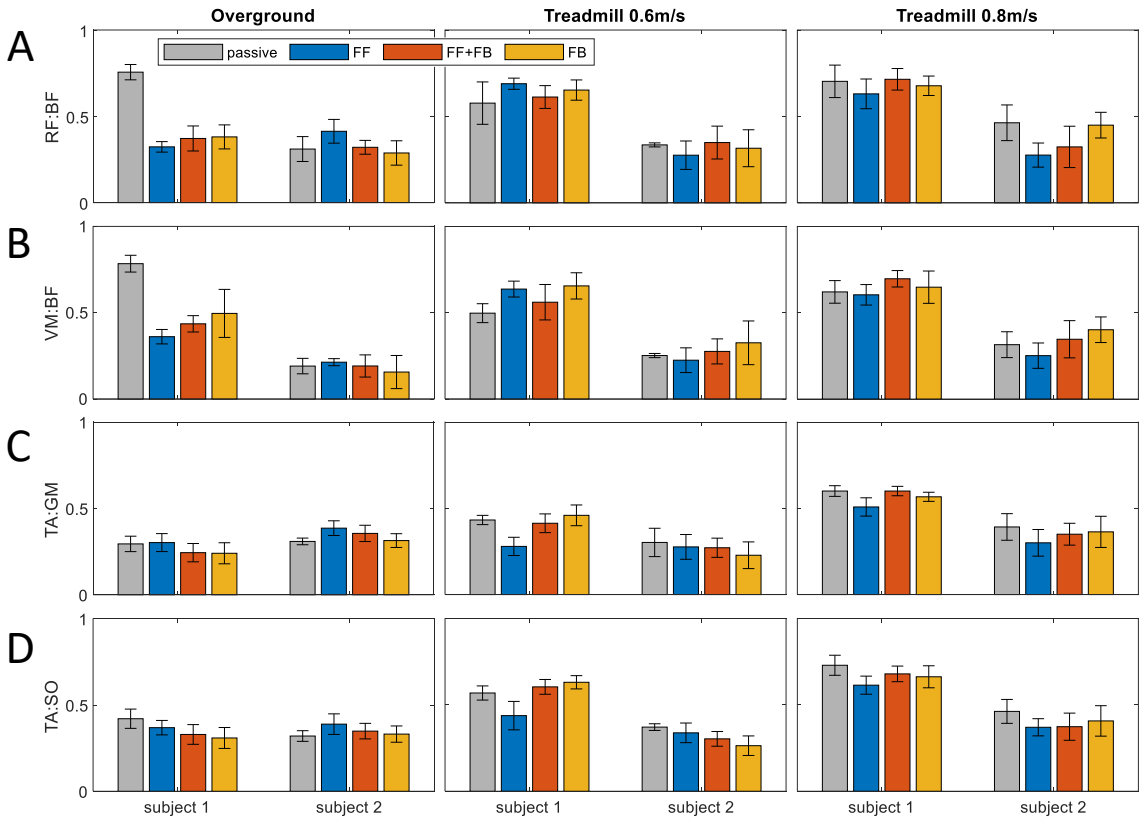

Figure 5.12: Fraction of gait cycle with co-contraction.

5.4 Conclusion

In this pilot study, an ideal feedforward control approach which was identified in Chapter 4, is implemented in combination with a feedback control. As the feedforward control was shown in Chapter 4 to sychronize well with the user and provide assistive torques,

without providing sufficient joint-level correction to obtain a natural gait, the purpose of the feedback control is to address this downfall.

The feedback control alone is able to improve upon the joint-level performance of the controller while sacrificing the spatiotemporal performance. Meanwhile the feedback control alone is better able to perform in terms of spatiotemporal performance rather than joint-level. This indicates that a combination of these two controls will be able to produce a balance of these two performance metrics. However, further testing with more subjects will be required to determine the combination which will be best able to do this.

The controllers were able to decrease the activation in knee extensor and ankle dorsiflexor muscles. This indicates that the active controllers are able to provide assistance. Meanwhile, there is an increase in knee extensor and little change in ankle plantarflexor muscles. The increase in knee extensor muscles is due to an increase in thigh co-contraction muscle pairs. However, this increase is small. The co-contraction measured in the shank muscles decreases with the active exoskeleton, which indicates decreased stiffness and in turn increased stability at this joint.

Chapter 6

Conclusion

The objective of this thesis is to develop a real-time joint torque estimator for use as a lower limb exoskeleton controller. The joint torque estimator was developed and validated against a gold standard approach with a variety of walking conditions and subjects. Once implemented as a controller, it was tested in treadmill and overground walking scenarios to evaluate its ability to assist and correct movements while walking.

The objective of an accurate a real-time approach to joint torque estimation was identified in Chapter 2.1. An approach without the use of force measurements allows for more versatility in applications. Such approaches, which rely on kinematic data only, enable biomechanical analysis during overground walking, and other scenarios where continuous force measurements is a challenge.

In Chapter 3, a hybrid inverse dynamic-neural network model was proposed and validated for treadmill walking. This model includes a data-driven component for GRF and ZMP estimation as well as an inverse dynamic model adjusted to simple anthropometric measures of each user. An alternative end-to-end feedforward neural network was also developed for joint torque estimation. Both the hybrid and end-to-end approaches were validated with 11 participants during treadmill walking with a variety of speeds and gait patterns. One additional subject, who wore a lower limb exoskeleton, was included for verification.

The end-to-end network has less errors in joint torque estimation than the hybrid model when comparing to a gold standard approach for walking conditions most similar to the training data. These conditions include treadmill walking with speed changes, starts and stops, asymmetrical walking, and varied stride lengths. However, in many cases, there is no statistically significant difference between the estimation errors of the end-to-end and

hybrid model. Conversely, in the case of the exoskeleton walking, the hybrid model is more accurate. This indicates that the explicit dynamics included in the hybrid model allows for better generalizability.

This hybrid model was then implemented as a joint torque control approach for a lower limb exoskeleton in Chapter 4. A separate pre-defined direct torque control was also developed such that the applied torques are a function of walking speed and gait phase alone. These two control approaches were investigated individually and in combination during treadmill and overground walking of 9 participants.

A combination, i.e. the weighted sum, of the two controllers, in which more weight is placed on the hybrid control, produced the highest overground walking speed. Spatiotemporal parameters, such as percent stance, step time, and step length, were closest to natural walking with this same combination of controllers. At joint-level, the controllers did not produce meaningfully different results. On average, this controller was able to decrease the muscle activation of four out of six measured leg muscles when compared to walking with the exoskeleton in passive mode. Specifically, the knee extensor and ankle plantarflexor muscles tend to show reduction in muscle activity. The decrease in overall muscle activity, and consequently effort level, indicates that the exoskeleton is able to assist in some of the required movements during the gait cycle. During overground walking, the co-contraction of the thigh muscle pairs tends to decrease while the shank muscle pairs increase. This indicates a decrease in joint stiffness and in turn an increase in stability provided from the exoskeleton at the hip joints while a decrease in stiffness and decrease in stability from the exoskeleton at the ankle joint. However, the decrease in stability at the ankle joint is likely caused by the significant increase in walking speed. In contrast during treadmill walking, the co-contraction of the shank muscles decreases, which indicates that at constant walking speed, the controller is able to decrease the need for stabilization and increase stability in the ankle joint. This combination of controllers with more weight placed on the hybrid control is identified as the ideal feedforward control from this test.

In order to improve the joint-level performance of the previously identified feedforward control, a position feedback control was added in Chapter 5. A pilot study with two participants investigated the effect of combining these two controllers. The feedback control was identified to have the best joint-level performance, while the feedforward control has the best spatiotemporal performance. The combination of both controllers is able to balance the performance of these controllers. However, further testing is required to confirm this hypothesis. In addition, optimizing the method in which these two controllers are combined is also an area for potential improvements. In particular, a weighted sum of the controllers with weights varied along the gait cycle.

All three of these controllers (FF, FB, FF-FB) were able to decrease activation in knee extensor and ankle dorsiflexor muscles in comparison to passive exoskeleton walking. This indicates some assistance is provided. There is a decrease in measured co-contraction of the shank muscles, indicating a decrease in joint stiffness required. Less joint stiffness indicates an increase in stability at the ankle joint resulting from the exoskeleton.

Further testing the performance of the controllers presented in Chapters 4 and 5 will further illuminate the best approach to take for lower limb exoskeleton control. Additional subjects and walking conditions will render the tests more conclusive. Having subjects with varying anthropometrics, and physical abilities, including physical impairments, will demonstrate whether the controllers will perform in a similar manner between subjects or whether the ideal controller is subject-specific. In the case of limited physical abilities, generating a set of desired joint trajectories that will feel natural to the user is another avenue for further improvement as it cannot be directly measured. Additional walking conditions such as speed changes, non-straight walking, or ramp walking may challenge the proposed controllers.

This thesis has demonstrated that a combination of controllers being implemented as a lower limb exoskeleton controller can have superior performance than a single control alone. With this knowledge research can be done to augment existing controllers together to reap the benefits of each controller. Various combinations of controllers has the potential to create a controller that can be easily tuned to accommodate for the needs of the user. For instance, with the feedforward-feedback controller being tested with this thesis, a user requiring more assistive than corrective torques, such as a military soldier using an exoskeleton for augmentation, can achieve this by placing more emphasis on the feedforward control. Meanwhile, a user who has physical impairments such as hemiparesis, requires more corrective torques to achieve a natural gait and would therefore put more emphasis on the feedback control.

References

[1] Mohammad Abdoli-Eramaki, Caroline Damecour, John Christenson, and Joan Stevenson. The effect of perspiration on the semg amplitude and power spectrum. *Journal of Electromyography and Kinesiology*, 22(6):908–913, 2012.

[2] Tine Alkjaer, Erik B. Simonsen, and Poul Dyhre-Poulsen. Comparison of inverse dynamics calculated by two- and three-dimensional models during walking. *Gait & Posture*, 13(2):73–77, 2001.

[3] Kamiar Aminian, Bijan Najafi, C Büla, P-F Leyvraz, and Ph Robert. Spatio-temporal parameters of gait measured by an ambulatory system using miniature gyroscopes. *Journal of biomechanics*, 35(5):689–699, 2002.

[4] Daisuke Aoyagi, Wade E. Ichinose, Susan J. Harkema, David J. Reinkensmeyer, and James E. Bobrow. A robot and control algorithm that can synchronously assist in naturalistic motion during body-weight-supported gait training following neurologic injury. *IEEE Transactions on Neural Systems and Rehabilitation Engineering*, 15(3):387–400, 2007.

[5] Arash Arami, Noémie Saint Raymond, and Kamiar Aminian. An accurate wearable foot clearance estimation system: Toward a real-time measurement system. *IEEE Sensors Journal*, 17(8):2542–2549, 2017.

[6] Arash Arami, Matteo Simoncini, Oguz Atasoy, Shafqat Ali, Willyan Hasenkamp, Arnaud Bertsch, Eric Meurville, Steve Tanner, Philippe Renaud, Catherine Dehollain, et al. Instrumented knee prosthesis for force and kinematics measurements. *IEEE transactions on automation science and engineering*, 10(3):615–624, 2013.

[7] Arash Arami, Nevio L Tagliamonte, Federica Tamburella, Hsieng-Yung Huang, Marco Molinari, and Etienne Burdet. A simple tool to measure spasticity in spinal

cord injury subjects. In *2017 International Conference on Rehabilitation Robotics (ICORR)*, pages 1590–1596. IEEE, 2017.

[8] Arash Arami, Axelle Vallet, and Kamiar Aminian. Accurate measurement of concurrent flexion–extension and internal–external rotations in smart knee prostheses. *IEEE Transactions on Biomedical Engineering*, 60(9):2504–2510, 2013.

[9] Joonbum Bae, Kyoungchul Kong, and Masayoshi Tomizuka. Real-time estimation of lower extremity joint torques in normal gait. *IFAC Proceedings Volumes*, 42(16):443–448, 2009.

[10] Sai K Banala, Seok Hun Kim, Sunil K Agrawal, and John P Scholz. Robot assisted gait training with active leg exoskeleton (alex). *IEEE transactions on neural systems and rehabilitation engineering*, 17(1):2–8, 2008.

[11] Rod S. Barrett, Thor F. Besier, and David G. Lloyd. Individual muscle contributions to the swing phase of gait: An emg-based forward dynamics modelling approach. *Simulation Modelling Practice and Theory*, 15(9):1146–1155, 2007.

[12] Romain Baud, Ali Reza Manzoori, Auke Ijspeert, and Mohamed Bouri. Review of control strategies for lower-limb exoskeletons to assist gait. *Journal of NeuroEngineering and Rehabilitation*, 18(1), 2021.

[13] Stefano Bertuletti, Ugo Della Croce, and Andrea Cereatti. A wearable solution for accurate step detection based on the direct measurement of the inter-foot distance. *Journal of biomechanics*, 84:274–277, 2019.

[14] Lucia Bizovska, Zdenek Svoboda, Patrik Kutilek, Miroslav Janura, Ales Gaba, and Zuzana Kovacikova. Variability of centre of pressure movement during gait in young and middle-aged women. *Gait & Posture*, 40(3):399–402, 2014.

[15] Julien Boudarham, Nicolas Roche, Didier Pradon, Celine Bonnyaud, Djamel Bensmail, and Raphael Zory. Variations in kinematics during clinical gait analysis in stroke patients. *PloS one*, 8(6):e66421, 2013.

[16] Thomas S. Buchanan, David G. Lloyd, Kurt Manal, and Thor F. Besier. Estimation of muscle forces and joint moments using a forward-inverse dynamics model. In *Medicine and Science in Sports and Exercise*, volume 37, pages 1911–1916, 2005.

[17] Kristina M Calder, Stacey M Acker, Neha Arora, Karen A Beattie, Jack P Callaghan, Jonathan D Adachi, and Monica R Maly. Knee power is an important parameter in

understanding medial knee joint load in knee osteoarthritis. *Arthritis care & research*, 66(5):687–694, 2014.

[18] I. Campanini, A. Merlo, P. Degola, R. Merletti, G. Vezzosi, and D. Farina. Effect of electrode location on emg signal envelope in leg muscles during gait. *Journal of Electromyography and Kinesiology*, 17(4):515–526, 2007.

[19] Elena Ceseracciu, Zimi Sawacha, and Claudio Cobelli. Comparison of markerless and marker-based motion capture technologies through simultaneous data collection during gait: proof of concept. *PloS one*, 9(3):e87640, 2014.

[20] Henry G Chambers and David H Sutherland. A practical guide to gait analysis. *JAAOS-Journal of the American Academy of Orthopaedic Surgeons*, 10(3):222–231, 2002.

[21] Michael S Cherry, Sridhar Kota, Aaron Young, and Daniel P Ferris. Running with an elastic lower limb exoskeleton. *Journal of applied biomechanics*, 32(3):269–277, 2016.

[22] Gery Colombo, Matthias Joerg, Reinhard Schreier, Volker Dietz, et al. Treadmill training of paraplegic patients using a robotic orthosis. *Journal of rehabilitation research and development*, 37(6):693–700, 2000.

[23] Roy D Crowninshield and Richard A Brand. A physiologically based criterion of muscle force prediction in locomotion. *Journal of biomechanics*, 14(11):793–801, 1981.

[24] S.L. Delp, J.P. Loan, M.G. Hoy, F.E. Zajac, E.L. Topp, and J.M. Rosen. An interactive graphics-based model of the lower extremity to study orthopaedic surgical procedures. *IEEE Transactions on Biomedical Engineering*, 37(8):757–767, Aug 1990.

[25] Paul DeVita and Tibor Hortobagyi. Age causes a redistribution of joint torques and powers during gait. *Journal of Applied Physiology*, 88(5):1804–1811, 2000. PMID: 10797145.

[26] Mohsen M Diraneyya, JuHyeong Ryu, Eihab Abdel-Rahman, and Carl T Haas. Inertial motion capture-based whole-body inverse dynamics. *Sensors*, 21(21):7353, 2021.

[27] Philip S. Dyer and Stacy J. Morris Bamberg. Instrumented insole vs. force plate: A comparison of center of plantar pressure. In *2011 Annual International Conference of the IEEE Engineering in Medicine and Biology Society*, pages 6805–6809, 2011.

[28] Florin Dzeladini, Amy R Wu, Daniel Renjewski, Arash Arami, Etienne Burdet, Edwin Van Asseldonk, Herman Van Der Kooij, and Auke J Ijspeert. Effects of a neuromuscular controller on a powered ankle exoskeleton during human walking. In *2016 6th IEEE International Conference on Biomedical Robotics and Biomechatronics (BioRob)*, pages 617–622. Ieee, 2016.

[29] Darryl D D'Lima, Nikolai Steklov, Shantanu Patil, and Clifford W Colwell. The mark coventry award: in vivo knee forces during recreation and exercise after knee arthroplasty. *Clinical orthopaedics and related research*, 466(11):2605–2611, 2008.

[30] Debbie D Espy, Feng Yang, Tanvi Bhatt, and Y-C Pai. Independent influence of gait speed and step length on stability and fall risk. *Gait & posture*, 32(3):378–382, 2010.

[31] Julien Favre, Matthieu Hayoz, Jennifer C. Erhart-Hledik, and Thomas P. Andriacchi. A neural network model to predict knee adduction moment during walking based on ground reaction force and anthropometric measurements. *Journal of Biomechanics*, 45(4):692–698, 2012.

[32] M. Fellinger, J. Passler, and W. Seggl. *Plug-in Gait Reference Guide*. 2018.

[33] Daniel P. Ferris and Cara L. Lewis. Robotic lower limb exoskeletons using proportional myoelectric control. In *2009 Annual International Conference of the IEEE Engineering in Medicine and Biology Society*, pages 2119–2124, 2009.

[34] David Forchelet, Matteo Simoncini, Arash Arami, Arnaud Bertsch, Eric Meurville, Kamiar Aminian, Peter Ryser, and Philippe Renaud. Enclosed electronic system for force measurements in knee implants. *Sensors*, 14(8):15009–15021, 2014.

[35] A. Forner-Cordero, H.J.F.M. Koopman, and F.C.T. van der Helm. Inverse dynamics calculations during gait with restricted ground reaction force information from pressure insoles. *Gait & Posture*, 23(2):189–199, 2006.

[36] Laurent Frossard, Laurence Cheze, and Raphael Dumas. Dynamic input to determine hip joint moments, power and work on the prosthetic limb of transfemoral amputees: ground reaction vs knee reaction. *Prosthetics and Orthotics International*, 35(2):140–149, 2011.

[37] Yasutaka Fujimoto, Satoshi Obata, and Atsuo Kawamura. Robust biped walking with active interaction control between foot and ground. *Proceedings - IEEE International Conference on Robotics and Automation*, 3(May):2030–2035, 1998.

[38] Sumire Futamure, Vincent Bonnet, Raphael Dumas, and Gentiane Venture. A sensitivity analysis method for the body segment inertial parameters based on ground reaction and joint moment regressor matrices. *Journal of Biomechanics*, 64:85–92, 2017.

[39] Andrej Gams, Tadej Petrič, Tadej Debevec, and Jan Babič. Effects of robotic knee exoskeleton on human energy expenditure. *IEEE Transactions on Biomedical Engineering*, 60(6):1636–1644, 2013.

[40] María Dolores Gor-García-Fogeda, Roberto Cano de la Cuerda, María Carratalá Tejada, Isabel Mª Alguacil-Diego, and Francisco Molina-Rueda. Observational gait assessments in people with neurological disorders: a systematic review. *Archives of physical medicine and rehabilitation*, 97(1):131–140, 2016.

[41] Robert D. Gregg, Timothy W. Bretl, and Mark W. Spong. A control theoretic approach to robot-assisted locomotor therapy. In *49th IEEE Conference on Decision and Control (CDC)*, pages 1679–1686, 2010.

[42] Laura Hak, Han Houdijk, Peter J Beek, and Jaap H van Dieën. Steps to take to enhance gait stability: the effect of stride frequency, stride length, and walking speed on local dynamic stability and margins of stability. *PloS one*, 8(12):e82842, 2013.

[43] Daniel Hamacher, NB Singh, Jaap H Van Dieën, MO Heller, and William R Taylor. Kinematic measures for assessing gait stability in elderly individuals: a systematic review. *Journal of The Royal Society Interface*, 8(65):1682–1698, 2011.

[44] Joseph Hamill and Kathleen M Knutzen. *Biomechanical basis of human movement*. Lippincott Williams & Wilkins, 2006.

[45] Gerald F Harris and Jacqueline J Wertsch. Procedures for gait analysis. *Archives of Physical Medicine and Rehabilitation*, 75(2):216–225, 1994.

[46] Bernd Heinlein, Ines Kutzner, Friedmar Graichen, Alwina Bender, Antonius Rohlmann, Andreas M Halder, Alexander Beier, and Georg Bergmann. Complete data of total knee replacement loading for level walking and stair climbing measured in vivo with a follow-up of 6–10 months. *Clin Biomech*, 24(4):315–326, 2009.

[47] Hertz. On the contact of elastic solids. *Crelle's Journal*, 92:156–171.

[48] Altinus Lucilus Hof and JW Van den Berg. Emg to force processing i: an electrical analogue of the hill muscle model. *Journal of biomechanics*, 14(11):747–758, 1981.

[49] Hsien Yung Huang, Arash Arami, Ildar Farkhatdinov, Domenico Formica, and Etienne Burdet. The influence of posture, applied force and perturbation direction on hip joint viscoelasticity. *IEEE Transactions on Neural Systems and Rehabilitation Engineering*, 28(5):1138–1145, 2020.

[50] K. H. Hunt and F. R. E. Crossley. Coefficient of Restitution Interpreted as Damping in Vibroimpact. *Journal of Applied Mechanics*, 42(2):440–445, 06 1975.

[51] Weiguang Huo, Samer Mohammed, Yacine Amirat, and Kyoungchul Kong. Active impedance control of a lower limb exoskeleton to assist sit-to-stand movement. In *2016 IEEE International Conference on Robotics and Automation (ICRA)*, pages 3530–3536, 2016.

[52] Weiguang Huo, Samer Mohammed, Yacine Amirat, and Kyoungchul Kong. Fast gait mode detection and assistive torque control of an exoskeletal robotic orthosis for walking assistance. *IEEE Transactions on Robotics*, 34(4):1035–1052, 2018.

[53] Mingoo Jeong, Hanseung Woo, and Kyoungchul Kong. A study on weight support and balance control method for assisting squat movement with a wearable robot, angel-suit. *International Journal of Control, Automation and Systems*, 18(1):114–123, 2020.

[54] Marjorie E Johnson, Marie-Laure Mille, Kathy M Martinez, Gwen Crombie, and Mark W Rogers. Age-related changes in hip abductor and adductor joint torques. *Archives of physical medicine and rehabilitation*, 85(4):593–597, 2004.

[55] Fabian Just, Özhan Özen, Stefano Tortora, Robert Riener, and Georg Rauter. Feedforward model based arm weight compensation with the rehabilitation robot armin. In *2017 International Conference on Rehabilitation Robotics (ICORR)*, pages 72–77. IEEE, 2017.

[56] Angelos Karatsidis, Moonki Jung, H. Martin Schepers, Giovanni Bellusci, Mark de Zee, Peter H. Veltink, and Michael Skipper Andersen. Musculoskeletal model-based inverse dynamic analysis under ambulatory conditions using inertial motion capture. *Medical Engineering & Physics*, 65:68–77, 2019.

[57] Saichon Kloyiam, Sarah Breen, Philip Jakeman, Joe Conway, and Yeshayahu Hutzler. Soccer-specific endurance and running economy in soccer players with cerebral palsy. *Adapted Physical Activity Quarterly*, 28(4):354–367, 2011.

[58] Weisheng Kong, Salvatore Sessa, Sarah Cosentino, Massimiliano Zecca, Kohei Saito, Chunbao Wang, Usama Imtiaz, Zhuohua Lin, Luca Bartolomeo, Hiroyuki Ishii, et al. Development of a real-time imu-based motion capture system for gait rehabilitation. In *2013 IEEE International Conference on Robotics and Biomimetics (ROBIO)*, pages 2100–2105. IEEE, 2013.

[59] Daniel TH Lai, Simon B Taylor, and Rezaul K Begg. Prediction of foot clearance parameters as a precursor to forecasting the risk of tripping and falling. *Human movement science*, 31(2):271–283, 2012.

[60] F Leboeuf, R Baker, A Barré, J Reay, R Jones, and M Sangeux. The conventional gait model, an open-source implementation that reproduces the past but prepares for the future. *Gait & Posture*, 69:235–241, 2019.

[61] Hyunglae Lee, Elliott J Rouse, and Hermano Igo Krebs. Summary of human ankle mechanical impedance during walking. *IEEE journal of translational engineering in health and medicine*, 4:1–7, 2016.

[62] Tommaso Lenzi, Maria Chiara Carrozza, and Sunil K. Agrawal. Powered hip exoskeletons can reduce the user's hip and ankle muscle activations during walking. *IEEE Transactions on Neural Systems and Rehabilitation Engineering*, 21(6):938–948, 2013.

[63] Mantian Li, Jing Deng, Fusheng Zha, Shiyin Qiu, Xin Wang, and Fei Chen. Towards online estimation of human joint muscular torque with a lower limb exoskeleton robot. *Applied Sciences (Switzerland)*, 8(9), 2018.

[64] Jian Liu and Thurmon E. Lockhart. Comparison of 3d joint moments using local and global inverse dynamics approaches among three different age groups. *Gait & Posture*, 23(4):480–485, 2006.

[65] Yu Liu, Shi-Min Shih, Shi-Liu Tian, Yun-Jian Zhong, and Li Li. Lower extremity joint torque predicted by using artificial neural network during vertical jump. *Journal of Biomechanics*, 42(7):906–911, 2009.

[66] Jer-Junn Luh, Gwo-Ching Chang, Cheng-Kung Cheng, Jin-Shin Lai, and Te-Son Kuo. Isokinetic elbow joint torques estimation from surface emg and joint kinematic

data: using an artificial neural network model. *Journal of Electromyography and Kinesiology*, 9(3):173–183, 1999.

[67] Bruce A. MacWilliams, Matthew Cowley, and Diane E. Nicholson. Foot kinematics and kinetics during adolescent gait. *Gait & Posture*, 17(3):214–224, 2003.

[68] Deepti Majumdar, Madhu Sudan Pal, and Dhurjati Majumdar. Effects of military load carriage on kinematics of gait. *Ergonomics*, 53(6):782–791, 2010.

[69] Benoit Mariani, Stephane Rochat, Christophe J Büla, and Kamiar Aminian. Heel and toe clearance estimation for gait analysis using wireless inertial sensors. *IEEE Transactions on Biomedical Engineering*, 59(11):3162–3168, 2012.

[70] Andrés Martínez, Brian Lawson, and Michael Goldfarb. A controller for guiding leg movement during overground walking with a lower limb exoskeleton. *IEEE Transactions on Robotics*, 34(1):183–193, 2018.

[71] Fabien Massé, Roman R Gonzenbach, Arash Arami, Anisoara Paraschiv-Ionescu, Andreas R Luft, and Kamiar Aminian. Improving activity recognition using a wearable barometric pressure sensor in mobility-impaired stroke patients. *Journal of neuroengineering and rehabilitation*, 12(1):1–15, 2015.

[72] Eckart Mayr, Michael Nogler, Maria-Grazia Benedetti, Oliver Kessler, Andrea Reinthaler, Martin Krismer, and Alberto Leardini. A prospective randomized assessment of earlier functional recovery in tha patients treated by minimally invasive direct anterior approach: a gait analysis study. *Clinical biomechanics*, 24(10):812–818, 2009.

[73] Timothy McGrath, Richard Fineman, and Leia Stirling. An auto-calibrating knee flexion-extension axis estimator using principal component analysis with inertial sensors. *Sensors*, 18(6):1882, 2018.

[74] Roberto Merletti and PJJEK Di Torino. Standards for reporting emg data. *J Electromyogr Kinesiol*, 9(1):3–4, 1999.

[75] Alvin W Moore and James W Jorgenson. Median filtering for removal of low-frequency background drift. *Analytical chemistry*, 65(2):188–191, 1993.

[76] Marion Mundt, Arnd Koeppe, Sina David, Franz Bamer, Wolfgang Potthast, and Bernd Markert. Prediction of ground reaction force and joint moments based on optical motion capture data during gait. *Medical Engineering & Physics*, 86:29–34, 2020.

[77] Spencer A Murray, Kevin H Ha, Clare Hartigan, and Michael Goldfarb. An assistive control approach for a lower-limb exoskeleton to facilitate recovery of walking following stroke. *IEEE transactions on neural systems and rehabilitation engineering*, 23(3):441–449, 2014.

[78] Takahiko Nakamura, Kazunari Saito, and Kazuhiro Kosuge. Control of wearable walking support system based on human-model and grf. In *Proceedings of the 2005 IEEE international conference on robotics and automation*, pages 4394–4399. IEEE, 2005.

[79] Rezvan Nasiri, Mohammad Shushtari, Hossein Rouhani, and Arash Arami. Virtual energy regulator: A time-independent solution for control of lower limb exoskeletons. *IEEE Robotics and Automation Letters*, 6(4):7699–7705, 2021.

[80] Milad Nazarahari, Alireza Noamani, Niloufar Ahmadian, and Hossein Rouhani. Sensor-to-body calibration procedure for clinical motion analysis of lower limb using magnetic and inertial measurement units. *Journal of Biomechanics*, 85:224–229, 2019.

[81] Seung Eel Oh, Ahnryul Choi, and Joung Hwan Mun. Prediction of ground reaction forces during gait based on kinematics and a neural network model. *Journal of Biomechanics*, 46(14):2372–2380, 2013.

[82] Michael J Pavol, Tammy M Owings, and Mark D Grabiner. Body segment inertial parameter estimation for the general population of older adults. *Journal of Biomechanics*, 35:707–712, 2002.

[83] Antonio Pedotti, VV Krishnan, and L Stark. Optimization of muscle-force sequencing in human locomotion. *Mathematical Biosciences*, 38(1-2):57–76, 1978.

[84] Daniel S Peterson and Philip E Martin. Effects of age and walking speed on coactivation and cost of walking in healthy adults. *Gait & posture*, 31(3):355–359, 2010.

[85] Serge Pfeifer, Heike Vallery, Michael Hardegger, Robert Riener, and Eric J Perreault. Model-based estimation of knee stiffness. *IEEE transactions on biomedical engineering*, 59(9):2604–2612, 2012.

[86] Xingda Qu and Joo Chuan Yeo. Effects of load carriage and fatigue on gait characteristics. *Journal of biomechanics*, 44(7):1259–1263, 2011.

[87] Jeffrey A Reinbolt, Raphael T Haftka, Terese L Chmielewski, and Benjamin J Fregly. Are patient-specific joint and inertial parameters necessary for accurate inverse dynamics analyses of gait? *IEEE transactions on biomedical engineering*, 54(5):782–793, 2007.

[88] Lei Ren, Richard K. Jones, and David Howard. Whole body inverse dynamics over a complete gait cycle based only on measured kinematics. *Journal of Biomechanics*, 41(12):2750–2759, 2008.

[89] H. Rouhani, J. Favre, X. Crevoisier, and K. Aminian. A wearable system for multisegment foot kinetics measurement. *Journal of Biomechanics*, 47(7):1704–1711, 2014.

[90] Jan Rueterbories, Erika G Spaich, Birgit Larsen, and Ole K Andersen. Methods for gait event detection and analysis in ambulatory systems. *Medical engineering & physics*, 32(6):545–552, 2010.

[91] Angelo M Sabatini, Chiara Martelloni, Sergio Scapellato, and Filippo Cavallo. Assessment of walking features from foot inertial sensing. *IEEE Transactions on biomedical engineering*, 52(3):486–494, 2005.

[92] Lorenzo Saccares, Anais Brygo, Ioannis Sarakoglou, and Nikos G Tsagarakis. A novel human effort estimation method for knee assistive exoskeletons. In *2017 International Conference on Rehabilitation Robotics (ICORR)*, pages 1266–1272. IEEE, 2017.

[93] Zimi Sawacha, Giuseppe Cristoferi, Gabriella Guarneri, Stefano Corazza, Giulia Donà, Paolo Denti, Andrea Facchinetti, Angelo Avogaro, and Claudio Cobelli. Characterizing multisegment foot kinematics during gait in diabetic foot patients. *Journal of NeuroEngineering and Rehabilitation*, 6(1), 2009.

[94] Carlin Senter and Sharon L Hame. Biomechanical analysis of tibial torque and knee flexion angle. *Sports Medicine*, 36(8):635–641, 2006.

[95] Francisco Sepulveda, Derek M. Wells, and Christopher L. Vaughan. A neural network representation of electromyography and joint dynamics in human gait. *Journal of Biomechanics*, 26(2):101–109, 1993.

[96] Hadar Shaulian, Deborah Solomonow-Avnon, Amir Herman, Nimrod Rozen, Amir Haim, and Alon Wolf. The effect of center of pressure alteration on the ground reaction force during gait: A statistical model. *Gait & Posture*, 66:107–113, 2018.

[97] Ching-Long Shih, William A Gruver, and Tsu-Tian Lee. Inverse kinematics and inverse dynamics for control of a biped walking machine. *Journal of Robotic Systems*, 10(4):531–555, 1993.

[98] Mohammad Shushtari, Hannah Dinovitzer, and Arash Arami. Ultra-robust real-time estimation of gait phase. *under review in IEEE Trans. Neural Systems and Rehabilitation Engineering*, 2022.

[99] Mohammad Shushtari, Rezvan Nasiri, and Arash Arami. Online reference trajectory adaptation: A personalized control strategy for lower limb exoskeletons. *IEEE Robotics and Automation Letters*, 7(1):128–134, 2021.

[100] Mohammad Shushtari, Atsushi Takagi, Judy Lee, Etienne Burdet, and Arash Arami. Balance strategy in hoverboard control. *Scientific reports*, 12(1):1–11, 2022.

[101] Stacey M Smith, Robert A Cockburn, Andrea Hemmerich, Rebecca M Li, and Urs P Wyss. Tibiofemoral joint contact forces and knee kinematics during squatting. *Gait & posture*, 27(3):376–386, 2008.

[102] ME Steiner, SR Simon, and JC Pisciotta. Early changes in gait and maximum knee torque following knee arthroplasty. *Clinical orthopaedics and related research*, (238):174—182, January 1989.

[103] Yuanxi Sun, Yuntao Tang, Jia Zheng, Dianbiao Dong, Xiaohong Chen, and Long Bai. From sensing to control of lower limb exoskeleton: a systematic review. *Annual Reviews in Control*, 2022.

[104] Daan van Kooten, Florentina Hettinga, Kim Duffy, Jo Jackson, and Matthew J.D. Taylor. Are there associations with age and sex in walking stability in healthy older adults? *Gait & Posture*, 60:65–70, 2018.

[105] G. Venugopal, M. Navaneethakrishna, and S. Ramakrishnan. Extraction and analysis of multiple time window features associated with muscle fatigue conditions using semg signals. *Expert Systems with Applications*, 41(6):2652–2659, 2014.

[106] Shiqian Wang, Letian Wang, Cory Meijneke, Edwin van Asseldonk, Thomas Hoellinger, Guy Cheron, Yuri Ivanenko, Valentina La Scaleia, Francesca Sylos-Labini, Marco Molinari, Federica Tamburella, Iolanda Pisotta, Freygardur Thorsteinsson, Michel Ilzkovitz, Jeremi Gancet, Yashodhan Nevatia, Ralf Hauffe, Frank Zanow, and Herman van der Kooij. Design and control of the mindwalker exoskeleton.

IEEE Transactions on Neural Systems and Rehabilitation Engineering, 23(2):277–286, 2015.

[107] David A Winter. Pathologic gait diagnosis with computer-averaged electromyographic profiles. *Archives of physical medicine and rehabilitation*, 65(7):393–398, 1984.

[108] David A Winter. Human balance and posture control during standing and walking. *Gait & posture*, 3(4):193–214, 1995.

[109] Shirin Yousefizadeh, Juan de Dios Flores Mendez, and Thomas Bak. Trajectory adaptation for an impedance controlled cooperative robot according to an operator's force. *Automation in Construction*, 103:213–220, 2019.

[110] Hao Yu and Bogdan M Wilamowski. Levenberg-marquardt training. *Industrial electronics handbook*, 5(12):1, 2011.

[111] Shuangyue Yu, Tzu-Hao Huang, Dianpeng Wang, Brian Lynn, Dina Sayd, Viktor Silivanov, Young Soo Park, Yingli Tian, and Hao Su. Design and control of a quasi-direct drive soft exoskeleton for knee injury prevention during squatting. *arXiv preprint arXiv:1902.07106*, 2019.

[112] Juanjuan Zhang, Pieter Fiers, Kirby A. Witte, Rachel W. Jackson, Katherine L. Poggensee, Christopher G. Atkeson, and Steven H. Collins. Human-in-the-loop optimization of exoskeleton assistance during walking. *Science*, 356(6344):1280–1284, 2017.

[113] Zongwei Zhang, Jizhuang Fan, Hongzhe Jin, Tianjiao Zheng, Sikai Zhao, Shun Ma, Jie Zhao, and Yanhe Zhu. Active knee joint exoskeleton for stair ascent augmentation. *Science China Information Sciences*, 64(3):1–3, 2021.

[114] Guoping Zhao, Maziar Sharbafi, Mark Vlutters, Edwin van Asseldonk, and Andre Seyfarth. Template model inspired leg force feedback based control can assist human walking. In *2017 International Conference on Rehabilitation Robotics (ICORR)*, pages 473–478, 2017.